AD-A086 813 DIKEWOOD INDUSTRIES INC ALBUQUERQUE NM F/G 20/14
DISCRETE AND CONTINUOUS SPECTRA OF FINITE-WIDTH, PARALLEL-PLATE--ETC(U)
MAY 80 F C YANG F29601-78-C-0045
UNCLASSIFIED DC-FR-1299-2 AFWL-TR-79-137 NL

1 OF 2
AD
A086813

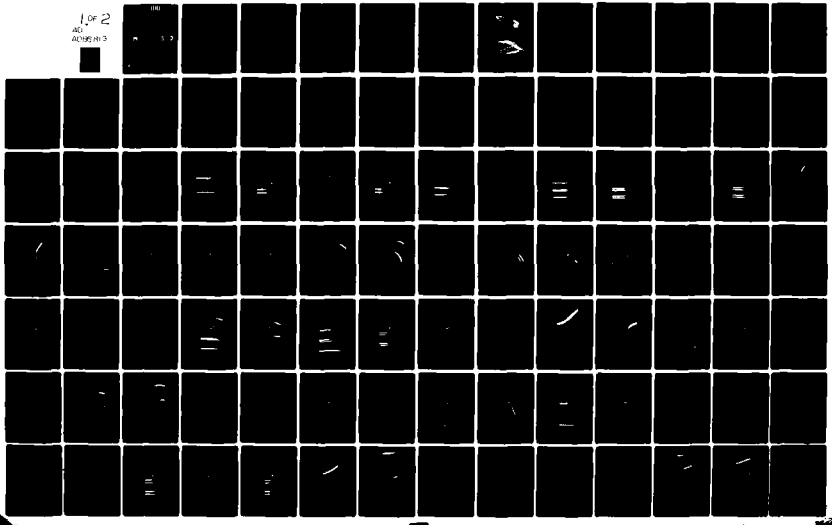

AFWL-TR-79-137

(2) LEVEL III

AD-E200518

AFWL-TR-79-137

ADA086813

DISCRETE AND CONTINUOUS SPECTRA OF FINITE-WIDTH, PARALLEL-PLATE SIMULATOR FIELDS

F. C. Yang

Dikewood Industries, Inc
1009 Bradbury Drive, SE
Albuquerque, NM 87106

May 1980

Final Report

DTIC
ELECTE
JUL 17 1980
S D
B

Approved for public release; distribution unlimited.

DDC FILE COPY

AIR FORCE WEAPONS LABORATORY
Air Force Systems Command
Kirtland Air Force Base, NM 87117

80 6 10 006

This final report was prepared by Dikewood Industries, Inc., Albuquerque, New Mexico, under Contract F29601-78-C-0045, Job Order 37630274 with the Air Force Weapons Laboratory, Kirtland Air Force Base, New Mexico. Captain Howard G. Hudson (NTYE) was the Laboratory Project Officer-in-Charge.

When US Government drawings, specifications, or other data are used for any purpose other than a definitely related Government procurement operation, the Government thereby incurs no responsibility nor any obligation whatsoever, and the fact that the Government may have formulated, furnished, or in any way supplied the said drawings, specifications, or other data, is not to be regarded by implication or otherwise, as in any manner licensing the holder or any other person or corporation, or conveying any rights or permission to manufacture, use, or sell any patented invention that may in any way be related thereto.

This report has been authored by a contractor of the United States Government. The United States Government retains a nonexclusive, royalty-free license to publish or reproduce the material contained herein, or allow others to do so, for the United States Government purposes.

This report has been reviewed by the Public Affairs Office and is releasable to the National Technical Information Service (NTIS). At NTIS, it will be available to the general public, including foreign nations.

This technical report has been reviewed and is approved for publication.

HOWARD G. HUDSON
Captain, USAF
Project Officer

J. PHILIP CASTILLO, PhD
Chief, Electromagnetics Branch

FOR THE DIRECTOR

THOMAS W. CIAMBRONE
Colonel, USAF
Chief, Applied Physics Division

DO NOT RETURN THIS COPY. RETAIN OR DESTROY.

UNCLASSIFIED

SECURITY CLASSIFICATION OF THIS PAGE (When Data Entered)

REPORT DOCUMENTATION PAGE	READ INSTRUCTIONS BEFORE COMPLETING FORM
1. REPORT NUMBER: AFWL-TR-79-137 ✓ 2. GOVT ACCESSION NO. AD-A086813	3. RECIPIENT'S CATALOG NUMBER
4. TITLE (and Subtitle): DISCRETE AND CONTINUOUS SPECTRA OF FINITE-WIDTH, PARALLEL-PLATE SIMULATOR FIELDS	5. TYPE OF REPORT & PERIOD COVERED: Final Report
	6. PERFORMING ORG. REPORT NUMBER: DC-FR-1299-2 ✓
7. AUTHOR(s): F. C. Yang	8. CONTRACT OR GRANT NUMBER(s): F29601-78-C-0045 ✓
9. PERFORMING ORGANIZATION NAME AND ADDRESS: Dikewood Industries, Inc. 1009 Bradbury Drive, S.E. Albuquerque, NM 87106	10. PROGRAM ELEMENT, PROJECT, TASK AREA & WORK UNIT NUMBERS: 64711F/37630274
11. CONTROLLING OFFICE NAME AND ADDRESS: Air Force Weapons Laboratory (NTYE) Kirtland Air Force Base, NM 87117	12. REPORT DATE: May 1980
	13. NUMBER OF PAGES: 106
14. MONITORING AGENCY NAME & ADDRESS (if different from Controlling Office)	15. SECURITY CLASS. (of this report): Unclassified
	15a. DECLASSIFICATION/DOWNGRADING SCHEDULE

16. DISTRIBUTION STATEMENT (of this Report)

Approved for public release; distribution unlimited.

17. DISTRIBUTION STATEMENT (of the abstract entered in Block 20, if different from Report)

18. SUPPLEMENTARY NOTES

19. KEY WORDS (Continue on reverse side if necessary and identify by block number)

Electromagnetic Pulse Simulator
Bounded Wave Simulator
Parallel Plate Simulator
TM, TE Higher-Order Modes
Continuous Spectrum

20. ABSTRACT (Continue on reverse side if necessary and identify by block number)

The discrete (referred as modes) and continuous spectra of finite-width, parallel-plate simulator fields are investigated. Formulas suitable for numerical calculation are obtained for both the transverse-magnetic (TM) and transverse-electric (TE) fields. Numerical results for the propagation constants and the field distributions of the higher order TM modes are presented. It is found that in the working volume of the parallel-plate simulator some of

DD FORM 1 JAN 73 1473

UNCLASSIFIED

SECURITY CLASSIFICATION OF THIS PAGE (When Data Entered)

20. ABSTRACT

the higher-order TM modes resemble those of a closed waveguide, and the field of the continuous spectrum decays at least as z^{-2} for waves propagating along the z-direction.

CONTENTS

Section		Page
I	INTRODUCTION	3
II	INTEGRAL EQUATION FORMULATION	6
	1. TM Fields	6
	2. TE Fields	8
III	MATRIX-EQUATION FORMULATION FOR THE TM FIELDS	10
IV	PROPAGATION CONSTANTS AND FIELD DISTRIBUTIONS OF DISCRETE TM MODES	16
V	CONTINUOUS SPECTRUM CONTRIBUTION	97
	REFERENCES	100
	APPENDIX	101

ACCESSION for
NTIS White Section ☑
DDC Buff Section ☐
UNANNOUNCED ☐
JUSTIFICATION
BY
DISTRIBUTION/AVAILABILITY CODES
Dist. AVAIL. and/or SPECIAL
A

SECTION I

INTRODUCTION

The bounded-wave electromagnetic-pulse (EMP) simulator makes use of two parallel finite-width plates as the guiding structure for the simulated EMP (figure 1). One reason for employing two parallel plates is that they support a transverse-electromagnetic (TEM) mode. Another reason is that over a significant portion of the region between the plates, the TEM-mode fields provide a good approximation to the free-space, plane-wave fields. Unfortunately, such a structure can also support higher-order transverse-magnetic (TM) and transverse-electric (TE) modes and a continuous spectrum (refs. 1,2,3, and 4). The TEM mode alone is not sufficient to completely describe the total simulator field.

The properties of the TEM mode on two parallel plates have been investigated extensively by the method of conformal mapping (refs. 5,6, and 7), whereas the higher-order modes and the continuous spectrum have been investigated only in some limiting cases. In reference 2, integral equations for the higher-order modes are formulated by using Green's theorem. The integral equations are analytically solved under the condition that the separation of the plates is much larger than their width (i.e., narrow plates). In reference 3, alternative integral equations for the higher-order modes are formulated by employing Laplace transforms and the Wiener-Hopf technique, and are solved for the plates with small separation-to-width ratios (i.e., wide plates). The integral equations derived in reference 2 are most useful for numerical treatment when the separation of the plates is comparable to or larger than their width, whereas those derived in reference 3 are most useful when the separation of the plates is comparable to or smaller than their width. The plate geometries discussed in this report have separation-to-width ratios of one, two and three. The integral equations derived in reference 2 are thus more appropriate. In this report, numerical results for the propagation constants and field distributions will be given for the TM modes. The TE modes, which are more highly attenuated away from the launching region (ref. 2), will be discussed in an appendix.

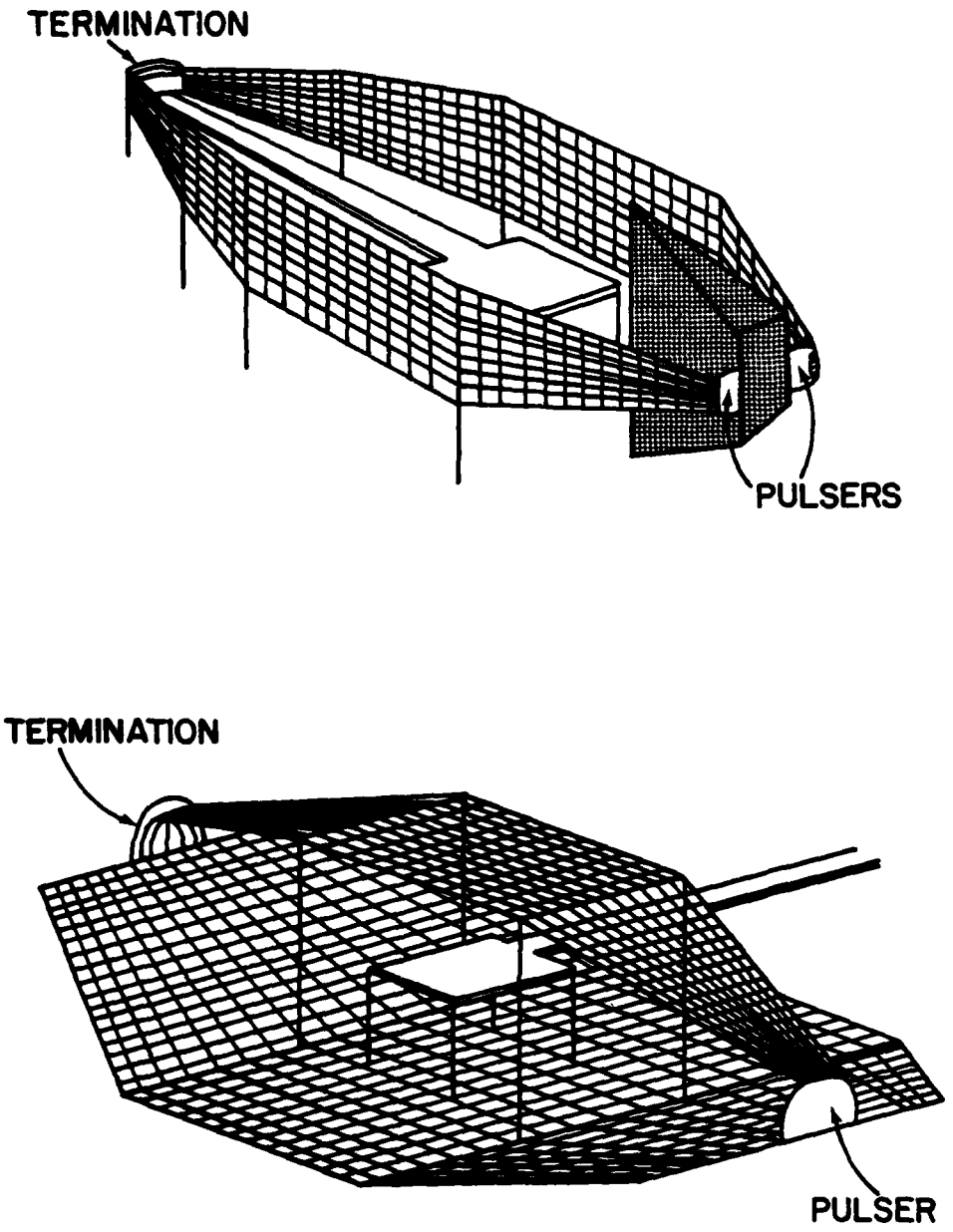

Figure 1. Schematic Picture of Bounded-Wave Simulators.

There is not much information available regarding the continuous spectrum of the two-parallel-plate simulator. In reference 1, an asymptotic analysis has been given to calculate the contribution of the continuous spectrum to the total field of two infinitely long parallel wires, which may be considered as a limiting case of a two-parallel-plate simulator. In this report, a preliminary asymptotic estimation of the continuous spectrum contribution to the TM field at a fixed frequency will be given.

To solve the integral equations derived in reference 2, one first transforms the integral equations into the Fredholm integral equations of the second kind by using Carleman's formula for singular integral equations (ref. 8). The resulting integral equations are transformed further into matrix equations which can be solved numerically by expanding the unknown functions in terms of Chebyshev polynomials. From the numerical solutions of the matrix equations, the propagation constants and field distributions of the higher-order modes as well as the properties of the continuous spectrum can be obtained by some straightforward calculations.

It should be mentioned that although the results in this report are obtained for the infinitely long plates, they can be directly applied to the real simulators where the lengths are finite.

SECTION II

INTEGRAL EQUATION FORMULATION

Two infinitely long, perfectly conducting, parallel plates of finite width are shown in figure 2. The width of each plate is 2w and the distance separating the plates is 2h. A coordinate system is introduced such that the z-axis coincides with the axis of the structure and the x-y plane is the transverse plane, with the x-axis parallel to the plates.

The transverse field components $\underline{E}_t(x,y,\zeta,s)$ and $\underline{H}_t(x,y,\zeta,s)$ in the Laplace transform domain (i.e., s, ζ domain) are related to the longitudinal field components, $E_z(x,y,\zeta,s)$ and $H_z(x,y,\zeta,s)$, via (ref. 2)

$$\begin{aligned} \underline{E}_t(x,y,\zeta,s) &= -\zeta p^{-2}\nabla_t E_z(x,y,\zeta,s) - s\mu_o p^{-2}\,\hat{z}\times\nabla_t H_z(x,y,\zeta,s) \\ \underline{H}_t(x,y,\zeta,s) &= -\zeta p^{-2}\nabla_t H_z(x,y,\zeta,s) + s\varepsilon_o p^{-2}\,\hat{z}\times\nabla_t E_z(x,y,\zeta,s) \end{aligned} \tag{1}$$

where the factor $\exp(\zeta z + st)$ has been suppressed, $p^2 = s^2/c^2 - \zeta^2$, c is the vacuum speed of light and ∇_t is the gradient in the transverse direction.

From equation 1, it is obvious that the fields can always be decomposed into two parts, the TM fields with $H_z = 0$ and the TE fields with $E_z = 0$. Each part will be discussed separately in the sequel.

1. TM FIELDS

As has been discussed above, a knowledge of E_z is sufficient for the determination of the TM field distributions. From reference 2, $E_z(x,y,\zeta,s)$ is given by

$$E_z(x,y,\zeta,s) = \int_{-w}^{w} G(x,y,x',h;p)f(x',h)dx' + \int_{-w}^{w} G(x,y,x',-h;p)f(x',-h)dx'$$

$$G(x,y,x',y';p) = \frac{1}{2\pi} K_o\left(p\sqrt{(x-x')^2 + (y-y')^2}\right) \tag{2}$$

$$f(x,\pm h) = \lim_{\varepsilon\to 0}\left(\frac{\partial}{\partial y} E_z(x,\pm h+\varepsilon,\zeta,s) - \frac{\partial}{\partial y} E_z(x,\pm h-\varepsilon,\zeta,s)\right)$$

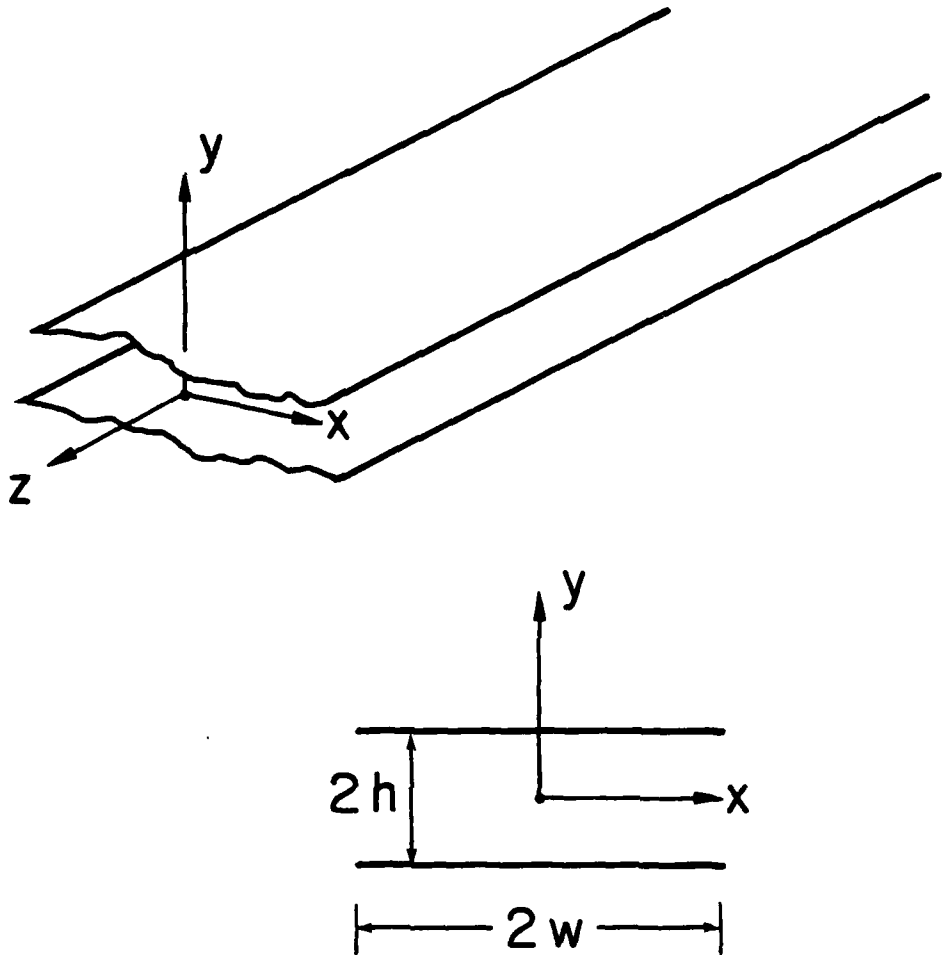

Figure 2. Two, Finitely Wide and Infinitely Long Parallel Plates.

where K_o is the modified Bessel function of the second kind and $f(x,\pm h)$ satisfy the following set of integral equations

$$\int_{-w}^{w} G(x,h,x',h;p)f(x',h)dx' + \int_{-w}^{w} G(x,h,x',-h;p)f(x',-h)dx' = \alpha(x,h)$$
$$\int_{-w}^{w} G(x,-h,x',h;p)f(x',h)dx' + \int_{-w}^{w} G(x,-h,x',-h;p)f(x',-h)dx' = \alpha(x,-h) \tag{3}$$

for $|x| \leq w$, with $\alpha(x,\pm h) = - E_z^{inc}(x,\pm h,\zeta,s)$ being the incident longitudinal electric fields at the plates.

2. TE FIELDS

The TE field distributions can be derived completely from $H_z(x,y,\zeta,s)$ which is given by the following formula (ref. 2)

$$s\mu_o H_z(x,y,\zeta,s) = - \int_{-w}^{w} \left[\frac{\partial G}{\partial y'}(x,y,x',y';p)g(x',h)dx'\right]_{y'=h}$$
$$- \int_{-w}^{w} \left[\frac{\partial G}{\partial y'}(x,y,x',y';p)g(x',-h)dx'\right]_{y'=-h} \tag{4a}$$

where $g(x,\pm h)$ are defined by

$$(s\mu_o)^{-1} g(x,\pm h) = \lim_{\varepsilon \to 0} \left(H_z(x,\pm h+\varepsilon,\zeta,s) - H_z(x,\pm h-\varepsilon,\zeta,s)\right) \tag{4b}$$

and satisfy the following set of differential-integral equations

$$\left(\frac{d^2}{dx^2} - p^2\right)\left(\int_{-w}^{w} G(x,h,x',h;p)g(x',h)dx' + \int_{-w}^{w} G(x,h,x',-h;p)g(x',-h)dx'\right)$$
$$= \beta(x,h), \qquad \text{for } |x| \leq w \tag{5}$$
$$\left(\frac{d^2}{dx^2} - p^2\right)\left(\int_{-w}^{w} G(x,-h,x',h;p)g(x',h)dx' + \int_{-w}^{w} G(x,-h,x',-h;p)g(x',-h)dx'\right)$$
$$= \beta(x,-h), \qquad \text{for } |x| \leq w$$

with $\beta(x,\pm h) = p^2 E_x^{inc}(x,\pm h,\zeta,s) + \zeta\,\partial E_z^{inc}(x,\pm h,\zeta,s)/\partial x$ being the source terms.

Although equations 3 and 5 look extremely complicated, they can be simplified by observing that for most parallel-plate simulators the source terms on the right-hand sides of equations 3 and 5 satisfy the following conditions

$$\begin{aligned} \alpha(x,h) &= -\,\alpha(x,-h) = \alpha(-x,h) = \alpha^{-e}(x) \\ \beta(x,h) &= -\,\beta(x,-h) = -\beta(-x,h) = \beta^{-o}(x) \end{aligned} \tag{6}$$

Accordingly, one has

$$f(x,h) = -\,f(x,-h) = f(-x,h) = f^{-e}(x)$$

for the TM fields, and

$$g(x,h) = -\,g(x,-h) = -\,g(-x,h) = g^{-o}(x)$$

for the TE fields. The superscript "$-$" in α^{-e}, β^{-o}, f^{-e}, g^{-o} is used to indicate that all these functions α, β, f, g are antisymmetric with respect to y, while the superscript "e" or "o" is used to indicate that the functions are either even or odd functions of x. Under the above conditions of equation 6, the two equations of either integral equation set 3 or 5 become identical.

In the following sections, the simplified equations will be used to investigate the properties of the higher-order modes and the continuous spectrum of the two-parallel-plate guiding structure.

SECTION III

MATRIX-EQUATION FORMULATION FOR THE TM FIELDS

In this section, the integral equations given by equation 3 for the TM fields will be transformed into matrix equations by expanding the unknown functions in terms of Chebyshev polynomials.

On account of the source condition of equation 6 the coupled integral equations 3 are reduced to a single integral equation

$$\int_{-w}^{w} \Big(G(x,h,x',h;p) - G(x,h,x',-h;p) \Big) f^{-e}(x')dx' = \alpha^{-e}(x), \quad |x| \leq w \tag{7}$$

It is easy to see that the kernel of the integral equation 7 has a logarithmic singularity. After separating out the singular term and normalizing the variables in the following manner

$$\begin{aligned} x &= w\xi, \quad x' = w\xi' \\ p &= \gamma/w, \quad h = wH \end{aligned} \tag{8}$$

the integral equation 7 becomes

$$\begin{aligned} &\int_{-1}^{1} \ln(|\xi-\xi'|) f^{-e}(\xi')d\xi' \\ &\quad = 2\pi \int_{-1}^{1} \Big(M(\xi-\xi';\gamma) - N(\xi-\xi';\gamma) \Big) f^{-e}(\xi')d\xi' - 2\pi\alpha^{-e}(\xi), \quad \text{for } |\xi| \leq 1 \end{aligned} \tag{9}$$

where

$$M(\xi-\xi';\gamma) = \frac{1}{2\pi} K_o(\gamma|\xi-\xi'|) + \frac{1}{2\pi} \ln(|\xi-\xi'|)$$

$$N(\xi-\xi';\gamma) = \frac{1}{2\pi} K_o\left(\gamma\sqrt{(\xi-\xi')^2 + 4H^2} \right)$$

Here, both M and N are regular functions of $\xi - \xi'$.

To facilitate the numerical solution of the integral equation 9, it is desirable to transform it into a Fredholm integral equation of the second kind. To do this, Carleman's formula for integral equations with logarithmic kernels is used to obtain (ref. 8)

$$f^{-e}(\xi) + \int_{-1}^{1} \Big(K(\xi,\xi';\gamma) - L(\xi,\xi';\gamma) \Big) f^{-e}(\xi')d\xi' = S^{-e}(\xi), \quad |\xi| \leq 1 \quad (10)$$

where

$$K(\xi,\xi';\gamma) = \frac{2}{\pi\sqrt{1-\xi^2}\,\ln 2} \int_{-1}^{1} \frac{M(\xi''-\xi';\gamma)}{\sqrt{1-\xi''^2}}\, d\xi''$$

$$+ \frac{2}{\pi\sqrt{1-\xi^2}} \fint_{-1}^{1} \frac{M'(\xi''-\xi';\gamma)\sqrt{1-\xi''^2}}{\xi-\xi''}\, d\xi''$$

$$L(\xi,\xi';\gamma) = \frac{2}{\pi\sqrt{1-\xi^2}\,\ln 2} \int_{-1}^{1} \frac{N(\xi''-\xi';\gamma)}{\sqrt{1-\xi''^2}}\, d\xi''$$

$$+ \frac{2}{\pi\sqrt{1-\xi^2}} \fint_{-1}^{1} \frac{N'(\xi''-\xi';\gamma)\sqrt{1-\xi''^2}}{\xi-\xi''}\, d\xi''$$

$$S^{-e}(\xi) = \frac{2}{\pi\sqrt{1-\xi^2}\,\ln 2} \int_{-1}^{1} \frac{\alpha^{-e}(\xi'')}{\sqrt{1-\xi''^2}}\, d\xi''$$

$$+ \frac{2}{\pi\sqrt{1-\xi^2}} \fint_{-1}^{1} \frac{\alpha^{-e'}(\xi'')\sqrt{1-\xi''^2}}{\xi-\xi''}\, d\xi''$$

Here, $\fint$ denotes the principal-value integral and the prime in M', N', $\alpha^{-e'}$ denotes differentiation with respect to the first argument.

The integral equation 10 can now be reduced to a set of algebraic equations suitable for numerical computation. The mathematical properties

of $K(\xi,\xi';\gamma)$, $L(\xi,\xi';\gamma)$ and $S^{-e}(\xi)$ together with the edge conditions and symmetry properties of $f^{-e}(\xi)$ suggest the expansion

$$f^{-e}(\xi) = \frac{1}{\sqrt{1-\xi^2}} \sum_{n=0}^{\infty} f_n^{-e} T_{2n}(\xi) \tag{11}$$

where $T_{2n}(\xi)$ are Chebyshev polynomials of the first kind. Then, with the aid of the orthogonality of the Chebyshev polynomials, the integral equation 10 is transformed to the following set of algebraic equations

$$f_n^{-e} + \sum_{m=0}^{\infty} \left(K_{nm}^{e} - L_{nm}^{e} \right) f_m^{-e} = S_n^{-e} \tag{12}$$

where

$$K_{nm}^{e} = \frac{2}{\pi\varepsilon_n} \int_{-1}^{1} \int_{-1}^{1} \frac{K(\xi,\xi';\gamma) T_{2n}(\xi) T_{2m}(\xi')}{\sqrt{1-\xi'^2}} \, d\xi' d\xi$$

$$L_{nm}^{e} = \frac{2}{\pi\varepsilon_n} \int_{-1}^{1} \int_{-1}^{1} \frac{L(\xi,\xi';\gamma) T_{2n}(\xi) T_{2m}(\xi')}{\sqrt{1-\xi'^2}} \, d\xi' d\xi$$

$$S_n^{-e} = \frac{2}{\pi\varepsilon_n} \int_{-1}^{1} S^{-e}(\xi) T_{2n}(\xi) d\xi$$

and

$$\varepsilon_n = \begin{cases} 2, & n = 0 \\ 1, & n \neq 0 \end{cases}$$

Or, in matrix form

$$\left[\delta_{nm} + K_{nm}^{e} - L_{nm}^{e} \right] \left[f_m^{-e} \right] = \left[S_n^{-e} \right] \tag{13}$$

where δ_{nm} is the Kronecker delta, which is zero when n is not equal to m and unity when n equals m, and $[r_{nm}]$ is a matrix whose elements are r_{nm}.

Both K^e_{nm} and L^e_{nm} are complicated triple integrals. They can be simplified by first integrating over ξ and then by making the change of variables $\xi'' - \xi' = 2\eta$ and $\xi'' + \xi' = 2\eta'$, to get

$$K^e_{nm} = \begin{cases} \dfrac{8}{\pi \ln 2} \displaystyle\int_0^1 M(2\eta;\gamma) G^e_m(\eta) d\eta & n = 0 \\ \dfrac{16}{\pi} \displaystyle\int_0^1 M'(2\eta;\gamma) F^e_{nm}(\eta) d\eta & n \geq 1 \end{cases}$$

$$L^e_{nm} = \begin{cases} \dfrac{8}{\pi \ln 2} \displaystyle\int_0^1 N(2\eta;\gamma) G^e_m(\eta) d\eta & n = 0 \\ \dfrac{16}{\pi} \displaystyle\int_0^1 N'(2\eta;\gamma) F^e_{nm}(\eta) d\eta & n \geq 1 \end{cases} \tag{14}$$

where

$$G^e_m(\eta) = \int_0^{1-|\eta|} \frac{T_{2m}(\eta' - \eta) + T_{2m}(\eta' + \eta)}{\sqrt{\left(1 - (\eta' + \eta)^2\right)\left(1 - (\eta' - \eta)^2\right)}} d\eta'$$

$$F^e_{nm}(\eta) = \int_{-1+|\eta|}^{1-|\eta|} \frac{\left(1 - (\eta' + \eta)^2\right) U_{2n-1}(\eta' + \eta) T_{2m}(\eta' - \eta)}{\sqrt{\left(1 - (\eta' + \eta)^2\right)\left(1 - (\eta' - \eta)^2\right)}} d\eta' \tag{15}$$

and $U_n(\eta)$ is the Chebyshev polynomial of the second kind. By using the explicit formulas for the Chebyshev polynomials in the integrals of equation 15, $G^e_m(\eta)$ and $F^e_{nm}(\eta)$ are further transformed into sums of complete elliptic integrals which are more suitable for numerical computation, viz.,

$$G^e_m(\eta) = \sum_{k=0}^{m} \sum_{j=0}^{k} t^e_{mk} b_j(0,2k) \eta^{2k-2j} D_j(\eta)$$

$$F^e_{nm}(\eta) = \sum_{k=0}^{m} \sum_{\ell=1}^{n} u^e_{n\ell} t^e_{mk} \left\{ \sum_{j=0}^{k+\ell-1} \left(b_j(2\ell-1,\ 2k) - \eta^2 b_j(2\ell+1,\ 2k) \right) \times \right. \tag{16}$$

$$\left. \times\ \eta^{2\ell + 2k - 2j - 1} D_j(\eta) - \eta\, b_{k+\ell}(2\ell+1,\ 2k) D_{k+\ell}(\eta) \right\}$$

where

$$u^e_{n\ell} = (-1)^{n-\ell} \frac{(n+\ell-1)!}{(n-\ell)!(2\ell-1)!} 2^{2\ell-1}$$

$$t^e_{mk} = (-1)^{m-k} \frac{(m+k-1)!m}{(m-k)!(2k)!} 2^{2k}, \qquad t^e_{oo} = 1$$

$$b_j(k,\ell) = \sum_{i=i_1}^{i_2} (-1)^{\ell+i-2j} \frac{k!\ell!}{i!(k-i)!(2j-i)!(\ell+i-2j)!}$$

$$i_1 = \max\{0, 2j-\ell\} \qquad i_2 = \min\{k, 2j\}$$

and the functions $D_j(\eta)$ are determined from the following recursion formulas

$$D_{j+2}(\eta) = 4\,\frac{j+1}{2j+3}\left(1+\eta^2\right)D_{j+1}(\eta) - \frac{2j+1}{2j+3}\left(1-\eta^2\right)^2 D_j(\eta)$$

$$D_1(\eta) = 2(1+\eta)\left\{F\left((1-\eta)/(1+\eta)\right) - E\left((1-\eta)/(1+\eta)\right)\right\} \tag{17}$$

$$D_o(\eta) = 2F\left((1-\eta)/(1+\eta)\right)\Big/(1+\eta)$$

Here, $F(\eta)$ and $E(\eta)$ are complete elliptic integrals

$$F(\eta) = \int_0^{\pi/2} \left(1-\eta^2\sin^2\phi\right)^{-\frac{1}{2}} d\phi$$

$$E(\eta) = \int_0^{\pi/2} \left(1-\eta^2\sin^2\phi\right)^{\frac{1}{2}} d\phi$$

The solution of the matrix equation 13 is simply given by

$$\left[f^{-e}_m\right] = \left[\delta_{nm} + K^e_{nm} - L^e_{nm}\right]^{-1}\left[S^{-e}_n\right] \tag{18}$$

Insertion of this solution into equations 11, 2 and 1 gives the Laplace transform domain TM fields.

In the next two sections certain important properties of the TM fields will be discussed by studying the singularities of equation 2 in the complex ζ-plane at a fixed $s = j\omega$.

SECTION IV

PROPAGATION CONSTANTS AND FIELD DISTRIBUTIONS OF DISCRETE TM MODES

In the previous sections, the formulas required to calculate the TM fields of two parallel-plates are obtained. At a given frequency ω, the field distributions are calculated from the inverse Laplace transform integrals

$$\begin{Bmatrix} \underline{E}(x,y,z,j\omega) \\ \\ \underline{H}(x,y,z,j\omega) \end{Bmatrix} = \frac{1}{2\pi j} \int_{C_\zeta} \begin{Bmatrix} \underline{E}(x,y,\zeta,j\omega) \\ \\ \underline{H}(x,y,\zeta,j\omega) \end{Bmatrix} e^{\zeta z} d\zeta \tag{19}$$

where C_ζ is the path of integration in the complex ζ-plane shown in figure 3 and $\underline{E}(x,y,\zeta,j\omega)$ and $\underline{H}(x,y,\zeta,j\omega)$ are given by equations 1 and 2. An examination of equation 2 shows that in the complex ζ-plane, there are branch points at $\zeta = \pm j\omega$ and poles at $\zeta_{k,\ell}$ where $\det\left[\delta_{nm} + K^e_{nm} - L^e_{nm}\right] = 0$. For the branch cuts shown in figure 3, the contour C_ζ can be deformed to the left half-plane for field points at $z > 0$ and sources at $z \leq 0$. The contour integral along C_ζ is thus reduced to the integral along the branch cut B_- (the so-called continuous spectrum contribution) plus the residues at the poles $\zeta_{k,\ell}$(the so-called modal fields). The reason why two indices are assigned to $\zeta_{k,\ell}$ will become clear later when numerical results are obtained.

Each modal field is required to be outgoing in the transverse direction and decaying in the +z direction. Thus, in the branch shown in figure 3, the poles can exist only in the region where $-\omega/c < \mathrm{Im}(\zeta) < 0$ and $\mathrm{Re}(\zeta) < 0$. It is also observed that $p_{k,\ell}$ have negative real parts, so that the modal field distributions increase indefinitely in the transverse direction. Hence, the branch shown in figure 3 is appropriate only when the field points are close to the plates. In the remaining part of this section, the propagation constants and field distributions of the TM modes will be discussed, while an estimation of the continuous-spectrum contribution will be relegated to the next section.

To calculate the propagation constants of the TM modes, one has to find first $p_{k,\ell}$ from the equation $\det\left[\delta_{nm} + K^e_{nm} - L^e_{nm}\right] = 0$. With these

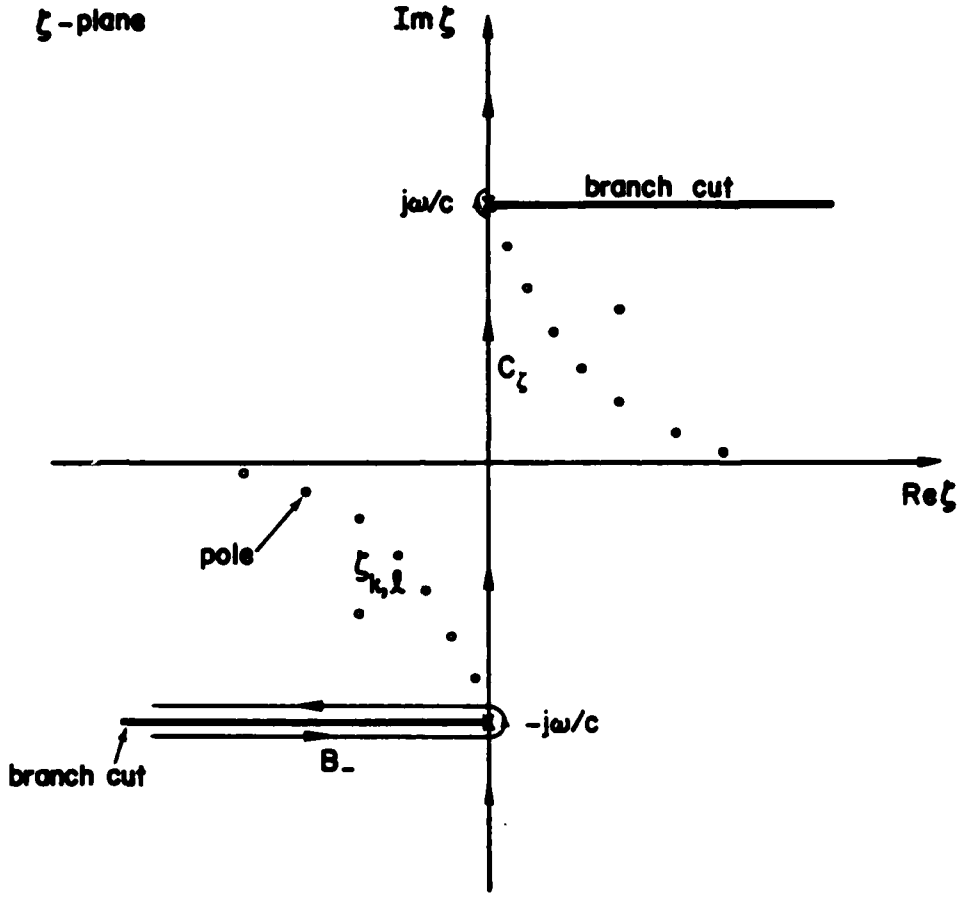

Figure 3. The Branch of $p = -j\sqrt{\zeta^2 + \omega^2/c^2}$. In this Branch, $\mathrm{Re}(p) < 0$ for $\{\zeta\colon \mathrm{Re}(\zeta) < 0 \text{ and } -\omega/c < \mathrm{Im}(\zeta) < 0\}$ and $\{\zeta\colon \mathrm{Re}(\zeta) > 0 \text{ and } \omega/c > \mathrm{Im}(\zeta) > 0\}$.

$p_{k,\ell}$ values (the so-called transverse propagation constants), the corresponding longitudinal propagation constants $\zeta_{k,\ell}$ are simply given by

$$\zeta_{k,\ell} = -j\sqrt{p_{k,\ell}^2 + \omega^2/c^2} \tag{20}$$

When $H = h/w >> 1$, i.e., the plates are extremely narrow, there exist possible $p_{k,\ell}$'s for which $|\gamma_{k,\ell}| = |p_{k,\ell}w| << 1$ and $\det\left[\delta_{nm} + K^e_{nm} - L^e_{nm}\right] = 0$. Actually, under the condition $|\gamma_{k,\ell}| << 1$, one can show that the $\gamma_{k,\ell}$'s satisfy

$$\det\left[\delta_{nm} + K^e_{nm} - L^e_{nm}\right] \simeq \det\left[\delta_{nm} + \delta_{no}\delta_{mo}(K^e_{oo} - L^e_{oo})\right]$$

$$\simeq 1 + \left(\ln 2 - \ln(\Gamma\gamma_{k,\ell}) - K_o(2\gamma_{k,\ell}H)\right)/\ln 2 = 0 \tag{21}$$

where $\Gamma \simeq 1.781$ is the exponent of Euler's constant. Equation 21 is the same as that obtained in reference 2, where its solutions are also given.

When the width of the plates is comparable to their separation, which is the case of interest here where $H = 1,2,3$, one must resort to numerical methods to solve the equation $\det\left[\delta_{nm} + K^e_{nm} - L^e_{nm}\right] = 0$ for the transverse propagation constants $p_{k,\ell}$. The method selected is first to locate the approximate positions of the zeros of the determinant from the constant-magnitude contours in the complex p-plane. Then these approximate positions are used as the starting points for the Newton-Raphson method, used to search for more accurate solutions for the transverse propagation constants $P_{k,\ell}$. It is found that three terms in the expansion 11 for $f^{-e}(\xi)$ are sufficient to obtain resonably accurate transverse propagation constants of the first several modes for $H \geq 1$. For each transverse propagation constant $p_{k,\ell}$, the f_n^{-e} are then determined within a multiplicative constant from the homogeneous equation of equation 13. These f_n^{-e} values can in turn be used in equations 1, 2 and 11 to calculate the corresponding modal field distributions.

The transverse propagation constants $p_{k,\ell}$ of the first several TM modes for H = 1,2,3 calculated by the above described approach with the aid of a CDC 6600/7600 computer are tabulated in table 1. The $\zeta_{k,\ell}$ values as functions of ω for the lowest TM modes with $k = 0,1$ and $\ell = 1,2$ are plotted in figures 4, 5 and 6. Four curves of $p_{0,\ell}$, $\ell = 1,2,3,4$ are also presented in figure 7 for H-values ranging from 50 to about 2. The numerical results of the modal field distributions for the $TM_{k,\ell}$ modes with $k = 0,1$, $\ell = 1,2$ are given in figures 8 through 19. The field distributions are plotted in terms of constant-value contours of the real parts, imaginary parts and magnitudes of the normalized field components.

From the field distribution plots of the $TM_{k,\ell}$ modes, especially the modes with $\ell > k$, it is observed that in the working volume of the simulator (i.e., x/w, $y/h < 1$) the fields vary almost sinusoidally as functions of x and y with periods of $2w/k$ and $2h/\ell$ respectively. The indices k,ℓ used in the $TM_{k,\ell}$ modes thus characterize the field variations in the x,y directions; and the use of two indices is justified. In this report, results are given only for $k = 0$ and 1. It is believed that if one goes even farther away from the imaginary axis, more $TM_{k,\ell}$ modes can be found for $k \geq 2$. However, for the modes with $k \geq 2$, the corresponding longitudinal propagation constants $\zeta_{k,\ell}$ will have decay constants so large that those modes become less important.

Table 1

TRANSVERSE PROPAGATION CONSTANTS OF TM MODES

h/w (H)	ℓ	k = 0		k = 1	
		$Re(p_{0,\ell}w)$	$Im(p_{0,\ell}w)$	$Re(p_{1,\ell}w)$	$Im(p_{1,\ell}w)$
1	1	-0.1274	3.2879	-1.5701	1.1930
	2	-0.0590	6.3890	-0.9827	4.3512
	3	-0.0353	9.5060	-0.5034	7.1986
	4	-0.0245	12.6321	-0.2935	10.1311
2	1	-0.1834	1.6686	-1.2325	0.7914
	2	-0.1260	3.2448	-1.1963	2.2510
	3	-0.0778	4.8067	-0.9098	3.9028
	4	-0.0575	6.3662	-0.6898	5.4269
3	1	-0.1779	1.0974	-1.0351	0.5888
	2	-0.1299	2.1721	-0.9925	1.4961
	3	-0.1006	3.2207	-0.9207	2.5827
	4	-0.0814	4.2662	-0.7896	3.6733

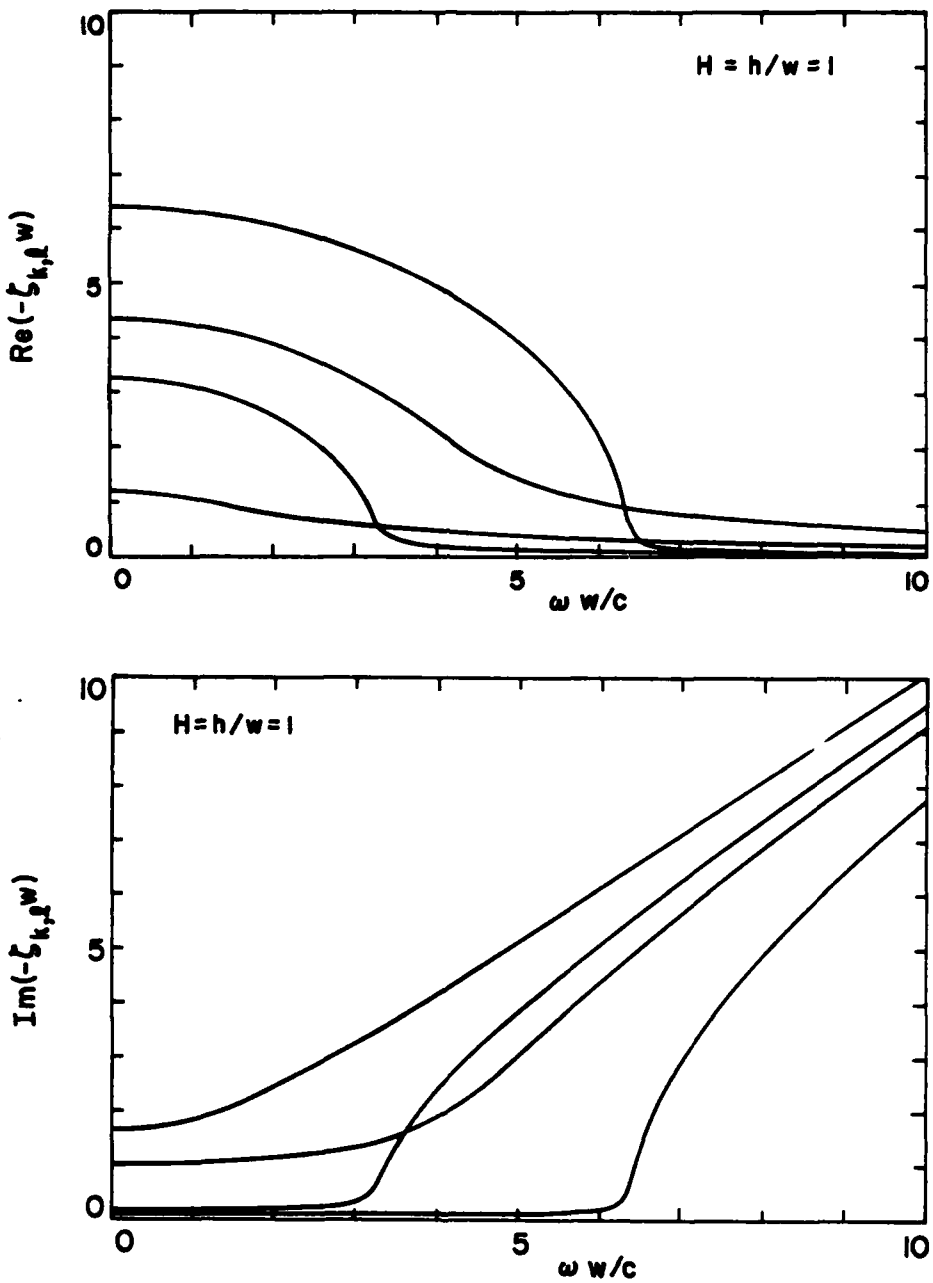

Figure 4. Frequency Variation of Longitudinal Propagation Constants $\zeta_{k,\ell}$ of Higher-Order TM Modes for $k = 0,1$, $\ell = 1,2$ when $h/w = 1$.

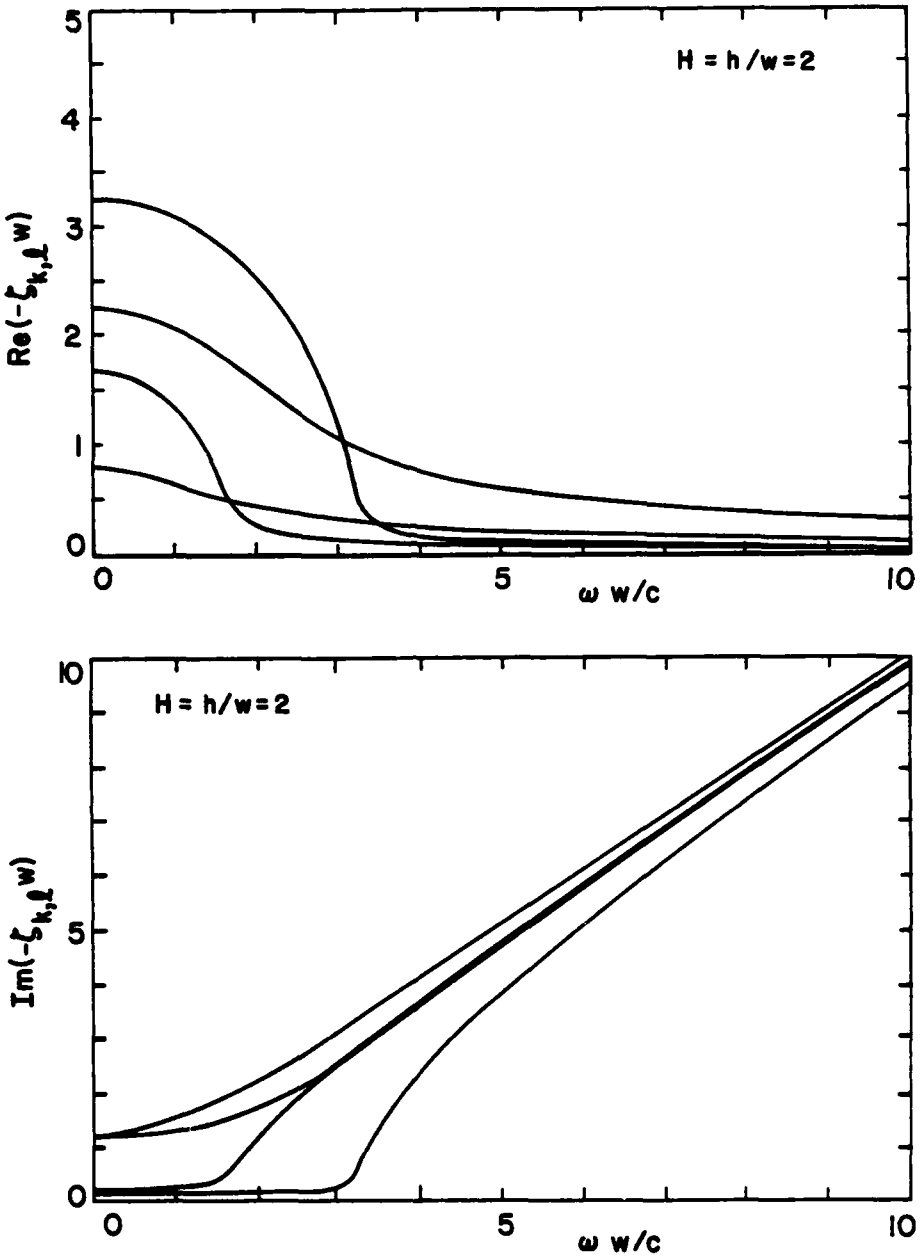

Figure 5. Frequency Variation of Longitudinal Propagation Constants $\zeta_{k,\ell}$ of Higher-Order TM Modes for $k = 0,1$, $\ell = 1,2$, when $h/w = 2$.

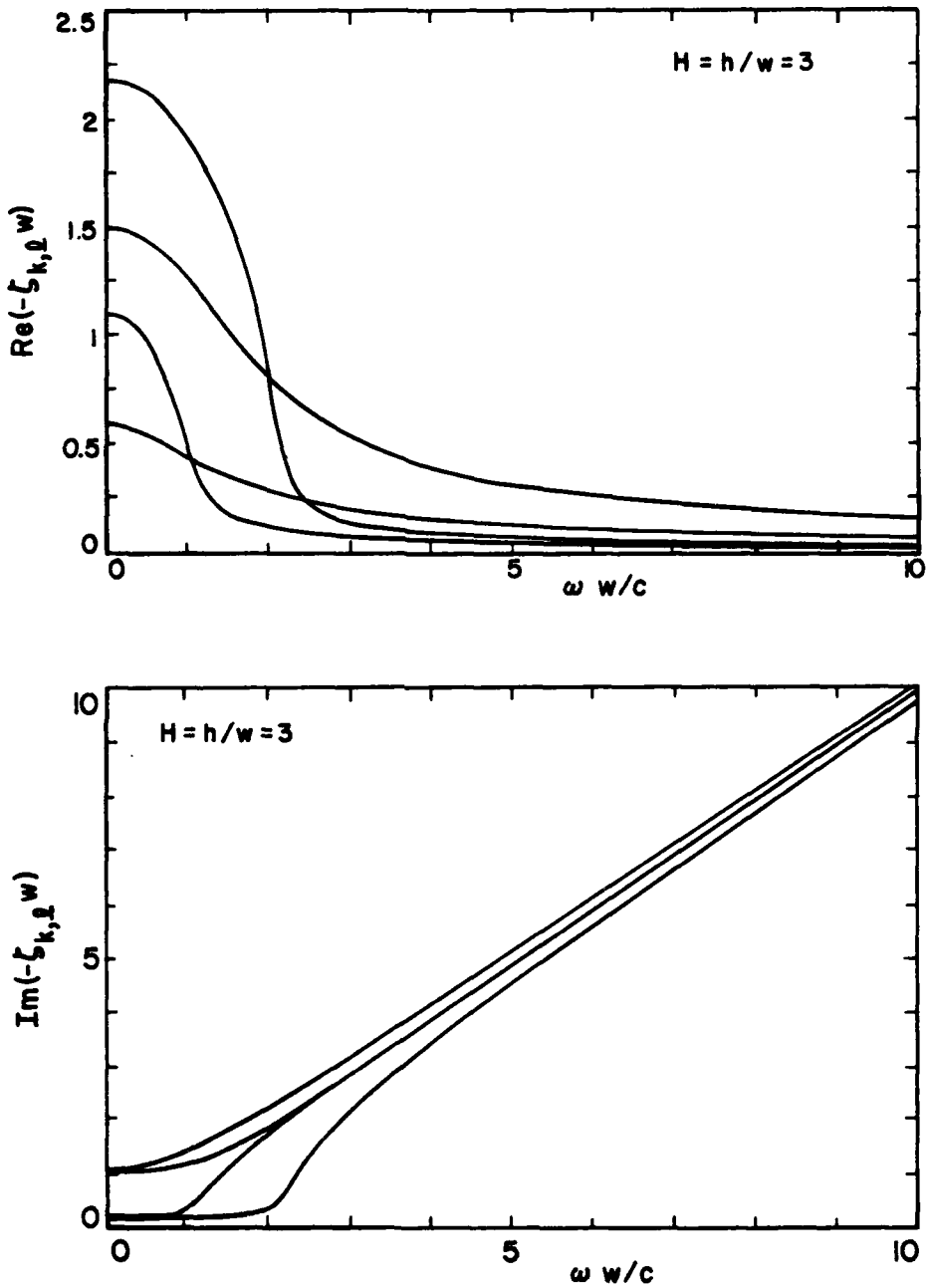

Figure 6. Frequency Variation of Longitudinal Propagation Constants $\zeta_{k,\ell}$ of Higher-Order TM Modes for $k = 0,1$, $\ell = 1,2$ when $h/w = 3$.

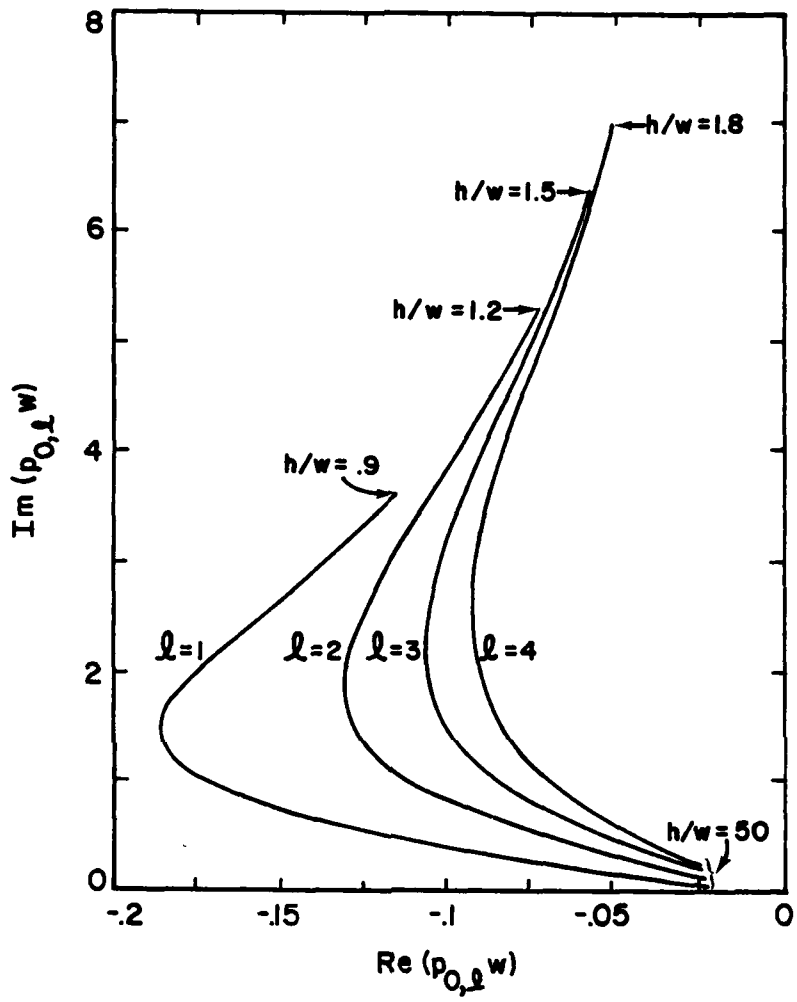

Figure 7. The Normalized Transverse Propagation Constants $p_{0,\ell}w$ as Functions of h/w for ℓ = 1,2,3,4.

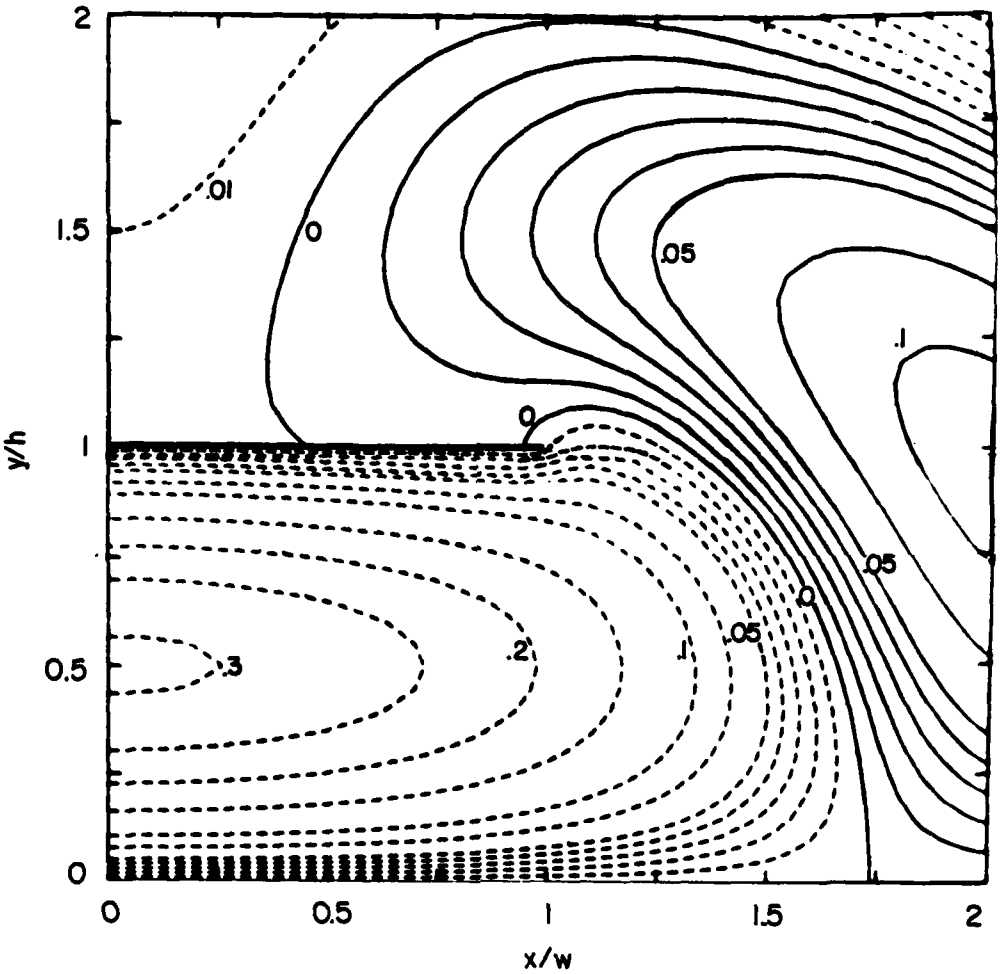

Figure 8a. Constant Value Contours for Normalized Field Component $Re(E_z/w)$ of the $TM_{0,1}$ Mode when $h/w = 1$. The Fields are Normalized so that $|p^2/\zeta|\sqrt{|E_x|^2 + |E_y|^2} = 1$ at $x = y = 0$. Broken Lines are for Negative Values.

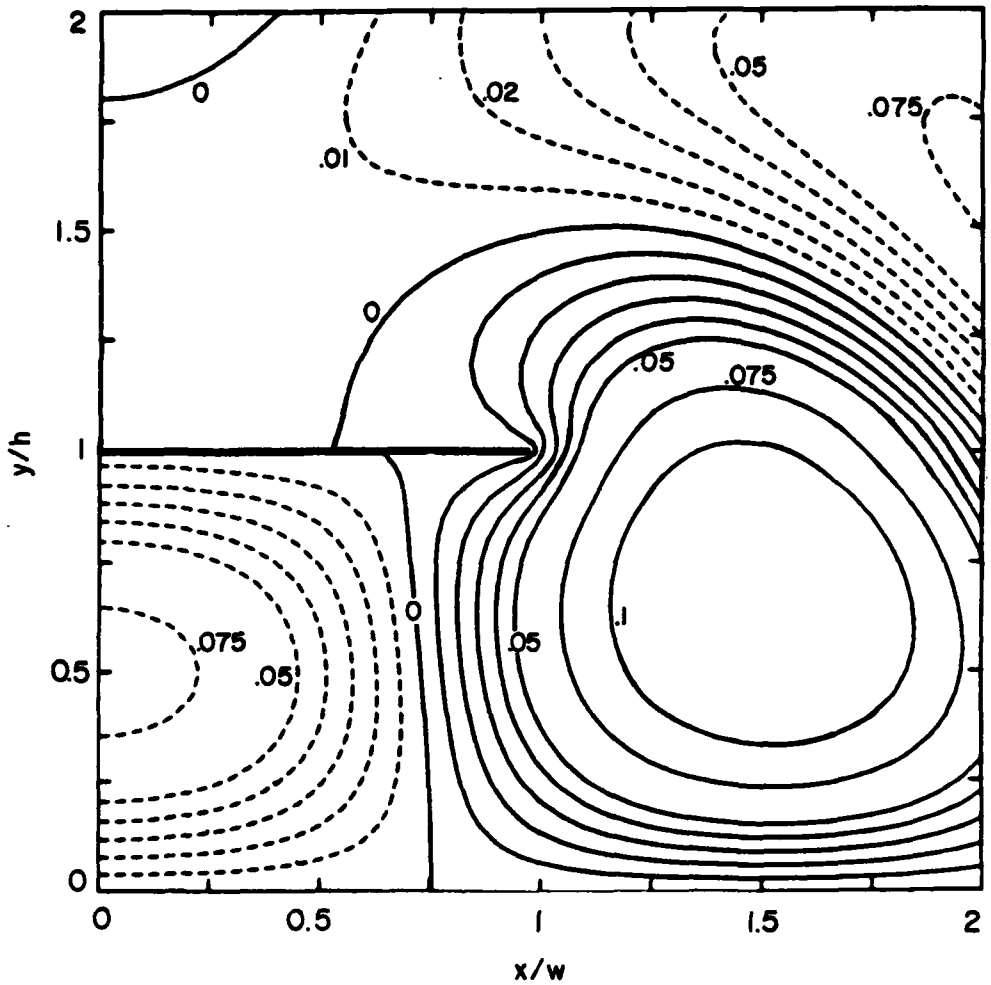

Figure 8b. Constant Value Contours for Normalized Field Component $\mathrm{Im}(E_z/w)$ of the $TM_{0,1}$ Mode when $h/w = 1$. The Fields are Normalized so that $|p^2/\zeta|\sqrt{|E_x|^2 + |E_y|^2} = 1$ at $x = y = 0$. Broken Lines are for Negative Values.

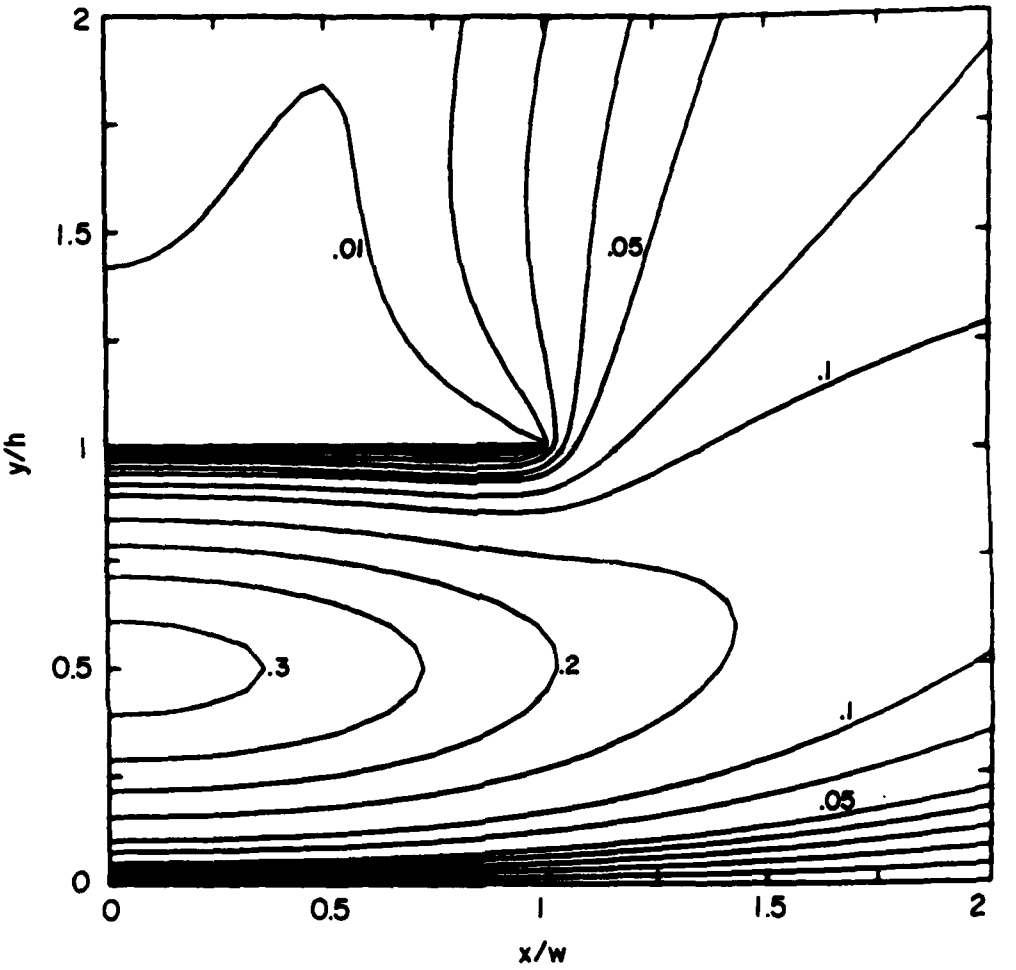

Figure 8c. Constant Value Contours for Normalized Field Component $|E_z/w|$, of the $TM_{0,1}$ Mode when $h/w = 1$. The Fields are Normalized so that $|p^2/\zeta|\sqrt{|E_x|^2 + |E_y|^2} = 1$ at $x = y = 0$.

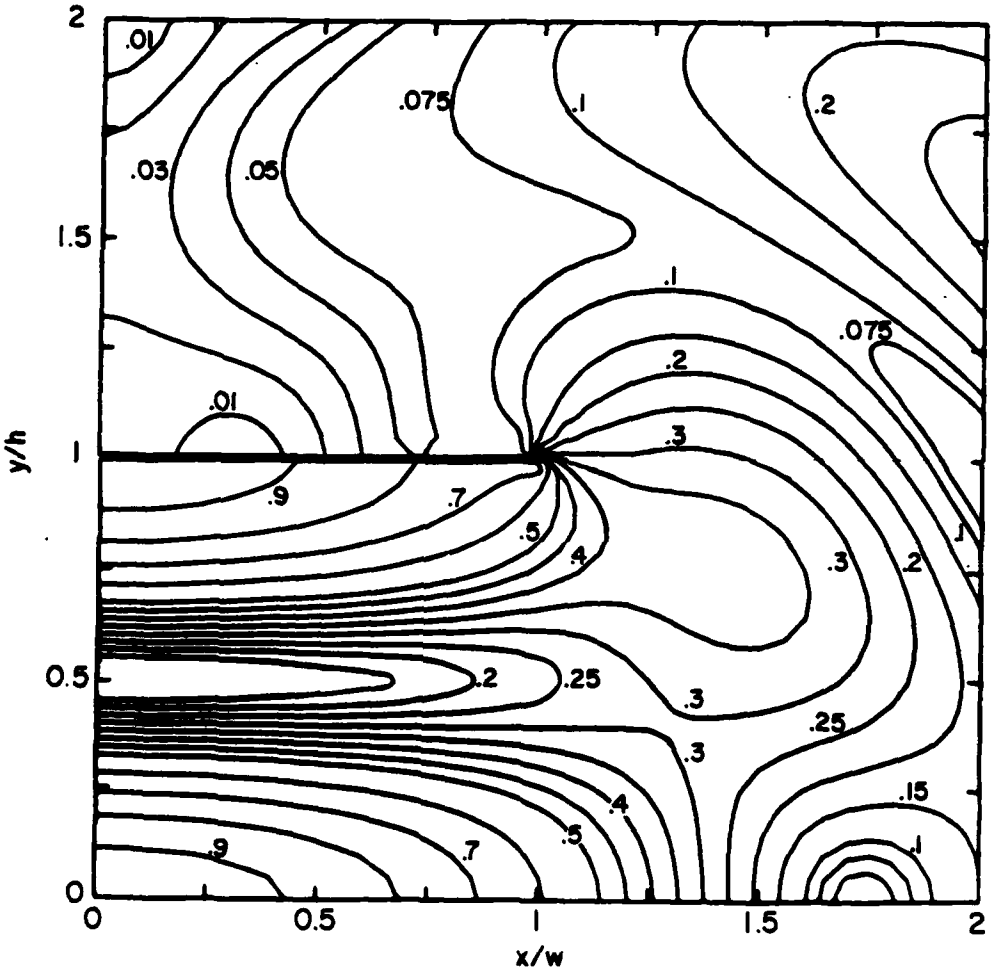

Figure 8d. Constant Value Contours for Normalized Field Component $\sqrt{(\mathrm{Re}(p^2E_x/\zeta))^2 + (\mathrm{Re}(p^2E_y/\zeta))^2} = \sqrt{(\mathrm{Re}(p^2H_y/s\varepsilon_o))^2 + (\mathrm{Re}(p^2H_x/s\varepsilon_o))^2}$ of the $TM_{0,1}$ Mode when $h/w = 1$. The Fields are Normalized so that $|p^2/\zeta|\sqrt{|E_x|^2 + |E_y|^2} = 1$ at $x = y = 0$.

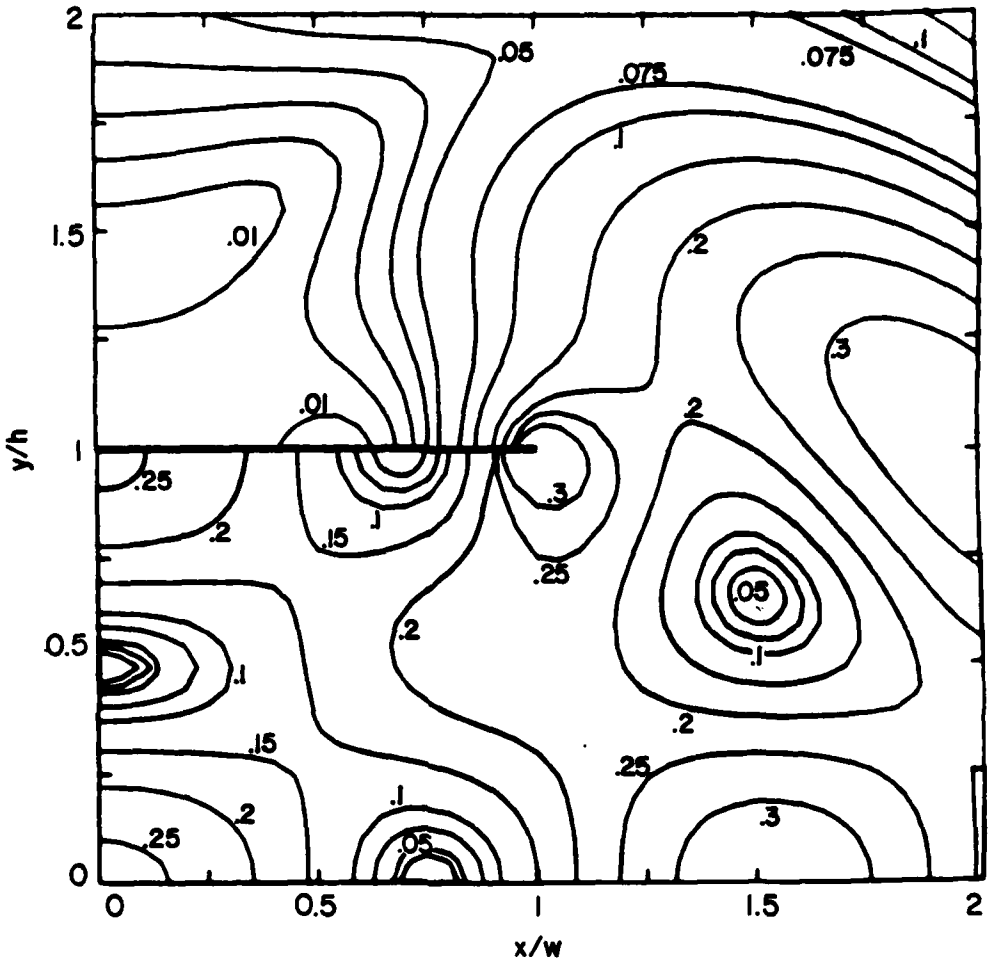

Figure 8e. Constant Value Contours for Normalized Field Component $\sqrt{(\mathrm{Im}(p^2E_x/\zeta))^2 + (\mathrm{Im}(p^2E_y/\zeta))^2} = \sqrt{(\mathrm{Im}(p^2H_y/s\varepsilon_o))^2 + (\mathrm{Im}(p^2H_x/s\varepsilon_o))^2}$ of the $TM_{0,1}$ Mode when $h/w = 1$. The Fields are Normalized so that $|p^2/\zeta|\sqrt{|E_x|^2 + |E_y|^2} = 1$ at $x = y = 0$.

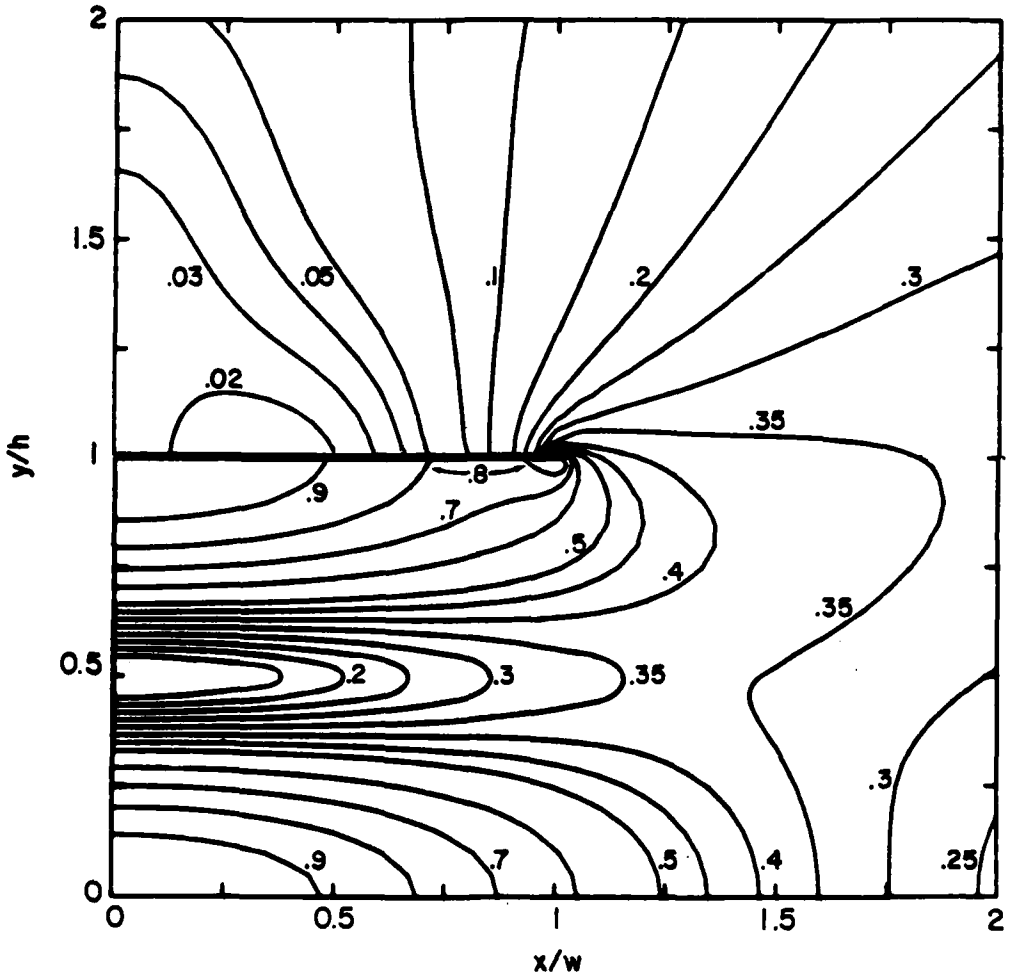

Figure 8f. Constant Value Contours for Normalized Field Component $|p^2/\zeta|\sqrt{|E_x|^2+|E_y|^2} = |p^2(s\varepsilon_o)^{-1}|\sqrt{|H_x|^2+|H_y|^2}$ of the $TM_{0,1}$ Mode when h/w = 1. The Fields are Normalized so that $|p^2/\zeta|\sqrt{|E_x|^2+|E_y|^2} = 1$ at $x = y = 0$.

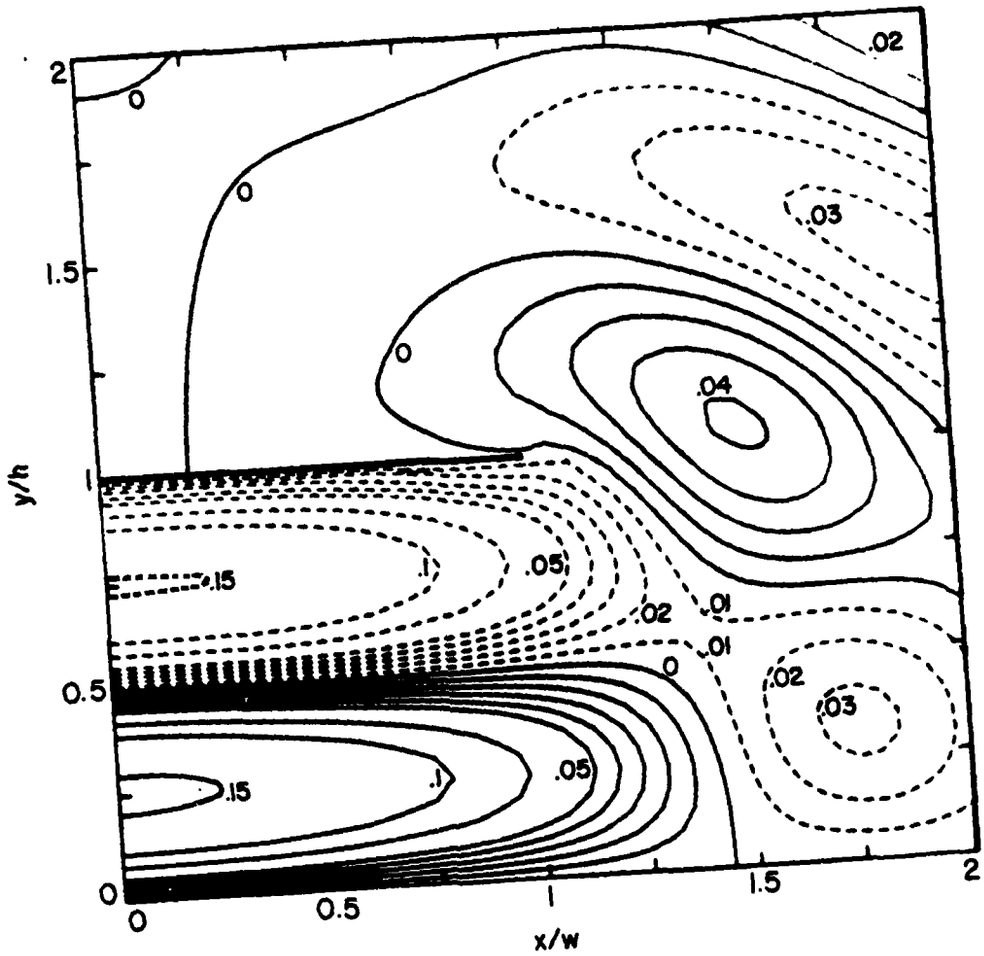

Figure 9a. Constant Value Contours for Normalized Field Component $Re(E_z/w)$ of the $TM_{0,2}$ Mode when $h/w = 1$. The Fields are Normalized so that $|p^2/\zeta|\sqrt{|E_x|^2 + |E_y|^2} = 1$ at $x = y = 0$. Broken Lines are for Negative Values.

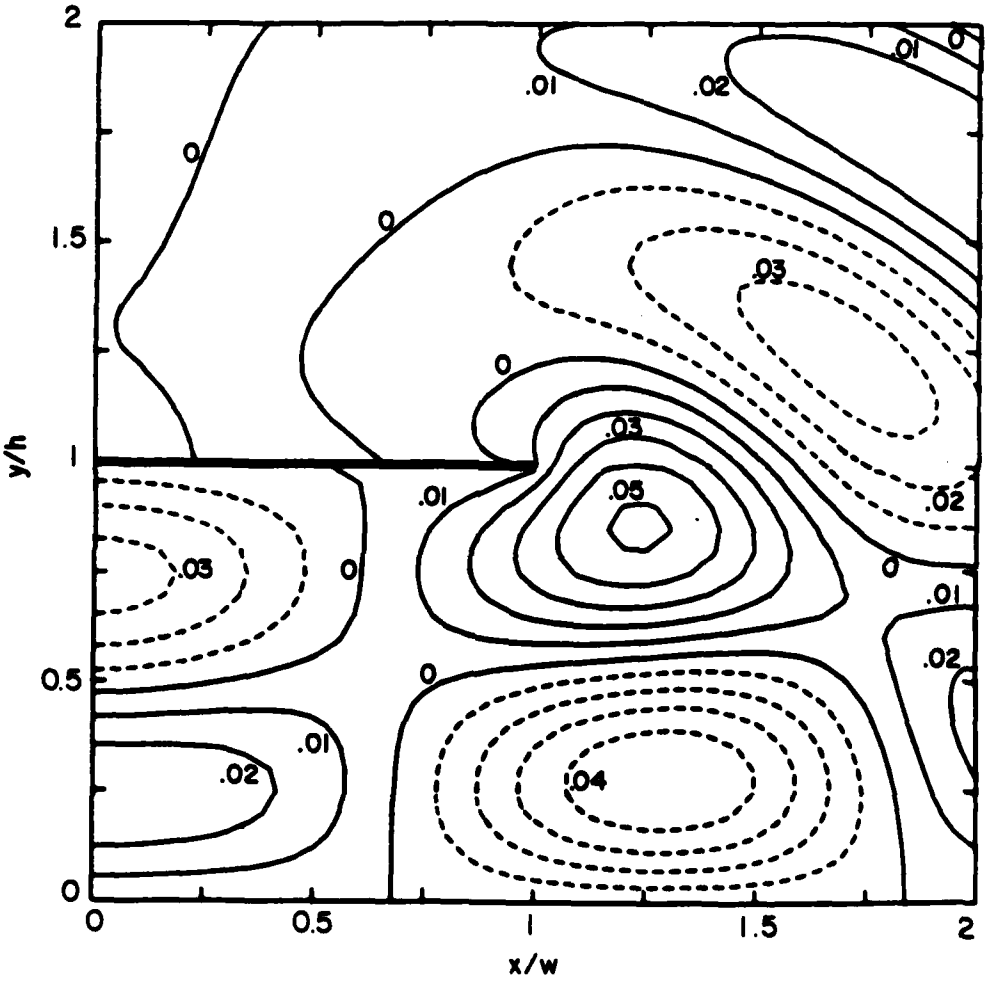

Figure 9b. Constant Value Contours for Normalized Field Component $\mathrm{Im}(E_z/w)$ of the $TM_{0,2_2}$ Mode when $h/w = 1$. The Fields are Normalized so that $|p^2/\zeta|\sqrt{|E_x|^2 + |E_y|^2} = 1$ at $x = y = 0$. Broken Lines are for Negative Values.

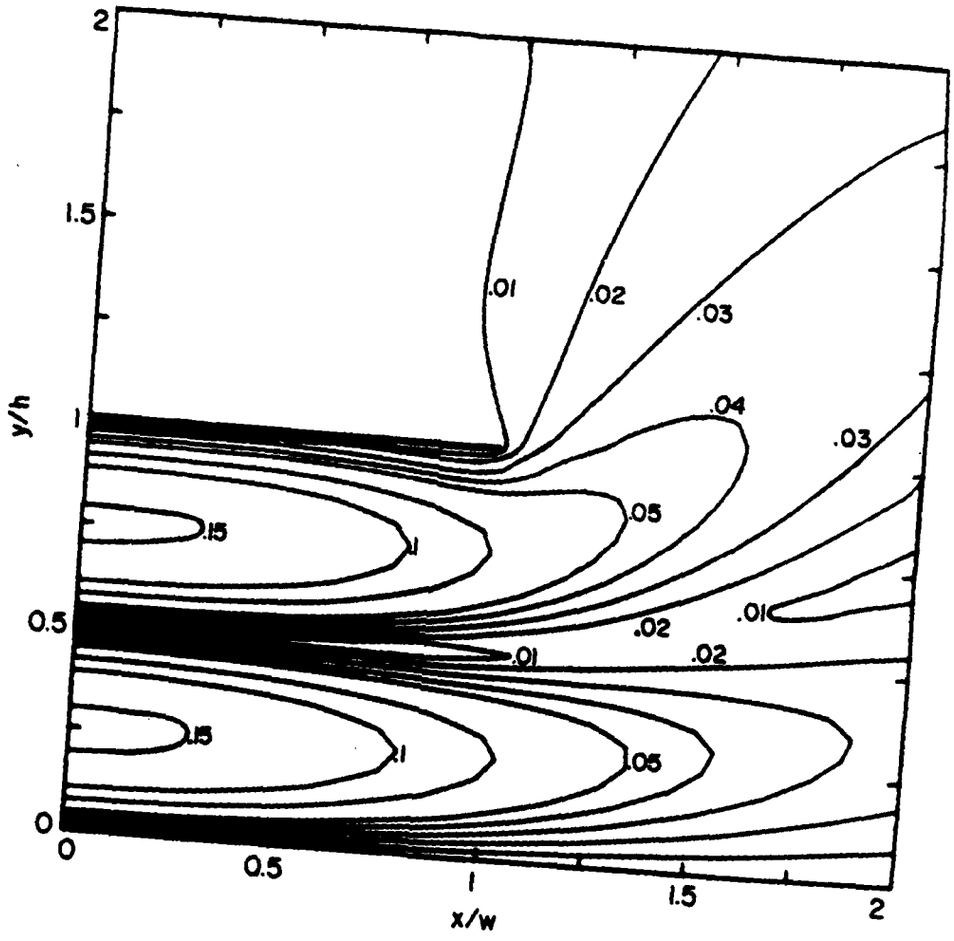

Figure 9c. Constant Value Contours for Normalized Field Component $|E_z/w|$ of the $TM_{0,2}$ Mode when $h/w = 1$. The Fields are Normalized so that $|p^2/\zeta|\sqrt{|E_x|^2 + |E_y|^2} = 1$ at $x = y = 0$.

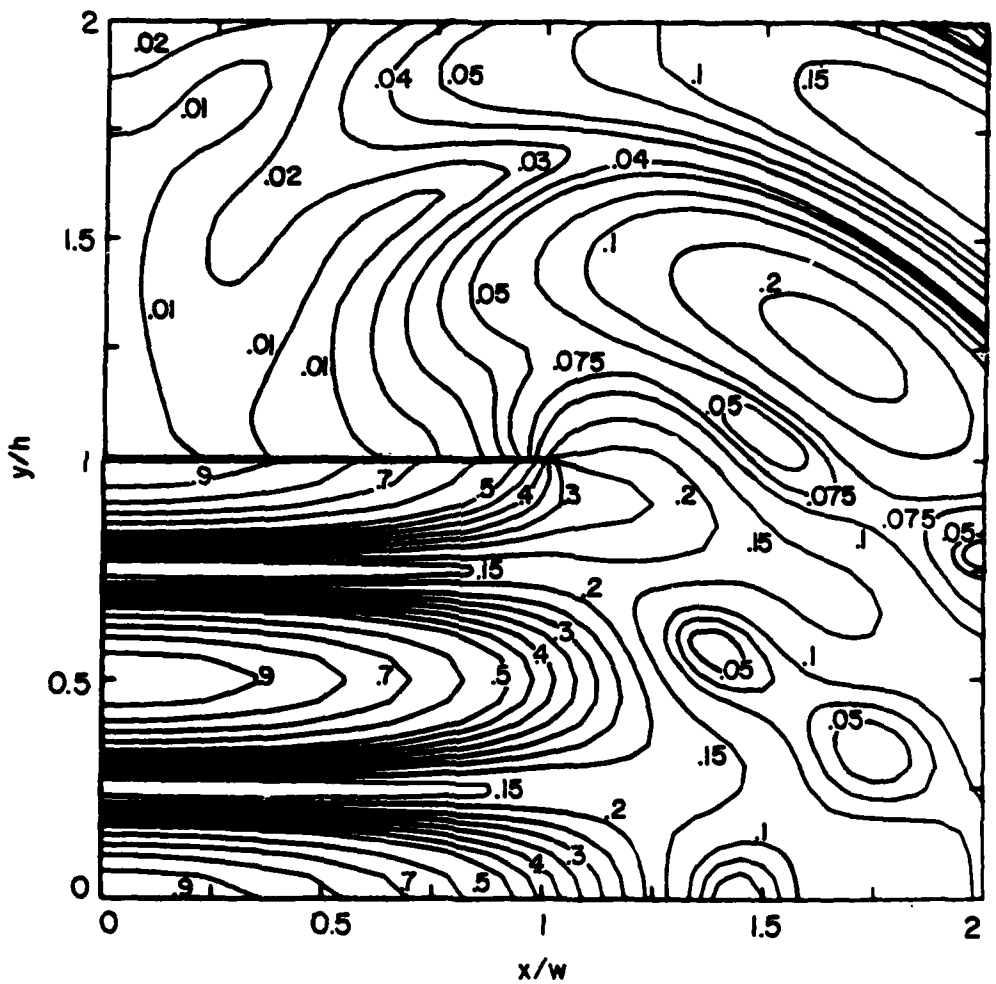

Figure 9d. Constant Value Contours for Normalized Field Component $\sqrt{(\mathrm{Re}(p^2E_x/\zeta))^2 + (\mathrm{Re}(p^2E_y/\zeta))^2} = \sqrt{(\mathrm{Re}(p^2H_y/s\varepsilon_o))^2 + (\mathrm{Re}(p^2H_x/s\varepsilon_o))^2}$ of the $TM_{0,2}$ Mode when $h/w = 1$. The Fields are Normalized so that $|p^2/\zeta|\sqrt{|E_x|^2 + |E_y|^2} = 1$ at $x = y = 0$.

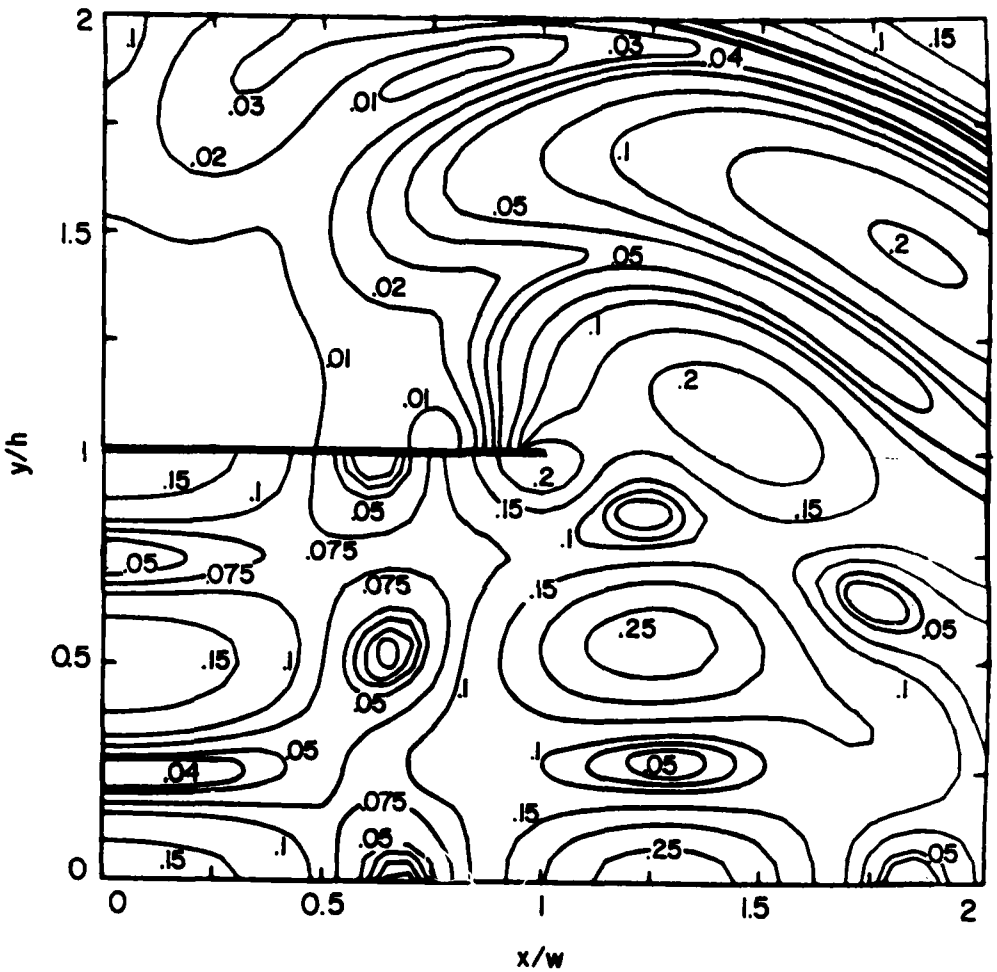

Figure 9e. Constant Value Contours for Normalized Field Component $\sqrt{(\mathrm{Im}(p^2E_x/\zeta))^2 + (\mathrm{Im}(p^2E_y/\zeta))^2} = \sqrt{(\mathrm{Im}(p^2H_y/s\varepsilon_o))^2 + (\mathrm{Im}(p^2H_x/s\varepsilon_o))^2}$ of the $TM_{0,2}$ Mode when $h/w = 1$. The Fields are Normalized so that $|p^2/\zeta|\sqrt{|E_x|^2 + |E_y|^2} = 1$ at $x = y = 0$.

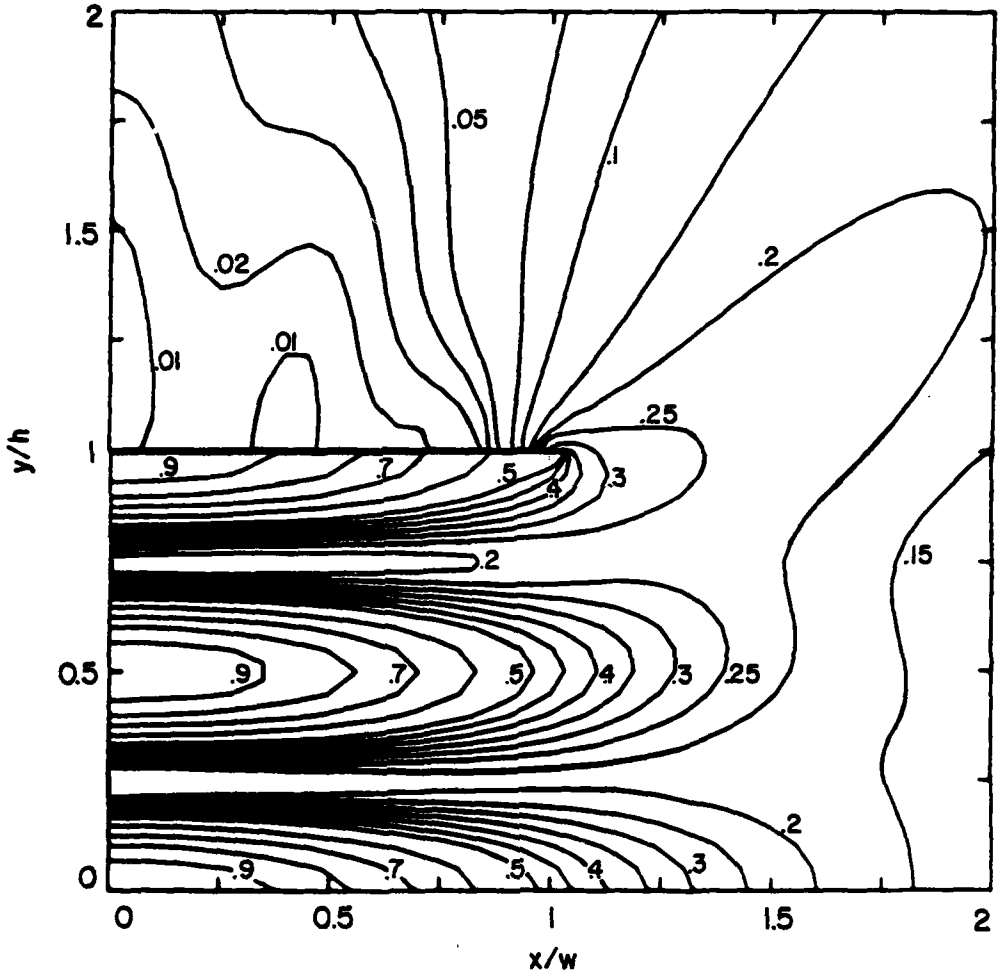

Figure 9f. Constant Value Contours for Normalized Field Component $|p^2/\zeta|\sqrt{|E_x|^2 + |E_y|^2} = |p^2(s\varepsilon_o)^{-1}|\sqrt{|H_x|^2 + |H_y|^2}$ of the $TM_{0,2}$ Mode when h/w = 1. The Fields are Normalized so that $|p^2/\zeta|\sqrt{|E_x|^2 + |E_y|^2} = 1$ at $x = y = 0$.

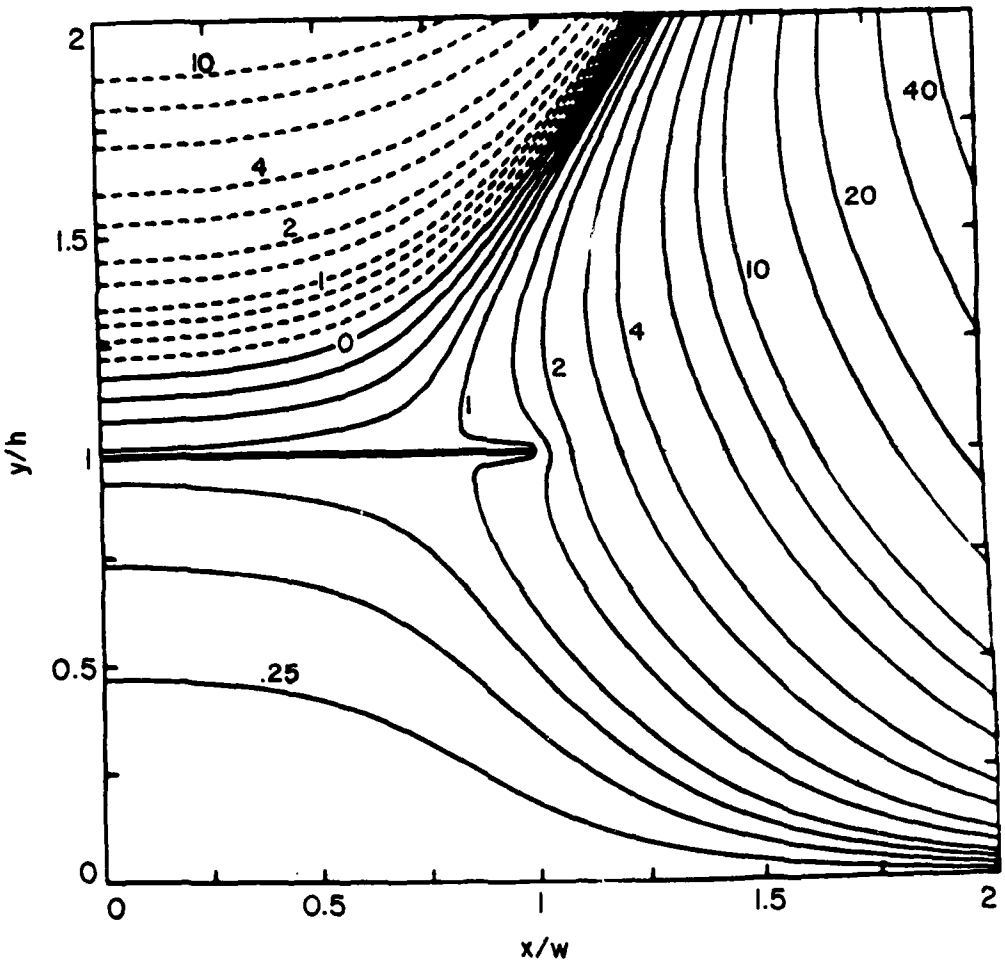

Figure 10a. Constant Value Contours for Normalized Field Component $Re(E_z/w)$ of the $TM_{1,1}$ Mode when $h/w = 1$. The Fields are Normalized so that $|p^2/\zeta|\sqrt{|E_x|^2 + |E_y|^2} = 1$ at $x = y = 0$. Broken Lines are for Negative Values.

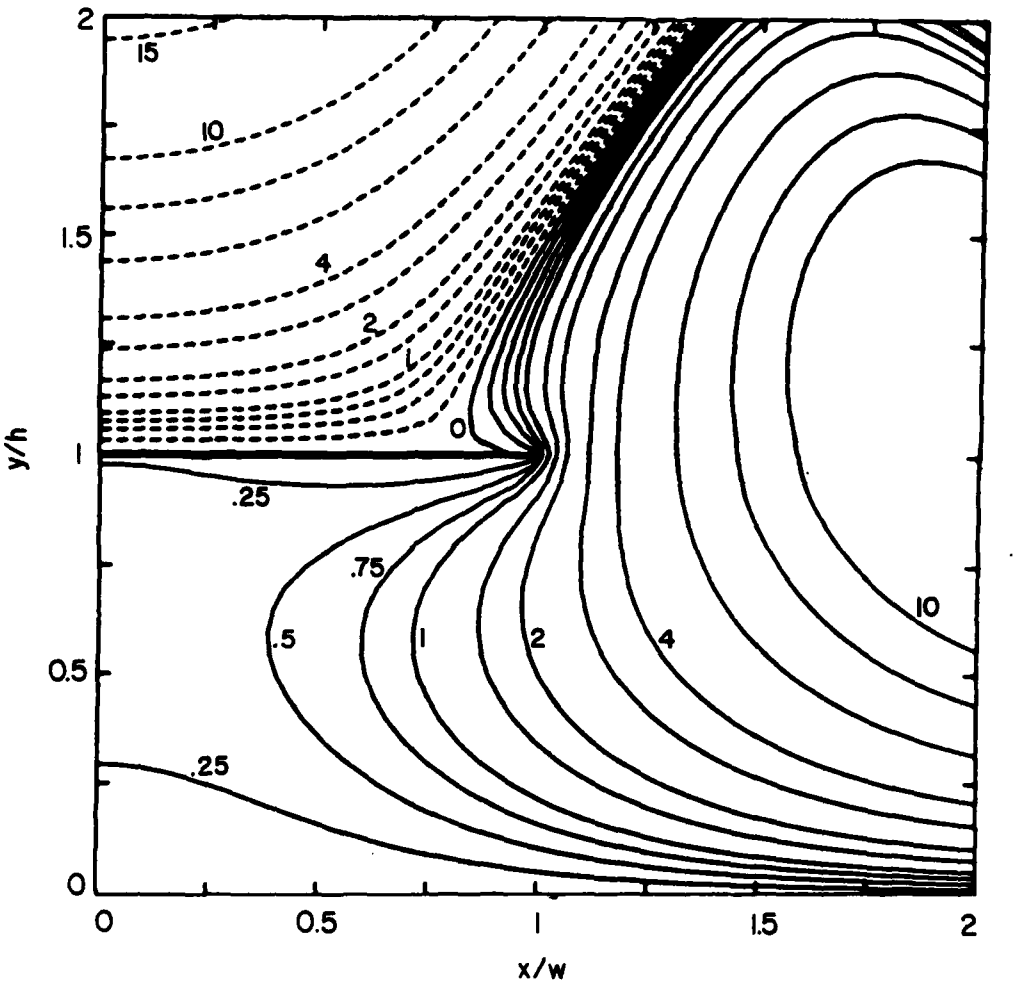

Figure 10b. Constant Value Contours for Normalized Field Component $\mathrm{Im}(E_z/w)$ of the $TM_{1,1}$ Mode when $h/w = 1$. The Fields are Normalized so that $|p^2/\zeta|\sqrt{|E_x|^2 + |E_y|^2} = 1$ at $x = y = 0$. Broken Lines are for Negative Values.

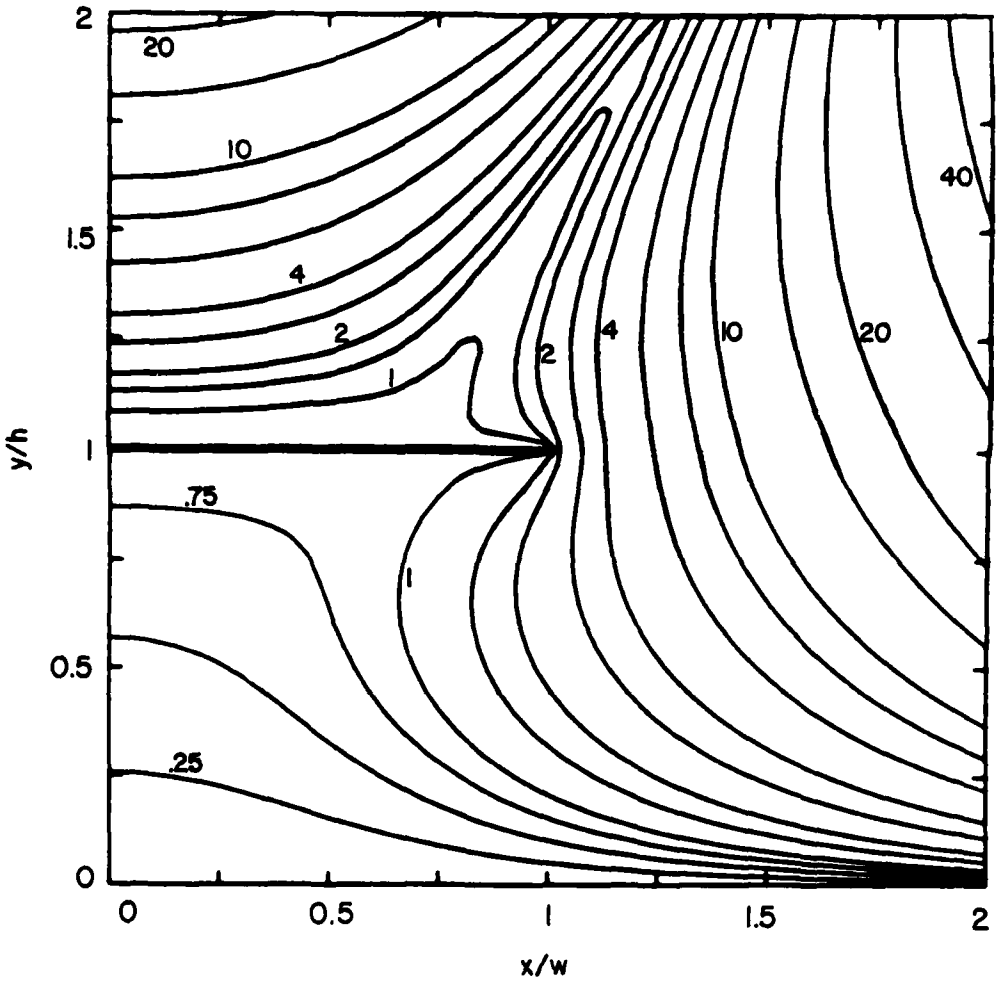

Figure 10c. Constant Value Contours for Normalized Field Component $|E_z/w|$ of the $TM_{1,1}$ Mode when $h/w = 1$. The Fields are Normalized so that $|p^2/\zeta|\sqrt{|E_x|^2 + |E_y|^2} = 1$ at $x = y = 0$.

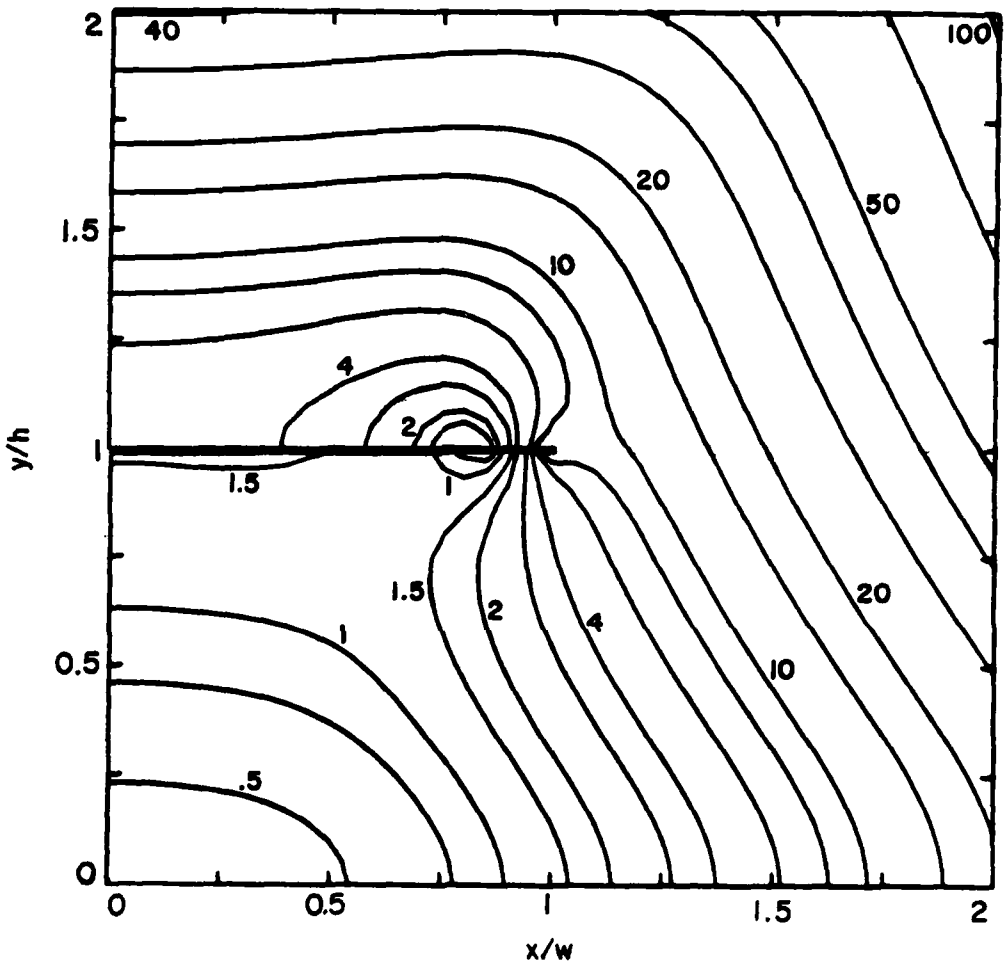

Figure 10d. Constant Value Contours for Normalized Field Component $\sqrt{(\mathrm{Re}(p^2E_x/\zeta))^2 + (\mathrm{Re}(p^2E_y/\zeta))^2} = \sqrt{(\mathrm{Re}(p^2H_y/s\varepsilon_o))^2 + (\mathrm{Re}(p^2H_x/s\varepsilon_o))^2}$ of the $TM_{1,1}$ Mode when $h/w = 1$. The Fields are Normalized so that $|p^2/\zeta|\sqrt{|E_x|^2 + |E_y|^2} = 1$ at $x = y = 0$.

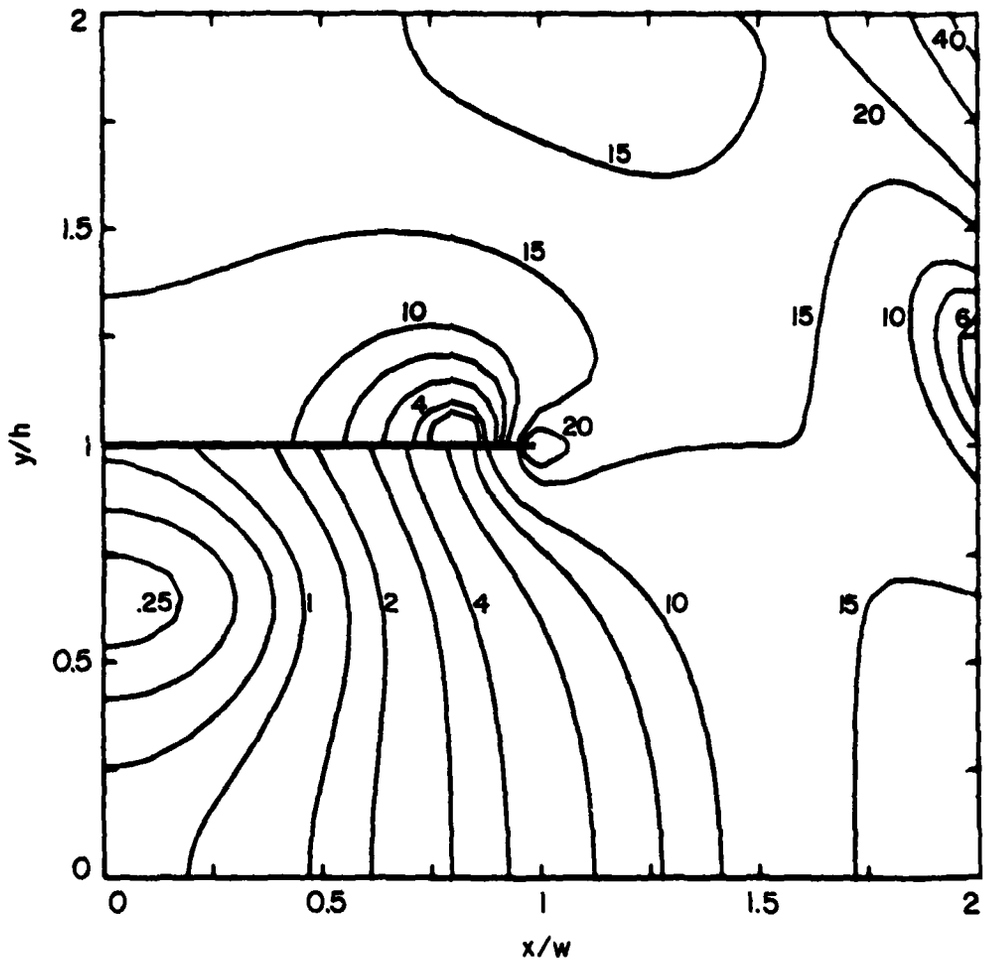

Figure 10e. Constant Value Contours for Normalized Field Component $\sqrt{(\mathrm{Im}(p^2E_x/\zeta))^2 + (\mathrm{Im}(p^2E_y/\zeta))^2} = \sqrt{(\mathrm{Im}(p^2H_y/s\varepsilon_o))^2 + (\mathrm{Im}(p^2H_x/s\varepsilon_o))^2}$ of the $TM_{1,1}$ Mode when $h/w = 1$. The Fields are Normalized so that $|p^2/\zeta|\sqrt{|E_x|^2 + |E_y|^2} = 1$ at $x = y = 0$.

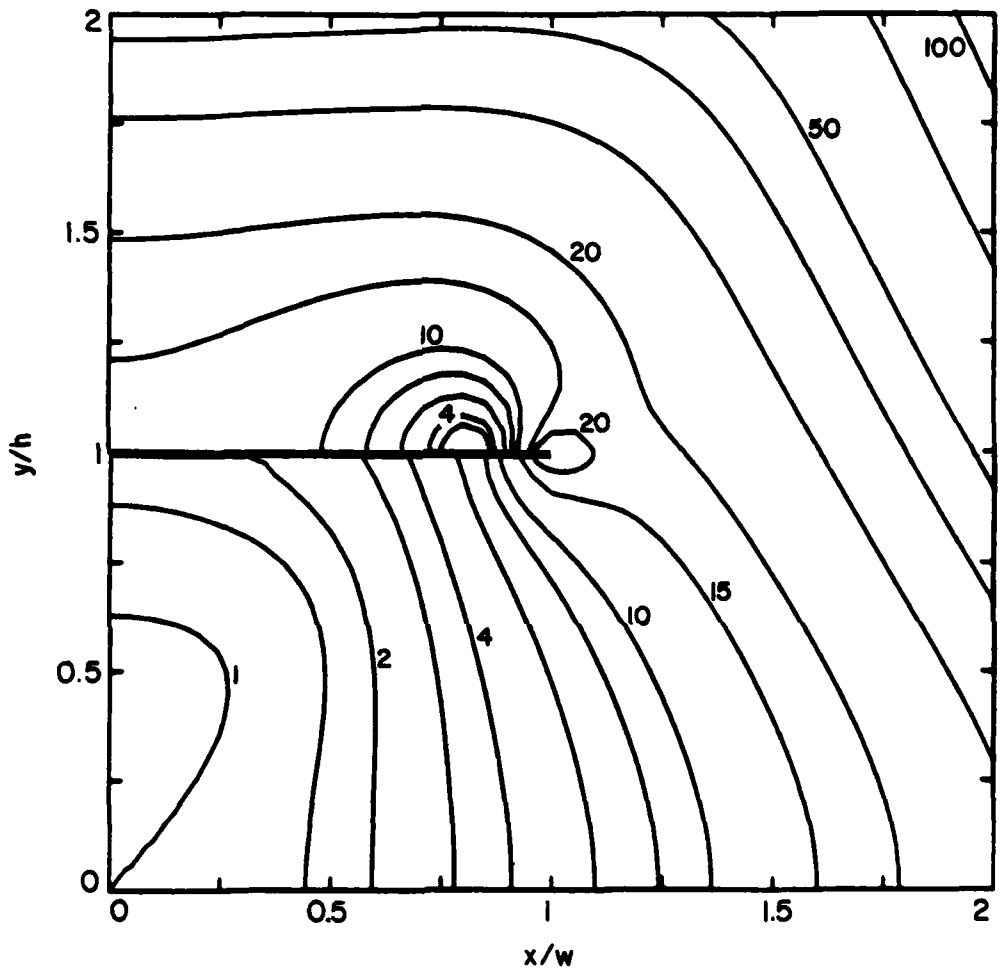

Figure 10f. Constant Value Contours for Normalized Field Component $|p^2/\zeta|\sqrt{|E_x|^2 + |E_y|^2} = |p^2(s\varepsilon_o)^{-1}|\sqrt{|H_x|^2 + |H_y|^2}$ of the $TM_{1,1}$ Mode when $h/w = 1$. The Fields are Normalized so that $|p^2/\zeta|\sqrt{|E_x|^2 + |E_y|^2} = 1$ at $x = y = 0$.

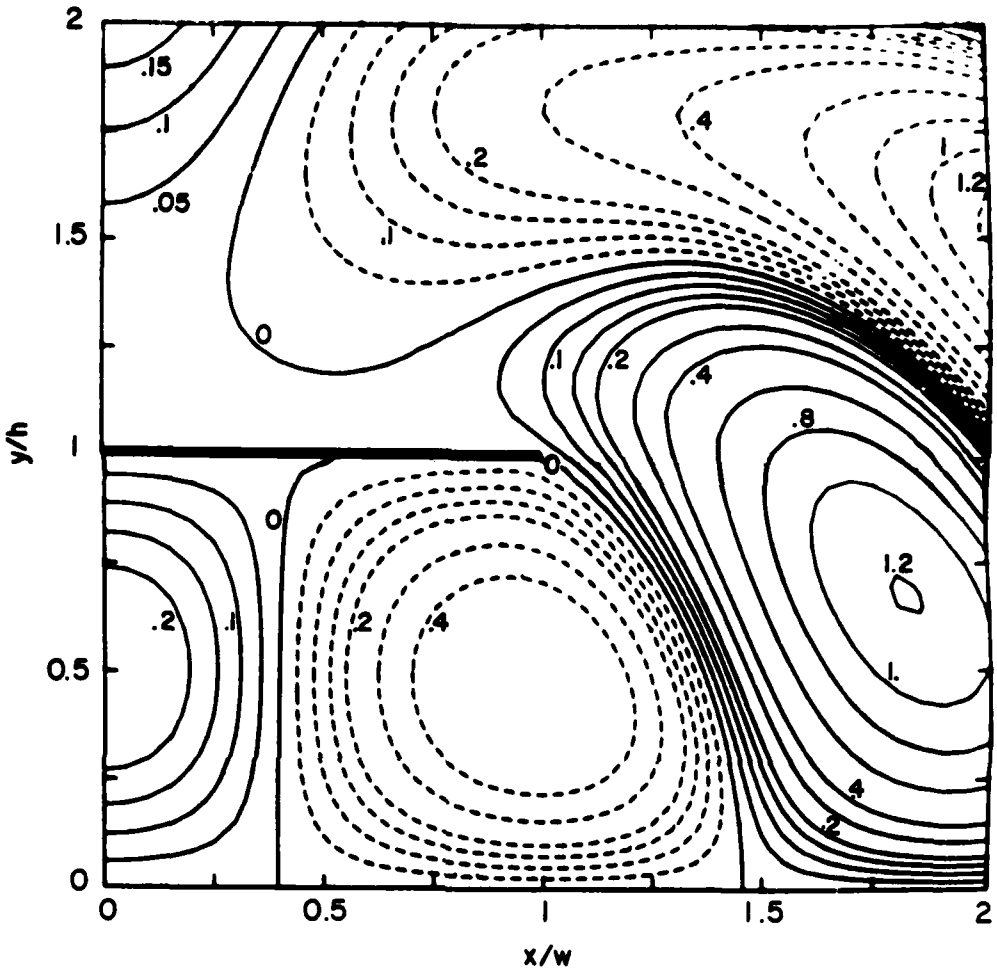

Figure 11a. Constant Value Contours for Normalized Field Component $Re(E_z/w)$ of the $TM_{1,2}$ Mode when $h/w = 1$. The Fields are Normalized so that $|p^2/\zeta|\sqrt{|E_x|^2 + |E_y|^2} = 1$ at $x = y = 0$. Broken Lines are for Negative Values.

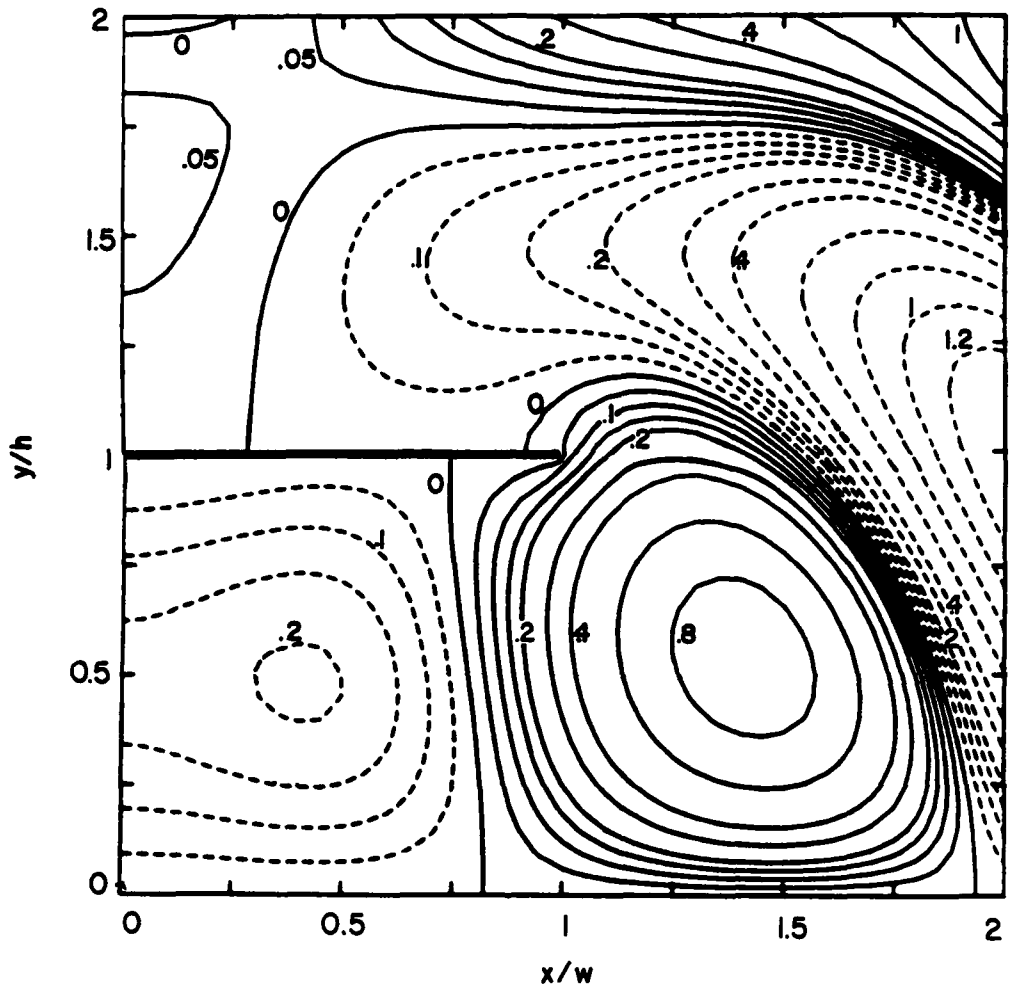

Figure 11b. Constant Value Contours for Normalized Field Component $\mathrm{Im}(E_z/w)$ of the $TM_{1,2}$ Mode when $h/w = 1$. The Fields are Normalized so that $|p^2/\zeta|\sqrt{|E_x|^2 + |E_y|^2} = 1$ at $x = y = 0$. Broken Lines are for Negative Values.

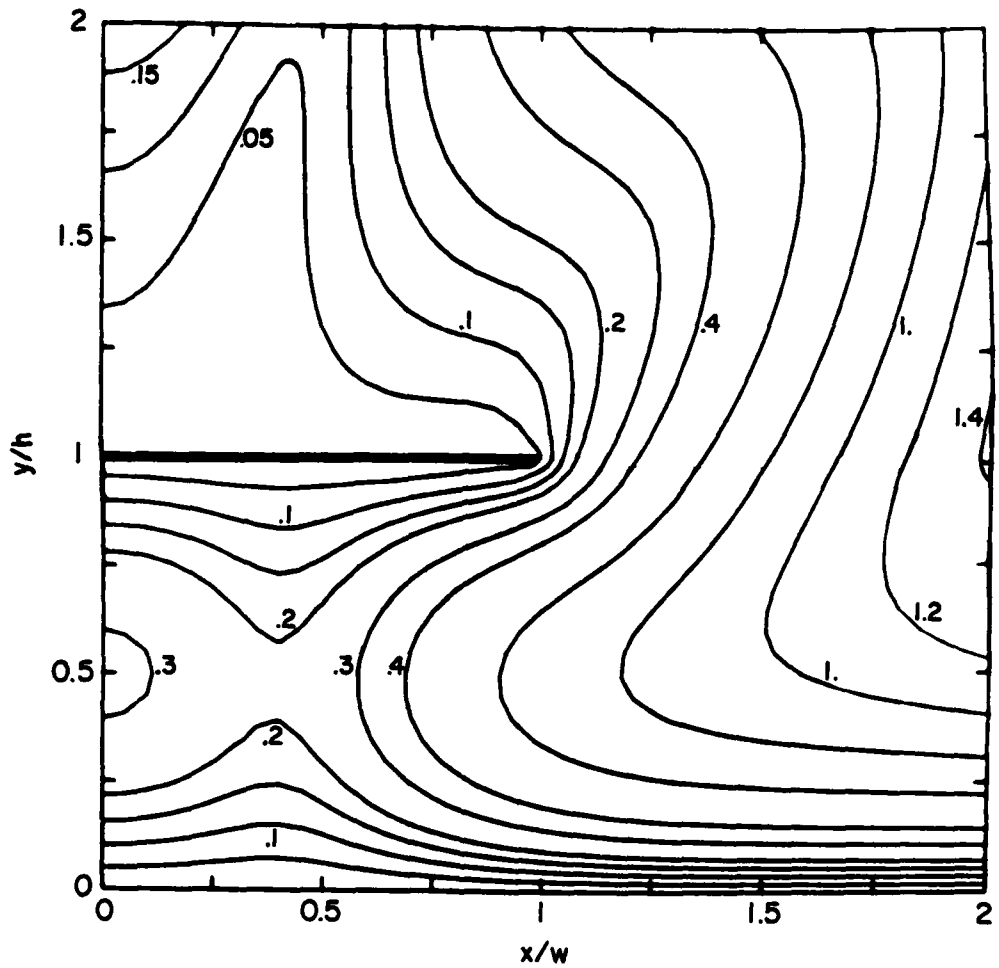

Figure 11c. Constant Value Contours for Normalized Field Component $|E_z/w|$ of the $TM_{1,2}$ Mode when $h/w = 1$. The Fields are Normalized so that $|p^2/\zeta|\sqrt{|E_x|^2 + |E_y|^2} = 1$ at $x = y = 0$.

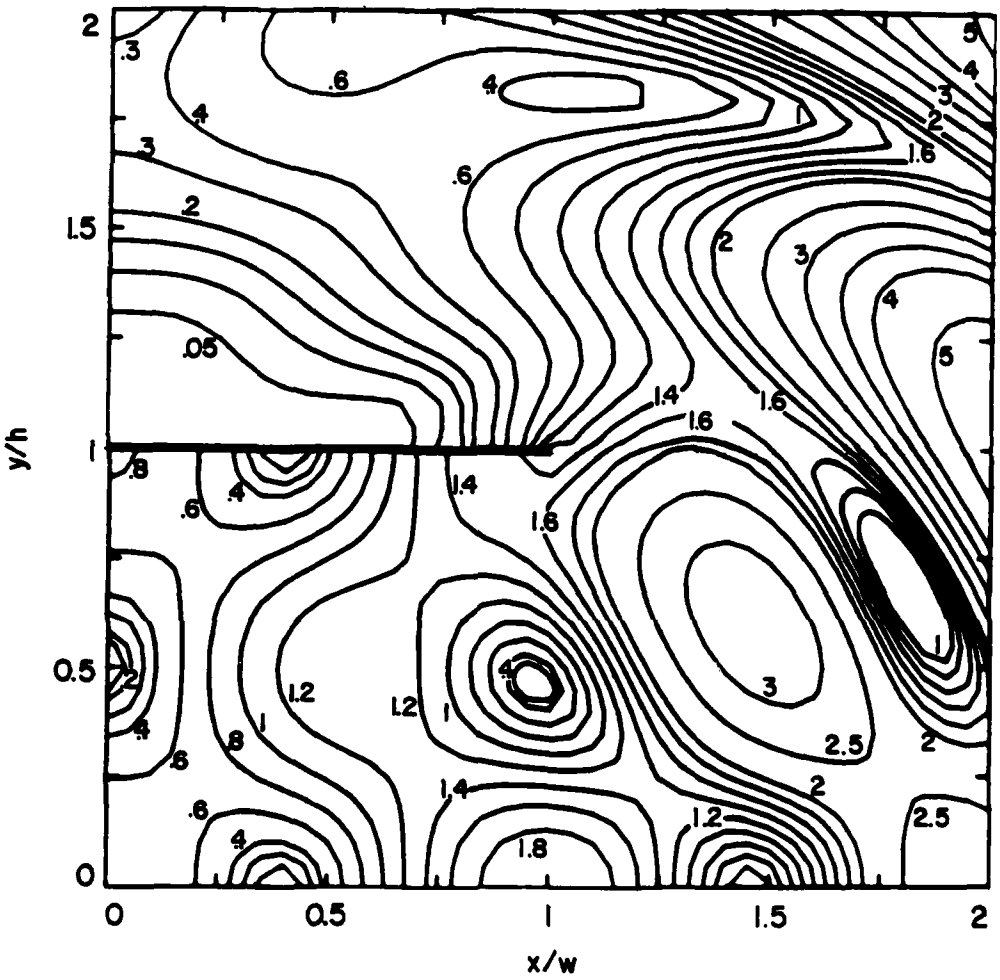

Figure 11d. Constant Value Contours for Normalized Field Component $\sqrt{(\mathrm{Re}(p^2E_x/\zeta))^2 + (\mathrm{Re}(p^2E_y/\zeta))^2} = \sqrt{(\mathrm{Re}(p^2H_y/s\varepsilon_o))^2 + (\mathrm{Re}(p^2H_x/s\varepsilon_o))^2}$ of the $TM_{1,2}$ Mode when $h/w = 1$. The Fields are Normalized so that $|p^2/\zeta|\sqrt{|E_x|^2 + |E_y|^2} = 1$ at $x = y = 0$.

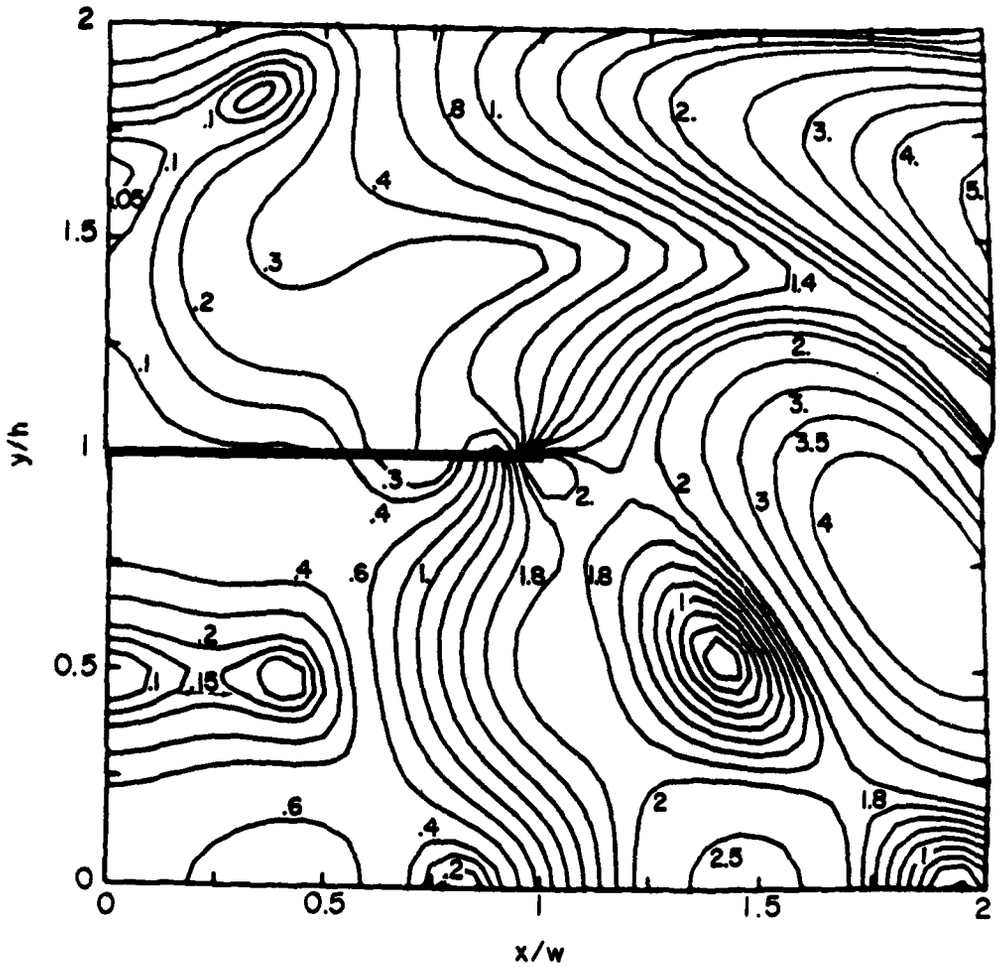

Figure 11e. Constant Value Contours for Normalized Field Component $\sqrt{(\mathrm{Im}(p^2E_x/\zeta))^2 + (\mathrm{Im}(p^2E_y/\zeta))^2} = \sqrt{(\mathrm{Im}(p^2H_y/s\varepsilon_o))^2 + \mathrm{Im}(p^2H_x/s\varepsilon_o))^2}$ of the $TM_{1,2}$ Mode when $h/w = 1$. The Fields are Normalized so that $|p^2/\zeta|\sqrt{|E_x|^2 + |E_y|^2} = 1$ at $x = y = 0$.

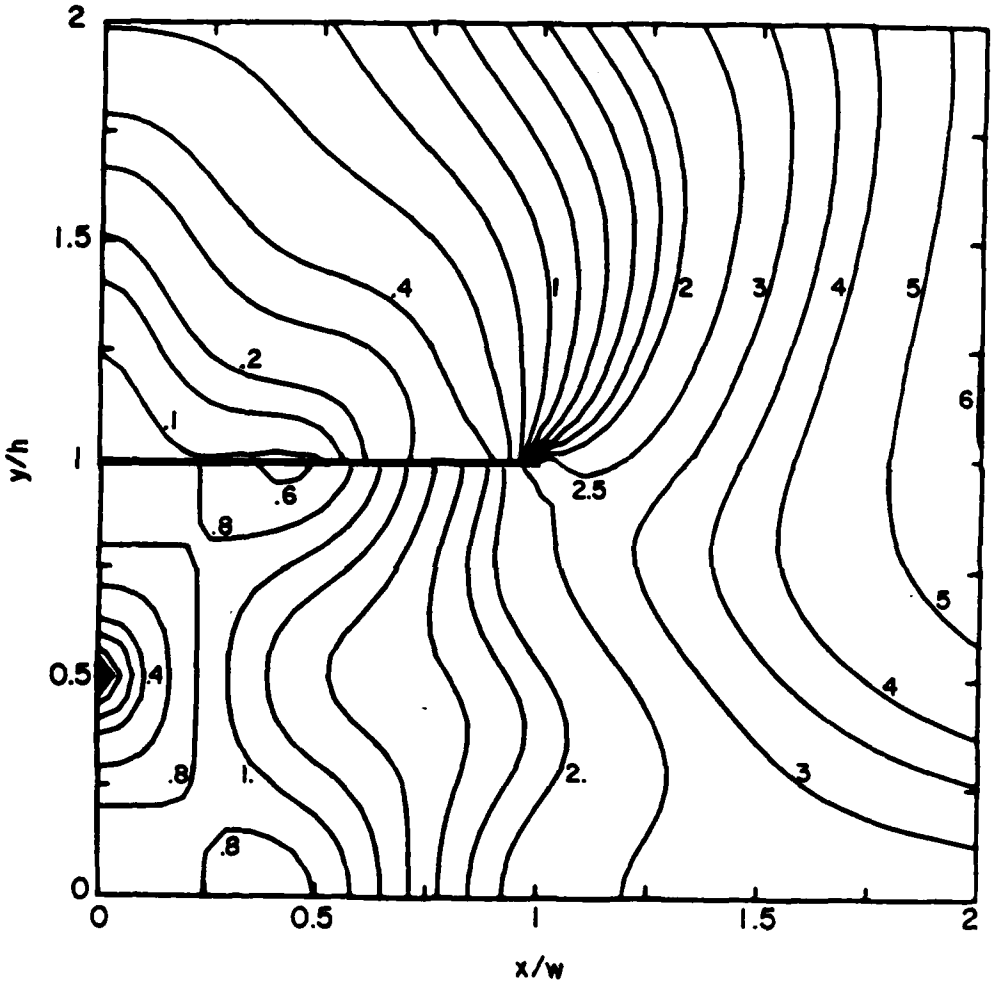

Figure 11f. Constant Value Contours for Normalized Field Component $|p^2/\zeta|\sqrt{|E_x|^2 + |E_y|^2} = |p^2(s\varepsilon_o)^{-1}|\sqrt{|H_x|^2 + |H_y|^2}$ of the $TM_{1,2}$ Mode when h/w = 1. The Fields are Normalized so that $|p^2/\zeta|\sqrt{|E_x|^2 + |E_y|^2} = 1$ at $x = y = 0$.

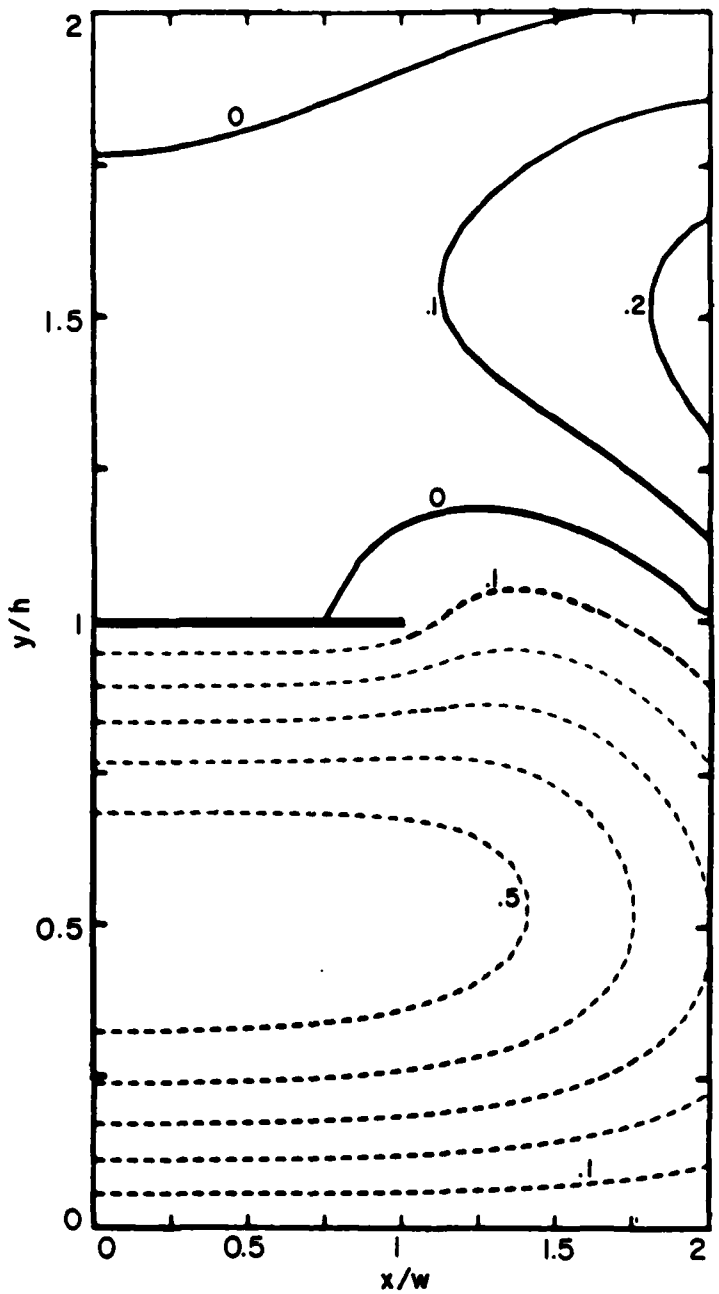

Figure 12a. Constant Value Contours for Normalized Field Component $Re(E_z/w)$ of the $TM_{0,1}$ Mode when $h/w = 2$. The Fields are Normalized so that $|p^2/\zeta|\sqrt{|E_x|^2 + |E_y|^2} = 1$ at $x = y = 0$. Broken Lines are for Negative Values.

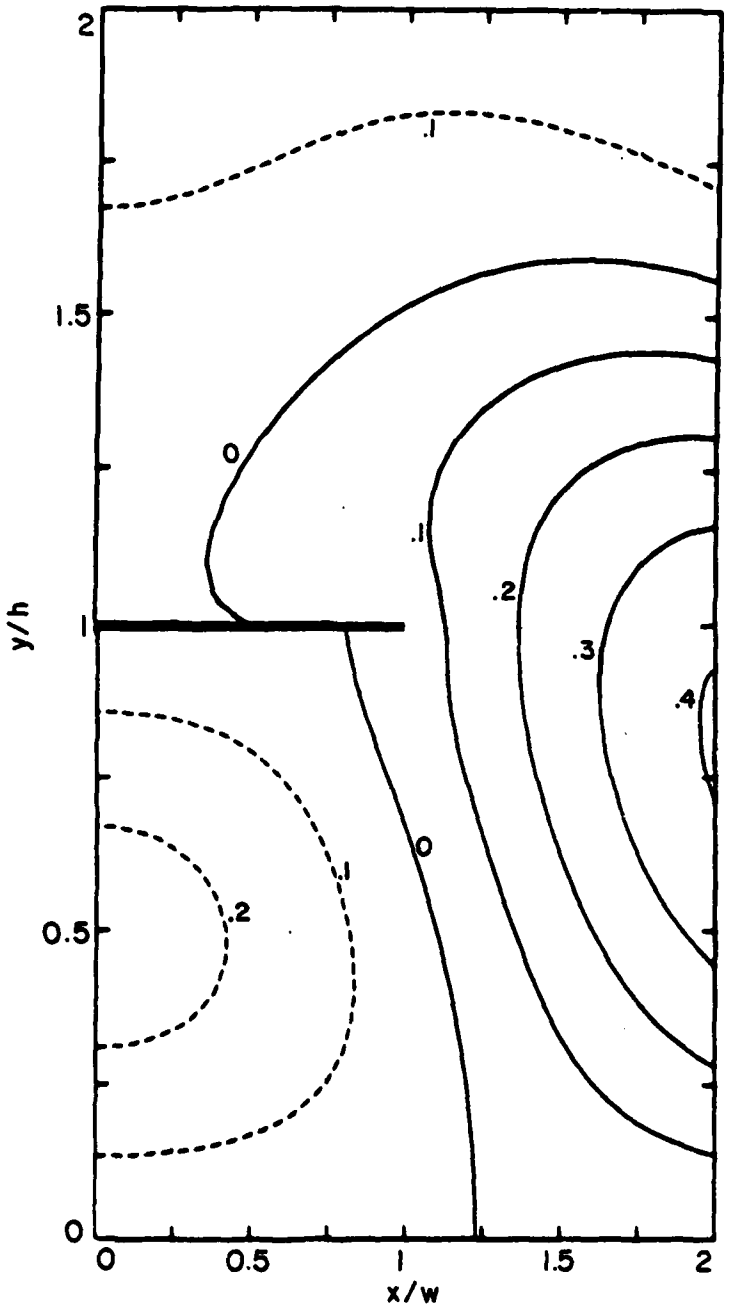

Figure 12b. Constant Value Contours for Normalized Field Component $\mathrm{Im}(E_z/w)$ of the $TM_{0,1}$ Mode when $h/w = 2$. The Fields are Normalized sothat $|p^2/\zeta|\sqrt{|E_x|^2 + |E_y|^2} = 1$ at $x = y = 0$. Broken Lines are for Negative Values.

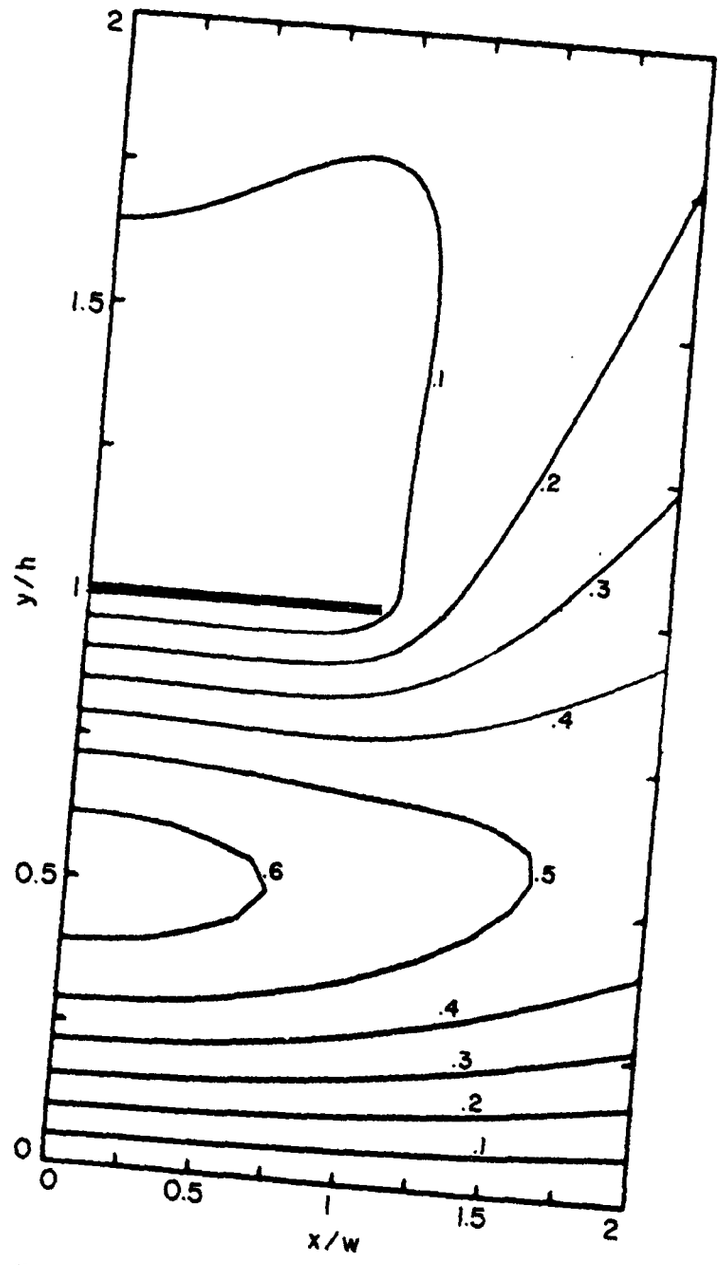

Figure 12c. Constant Value Contours for Normalized Field Component $|E_z/w|$ of the $TM_{0,1}$ Mode when $h/w = 2$. The Fields are Normalized so that $|p^2/\zeta|\sqrt{|E_x|^2 + |E_y|^2} = 1$ at $x = y = 0$.

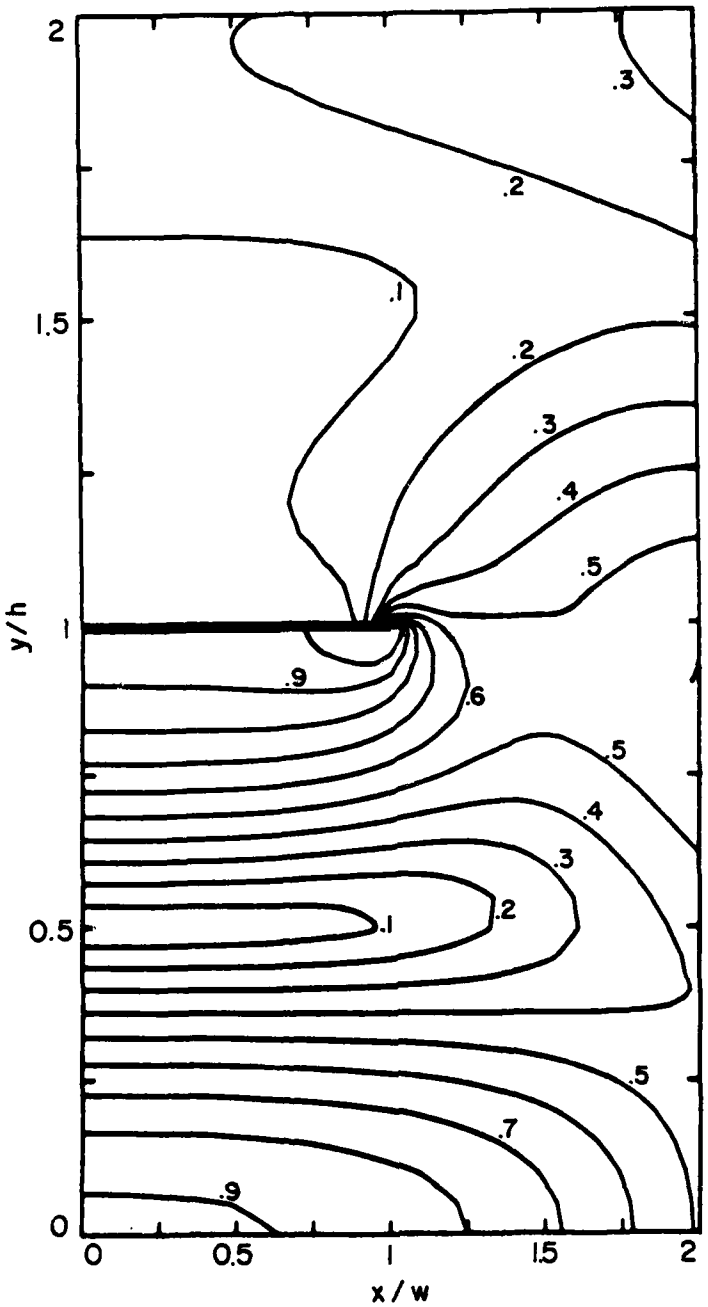

Figure 12d. Constant Value Contours for Normalized Field Component $\sqrt{(\mathrm{Re}(p^2E_x/\zeta))^2 + (\mathrm{Re}(p^2E_y/\zeta))^2} = \sqrt{(\mathrm{Re}(p^2H_y/s\varepsilon_o))^2 + (\mathrm{Re}(p^2H_x/s\varepsilon_o))^2}$ of the $TM_{0,1}$ Mode when $h/w = 2$. The Fields are Normalized so that $|p^2/\zeta|\sqrt{|E_x|^2 + |E_y|^2} = 1$ at $x = y = 0$.

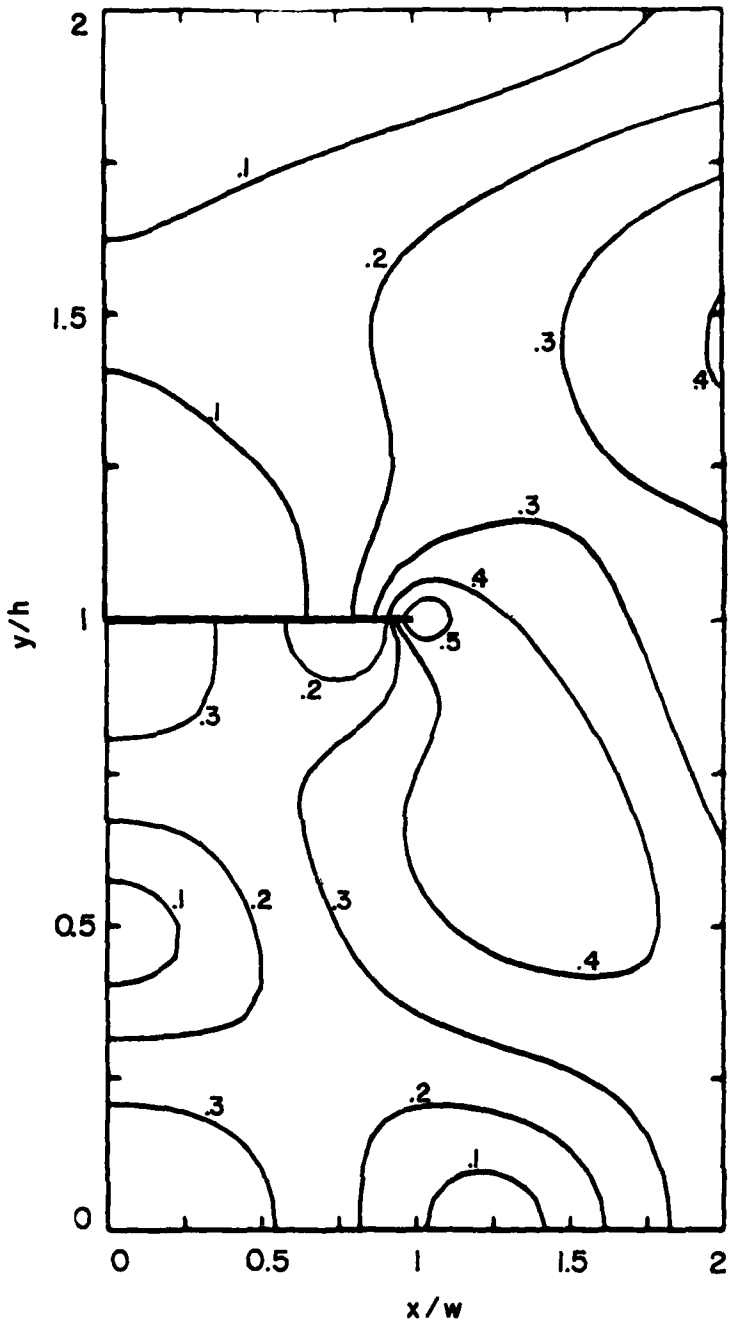

Figure 12e. Constant Value Contours for Normalized Field Component $\sqrt{(\mathrm{Im}(p^2E_x/\zeta))^2 + (\mathrm{Im}(p^2E_y/\zeta))^2} = \sqrt{(\mathrm{Im}(p^2H_y/s\varepsilon_o))^2 + (\mathrm{Im}(p^2H_x/s\varepsilon_o))^2}$ of the $TM_{0,1}$ Mode when $h/w = 2$. The Fields are Normalized so that $|p^2/\zeta|\sqrt{|E_x|^2 + |E_y|^2} = 1$ at $x = y = 0$.

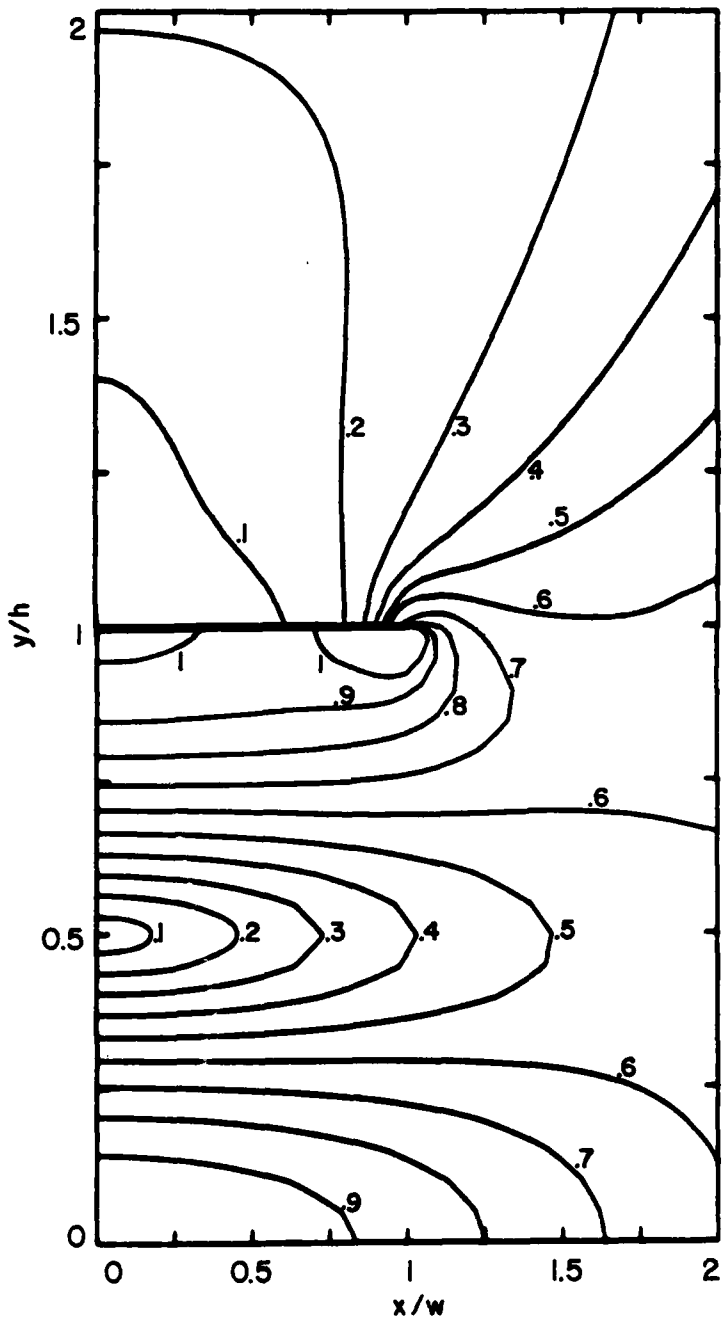

Figure 12f. Constant Value Contours for Normalized Field Component $|p^2/\zeta|\sqrt{|E_x|^2 + |E_y|^2} = |p^2(s\varepsilon_o)^{-1}|\sqrt{|H_x|^2 + |H_y|^2}$ of the $TM_{0,1}$ Mode when h/w = 2. The Fields are Normalized so that $|p^2/\zeta|\sqrt{|E_x|^2 + |E_y|^2} = 1$ at $x = y = 0$.

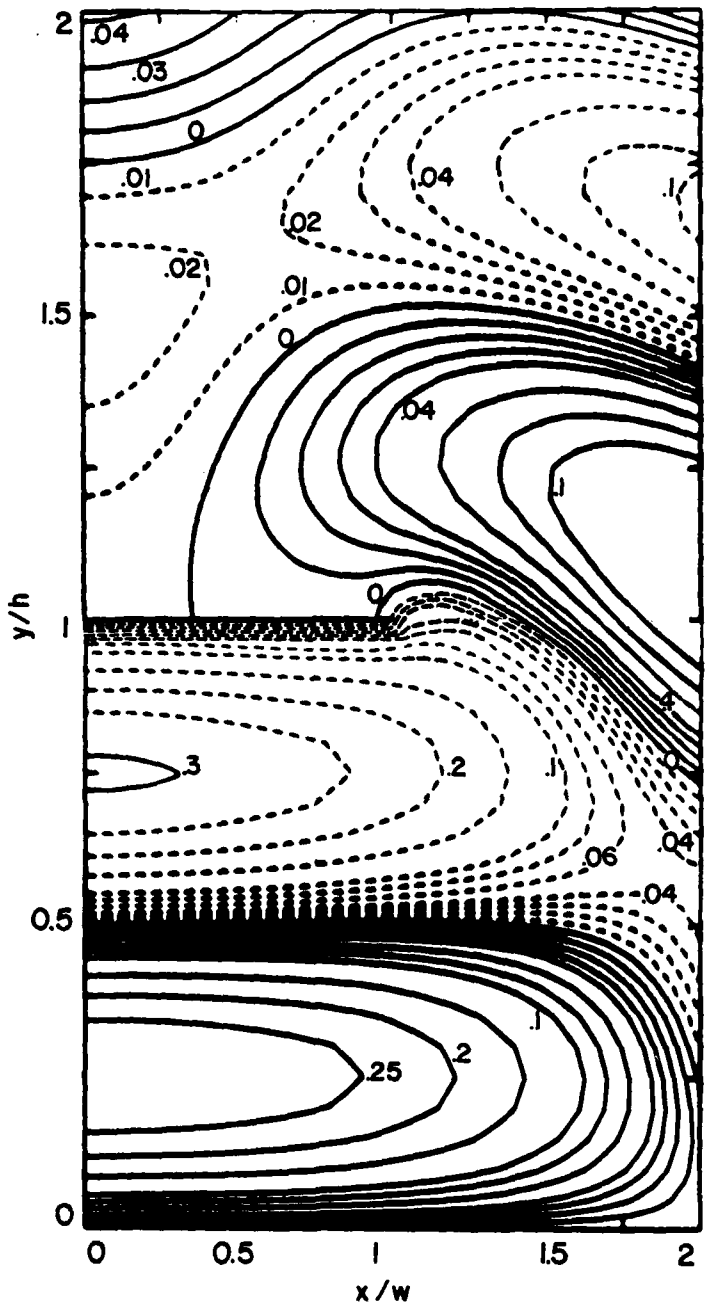

Figure 13a. Constant Value Contours for Normalized Field Component $Re(E_z/w)$ of the $TM_{0,2}$ Mode when $h/w = 2$. The Fields are Normalized so that $|p^2/\zeta|\sqrt{|E_x|^2 + |E_y|^2} = 1$ at $x = y = 0$. Broken Lines are for Negative Values.

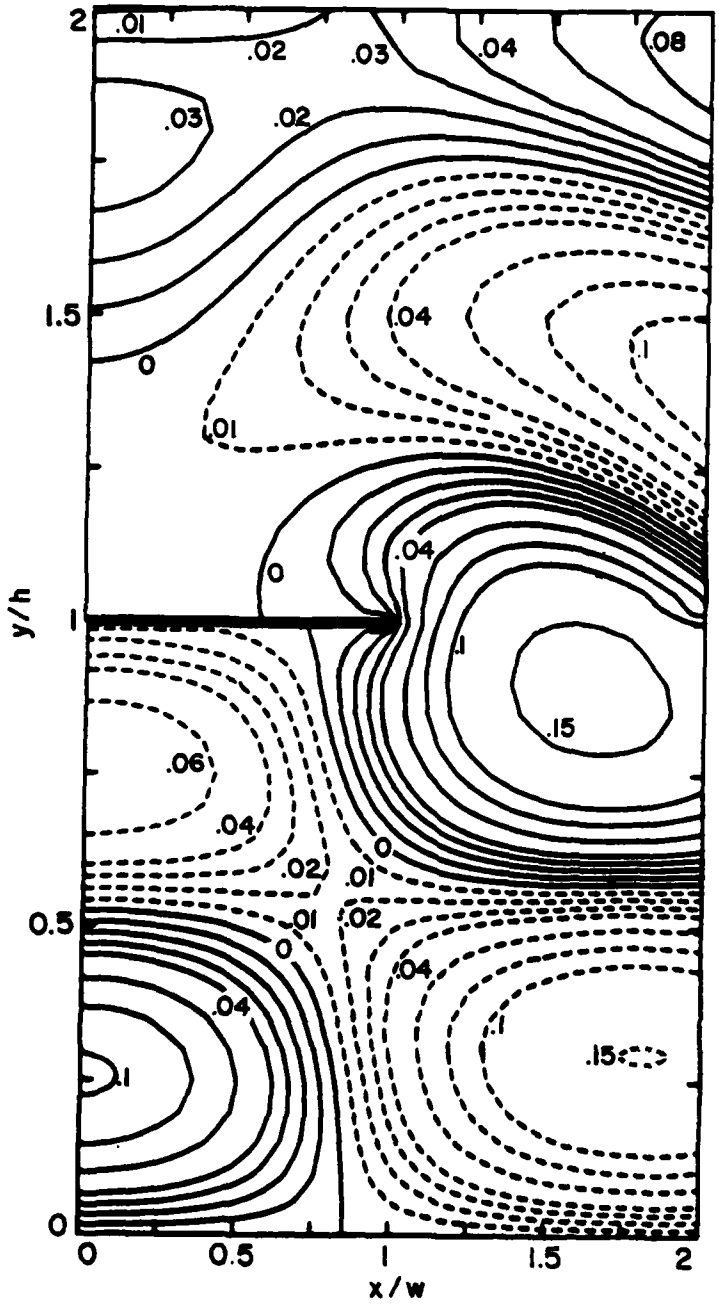

Figure 13b. Constant Value Contours for Normalized Field Component $\mathrm{Im}(E_z/w)$ of the $TM_{0,2}$ Mode when $h/w = 2$. The Fields are Normalized so that $|p^2/\zeta|\sqrt{|E_x|^2 + |E_y|^2} = 1$ at $x = y = 0$. Broken Lines are for Negative Values.

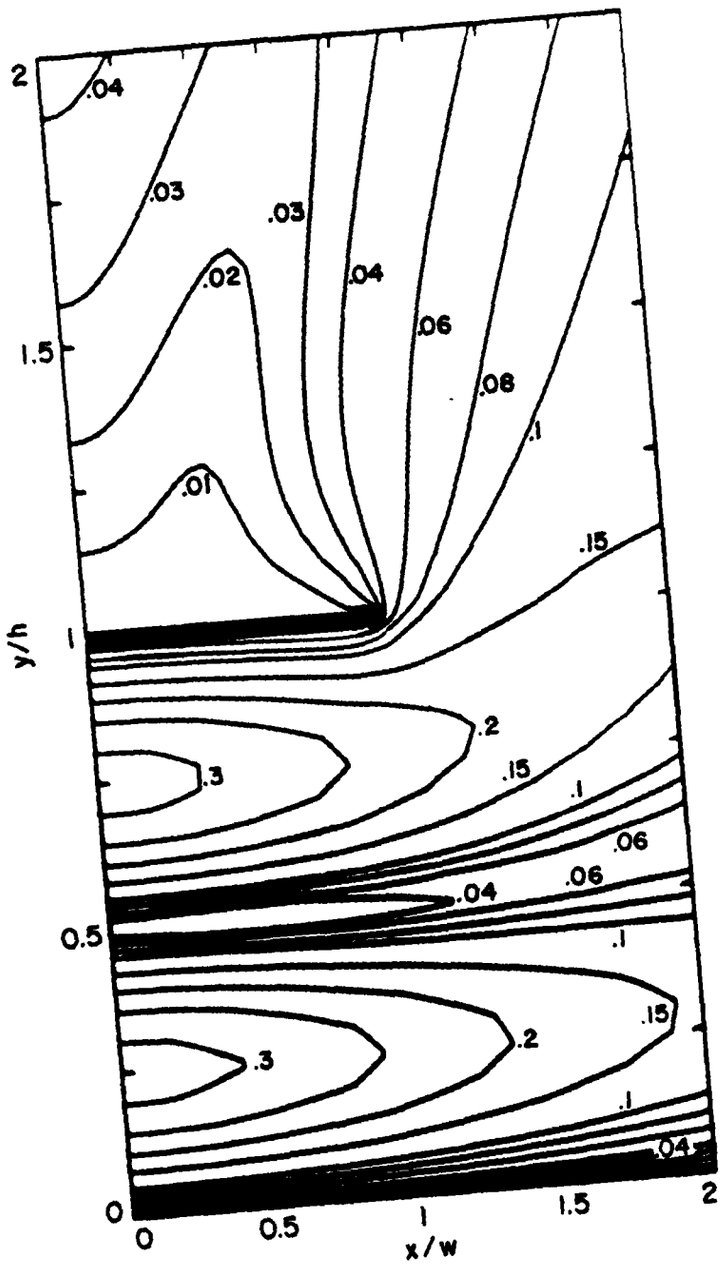

Figure 13c. Constant Value Contours for Normalized Field Component $|E_z/w|$ of the $TM_{0,2}$ Mode when $h/w = 2$. The Fields are Normalized so that $|p^2/\zeta|\sqrt{|E_x|^2 + |E_y|^2} = 1$ at $x = y = 0$.

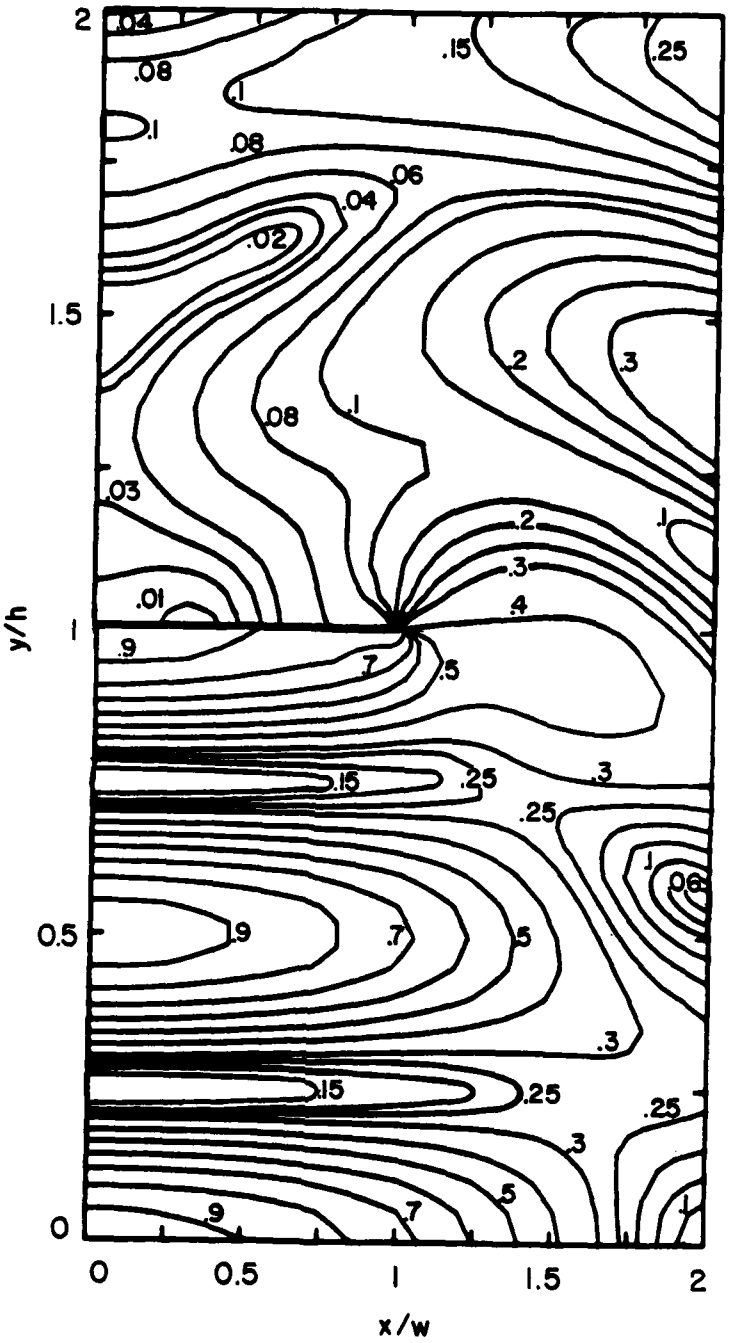

Figure 13d. Constant Value Contours for Normalized Field Component $\sqrt{(\mathrm{Re}(p^2E_x/\zeta))^2 + (\mathrm{Re}(p^2E_y/\zeta))^2} = \sqrt{(\mathrm{Re}(p^2H_y/s\varepsilon_o))^2 + (\mathrm{Re}(p^2H_x/s\varepsilon_o))^2}$ of the $TM_{0,2}$ Mode when $h/w = 2$. The Fields are Normalized so that $|p^2/\zeta|\sqrt{|E_x|^2 + |E_y|^2} = 1$ at $x = y = 0$.

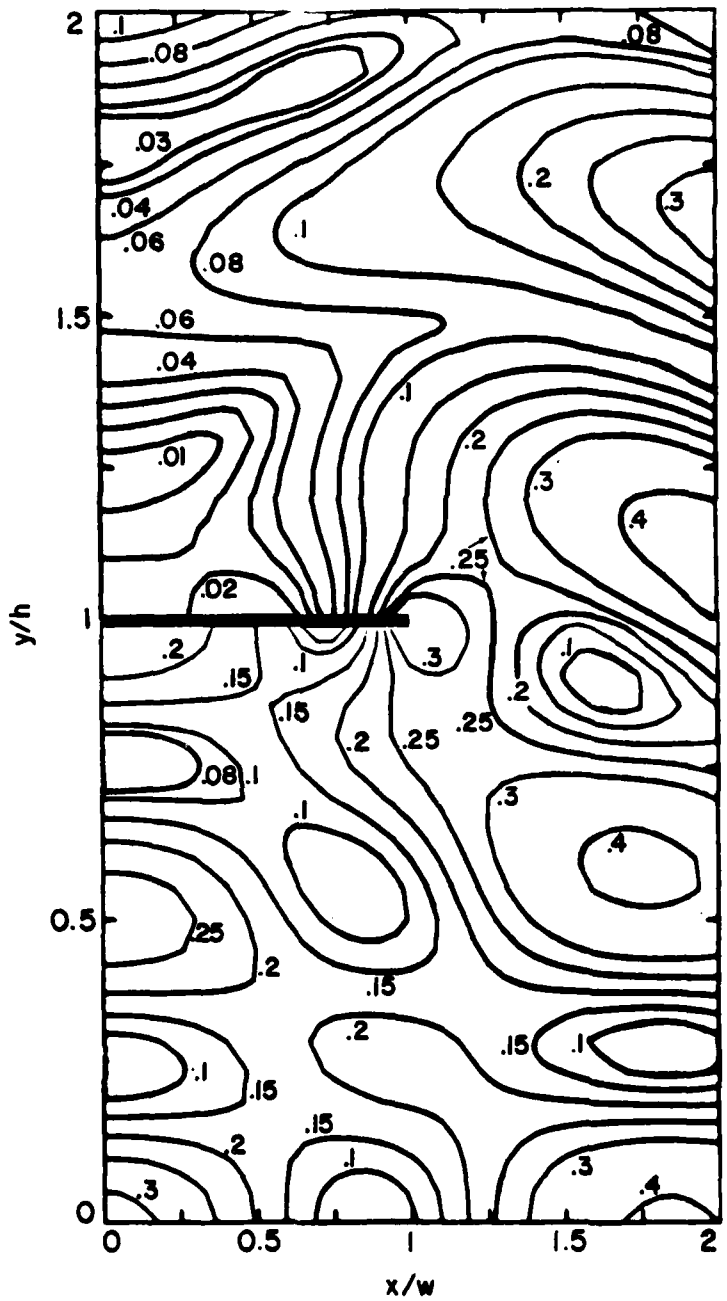

Figure 13e. Constant Value Contours for Normalized Field Component $\sqrt{(\mathrm{Im}(p^2E_x/\zeta))^2 + (\mathrm{Im}(p^2E_y/\zeta))^2} = \sqrt{(\mathrm{Im}(p^2H_y/s\varepsilon_o))^2 + (\mathrm{Im}(p^2H_x/s\varepsilon_o))^2}$ of the $TM_{0,2}$ Mode when $h/w = 2$. The Fields are Normalized so that $|p^2/\zeta|\sqrt{|E_x|^2 + |E_y|^2} = 1$ at $x = y = 0$.

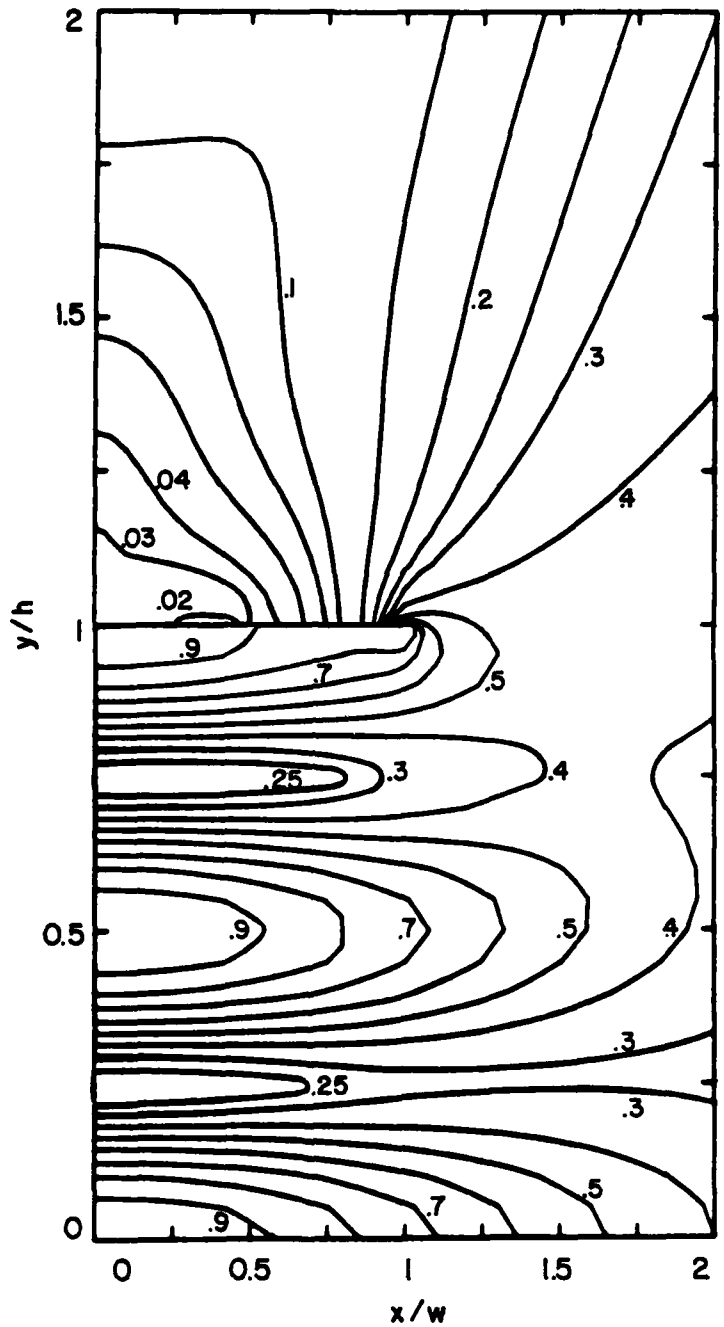

Figure 13f. Constant Value Contours for Normalized Field Component $|p^2/\zeta|\sqrt{|E_x|^2 + |E_y|^2} = |p^2(s\varepsilon_o)^{-1}|\sqrt{|H_x|^2 + |H_y|^2}$ of the $TM_{0,2}$ Mode when h/w = 2. The Fields are Normalized so that $|p^2/\zeta|\sqrt{|E_x|^2 + |E_y|^2} = 1$ at $x = y = 0$.

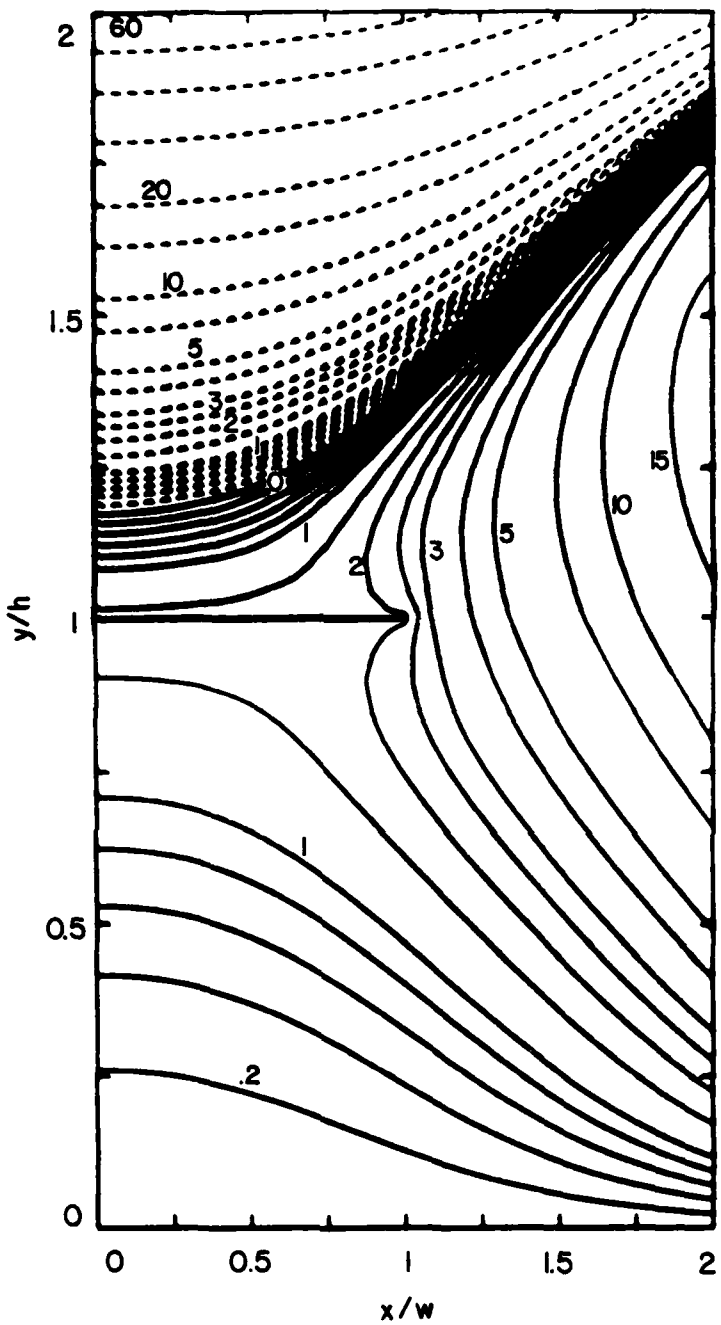

Figure 14a. Constant Value Contours for Normalized Field Component $Re(E_z/w)$ of the $TM_{1,1_2}$ Mode when $h/w = 2$. The Fields are Normalized so that $|p^2/\zeta|\sqrt{|E_x|^2 + |E_y|^2} = 1$ at $x = y = 0$. Broken Lines are for Negative Values.

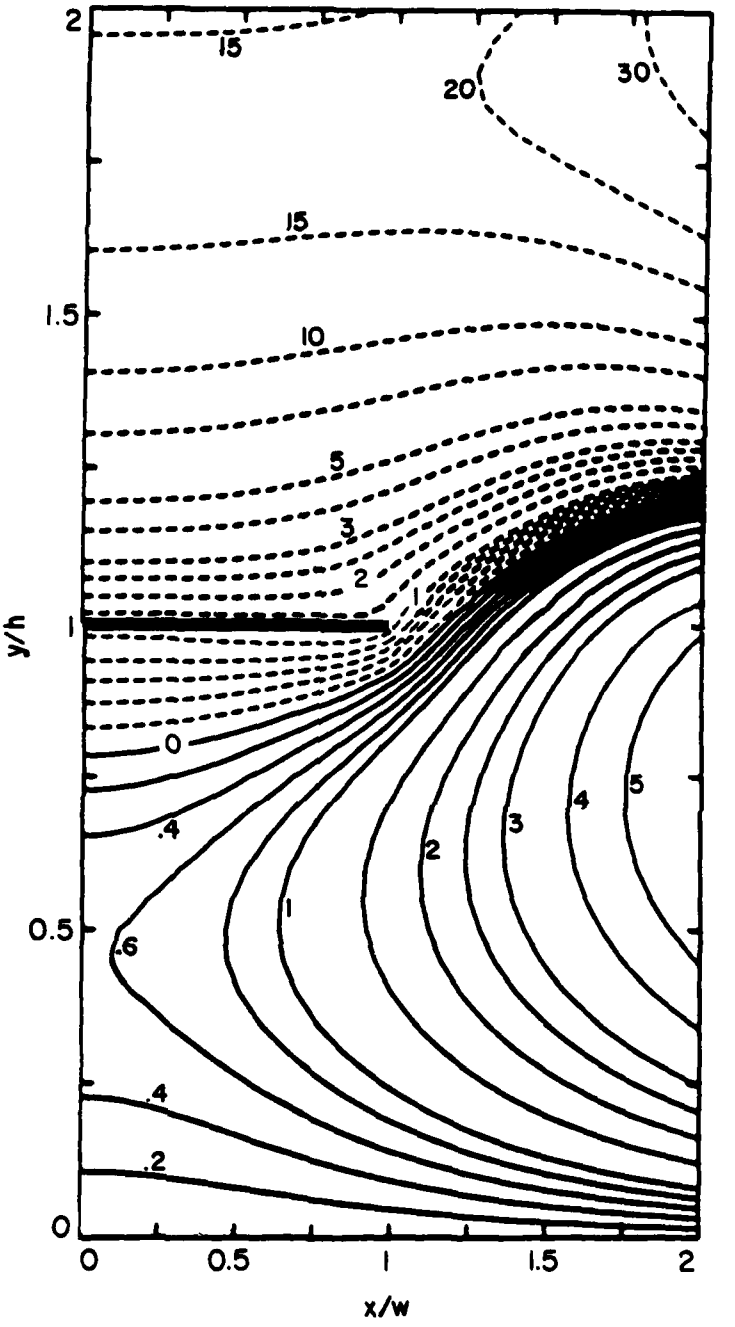

Figure 14b. Constant Value Contours for Normalized Field Component $\mathrm{Im}(E_z/w)$ of the $TM_{1,1}$ Mode when $h/w = 2$. The Fields are Normalized so that $|p^2/\zeta|\sqrt{|E_x|^2 + |E_y|^2} = 1$ at $x = y = 0$. Broken Lines are for Negative Values.

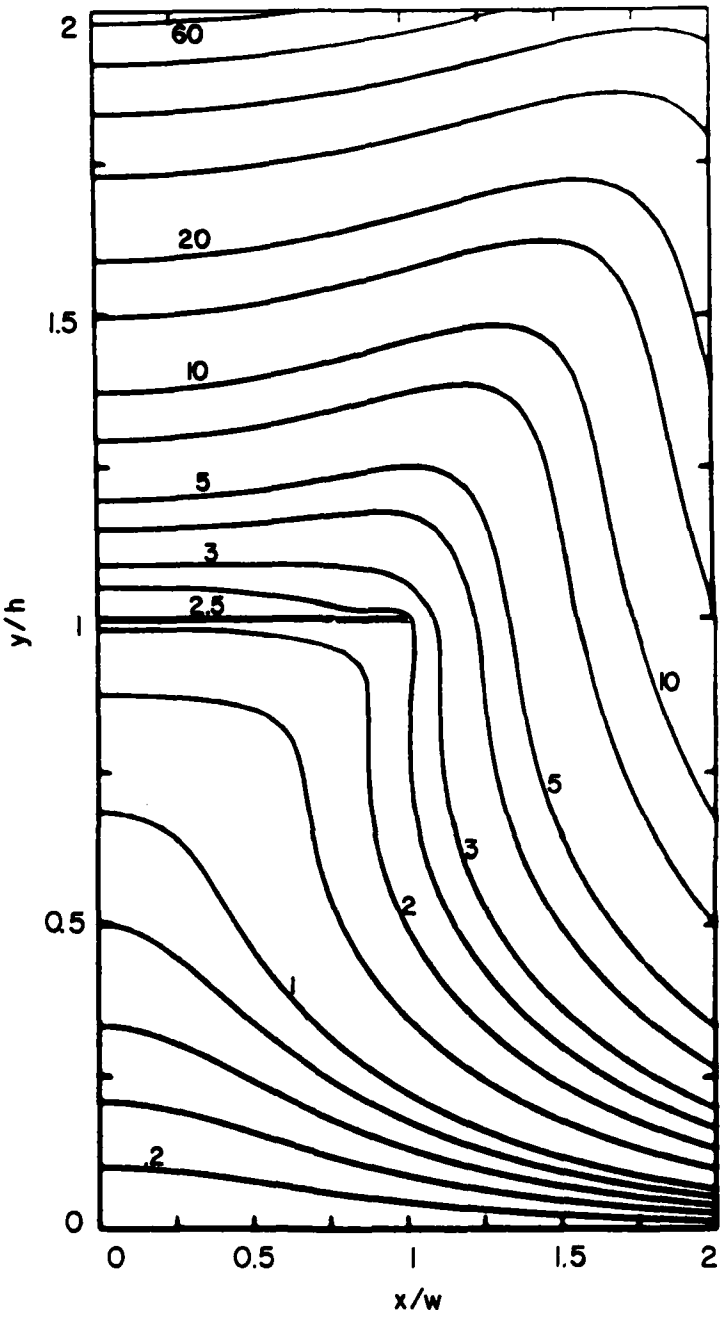

Figure 14c. Constant Value Contours for Normalized Field Component $|E_z/w|$ of the $TM_{1,1}$ Mode when $h/w = 2$. The Fields are Normalized so that $|p^2/\zeta|\sqrt{|E_x|^2 + |E_y|^2} = 1$ at $x = y = 0$.

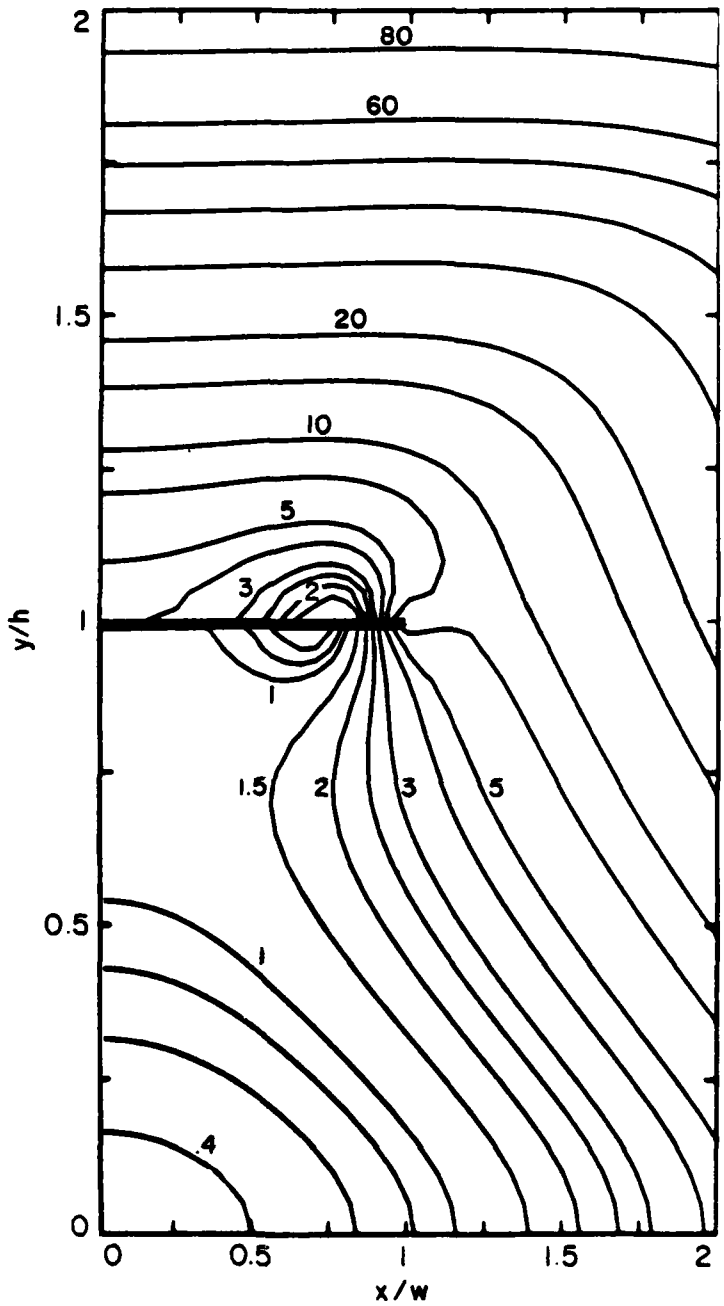

Figure 14d. Constant Value Contours for Normalized Field Component $\sqrt{(\mathrm{Re}(p^2E_x/\zeta))^2 + (\mathrm{Re}(p^2E_y/\zeta))^2} = \sqrt{(\mathrm{Re}(p^2H_y/s\varepsilon_o))^2 + (\mathrm{Re}(p^2H_x/s\varepsilon_o))^2}$ of the $TM_{1,1}$ Mode when $h/w = 2$. The Fields are Normalized so that $|p^2/\zeta|\sqrt{|E_x|^2 + |E_y|^2} = 1$ at $x = y = 0$.

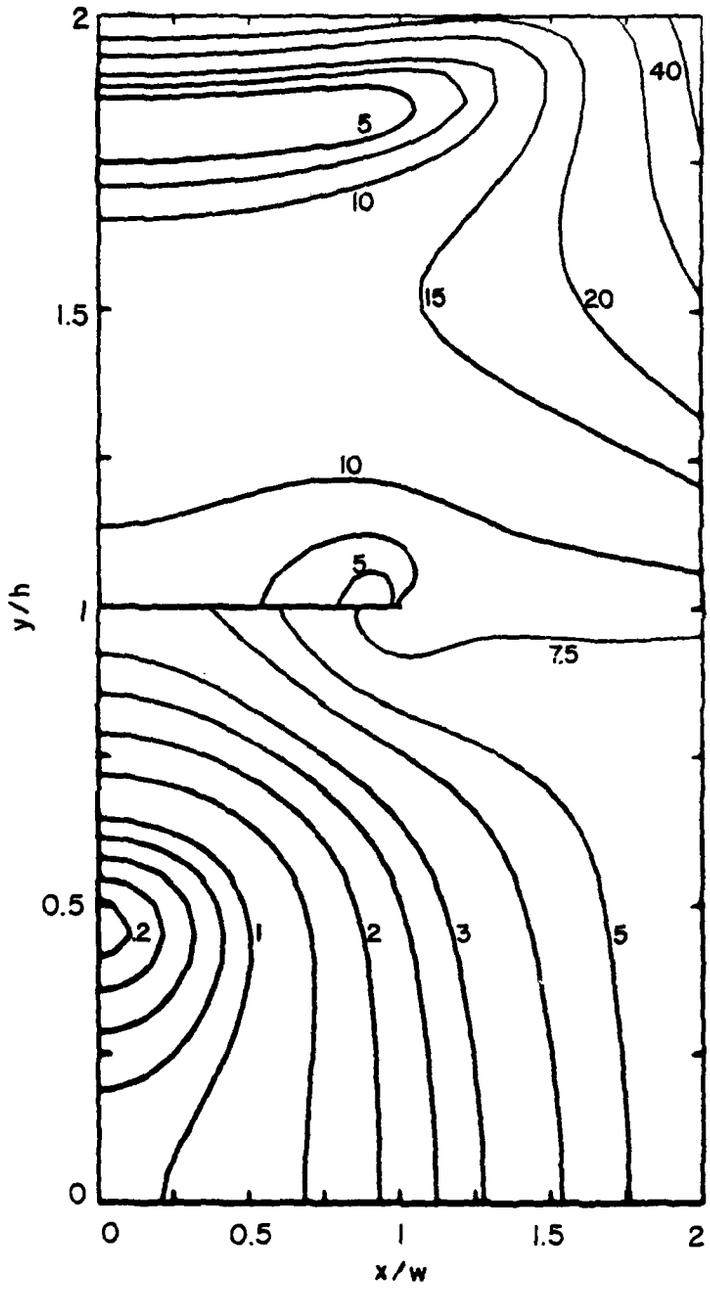

Figure 14e. Constant Value Contours for Normalized Field Component $\sqrt{(\mathrm{Im}(p^2E_x/\zeta))^2 + (\mathrm{Im}(p^2E_y/\zeta))^2} = \sqrt{(\mathrm{Im}(p^2H_y/s\varepsilon_o))^2 + (\mathrm{Im}(p^2H_x/s\varepsilon_o))^2}$ of the $TM_{1,1}$ Mode when $h/w = 2$. The Fields are Normalized so that $|p^2/\zeta|\sqrt{|E_x|^2 + |E_y|^2} = 1$ at $x = y = 0$.

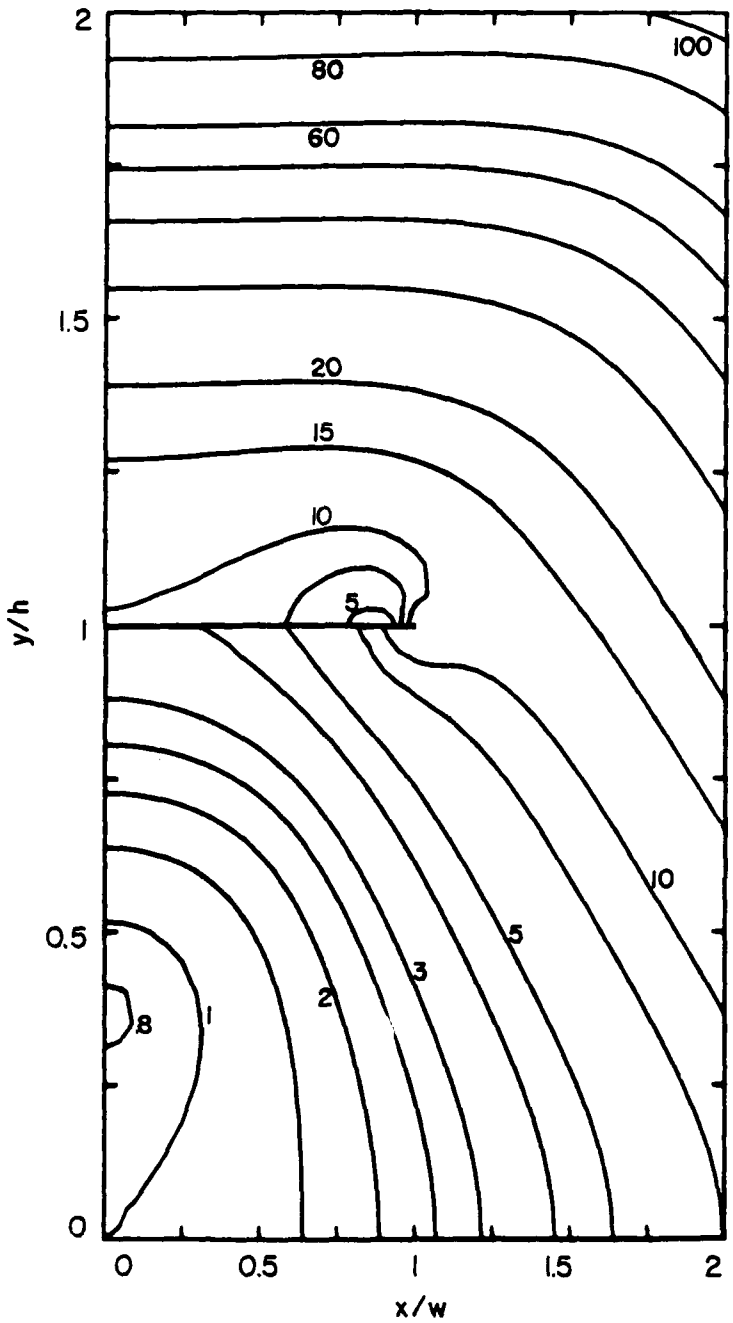

Figure 14f. Constant Value Contours for Normalized Field Component $|p^2/\zeta|\sqrt{|E_x|^2 + |E_y|^2} = |p^2(s\varepsilon_o)^{-1}|\sqrt{|H_x|^2 + |H_y|^2}$ of the $TM_{1,1}$ Mode when $h/w = 2$. The Fields are Normalized so that $|p^2/\zeta|\sqrt{|E_x|^2 + |E_y|^2} = 1$ at $x = y = 0$.

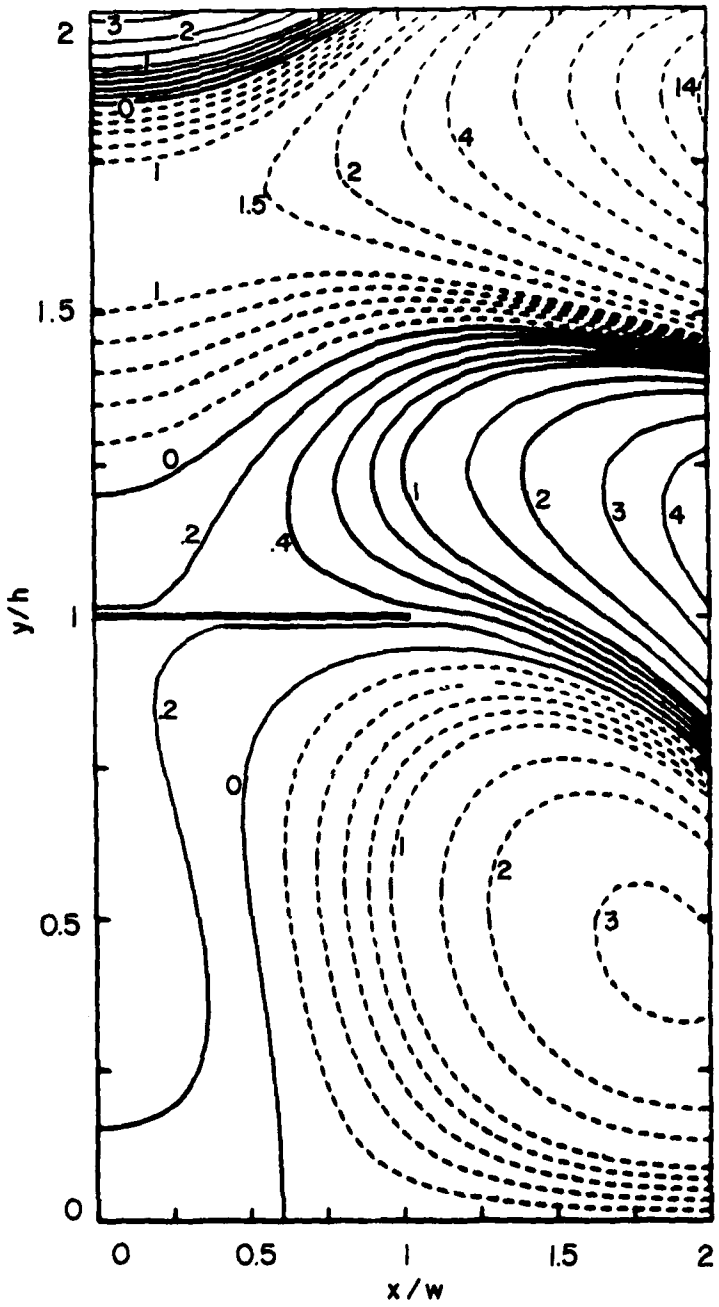

Figure 15a. Constant Value Contours for Normalized Field Component $Re(E_z/w)$ of the $TM_{1,2}$ Mode when $h/w = 2$. The Fields are Normalized so that $|p^2/\zeta|\sqrt{|E_x|^2 + |E_y|^2} = 1$ at $x = y = 0$. Broken Lines are for Negative Values.

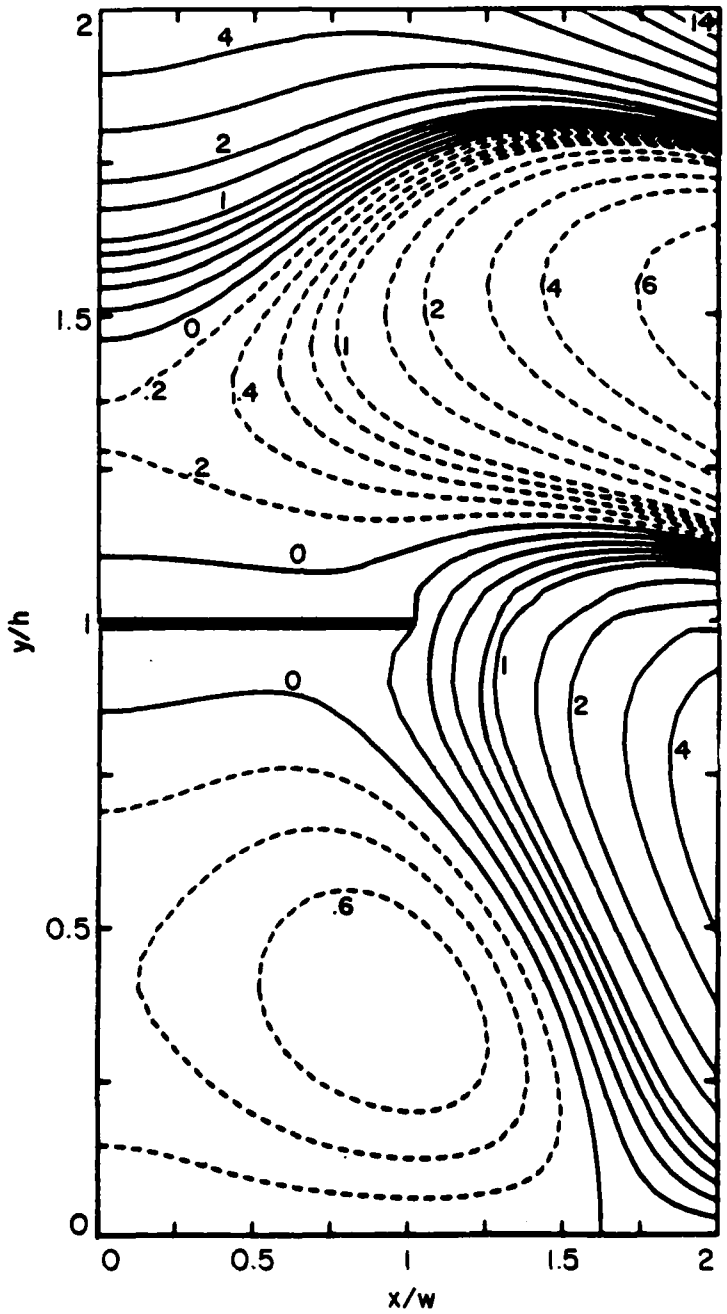

Figure 15b. Constant Value Contours for Normalized Field Component $\mathrm{Im}(E_z/w)$ of the $TM_{1,2}$ Mode when $h/w = 2$. The Fields are Normalized so that $|p^2/\zeta|\sqrt{|E_x|^2 + |E_y|^2} = 1$ at $x = y = 0$. Broken Lines are for Negative Values.

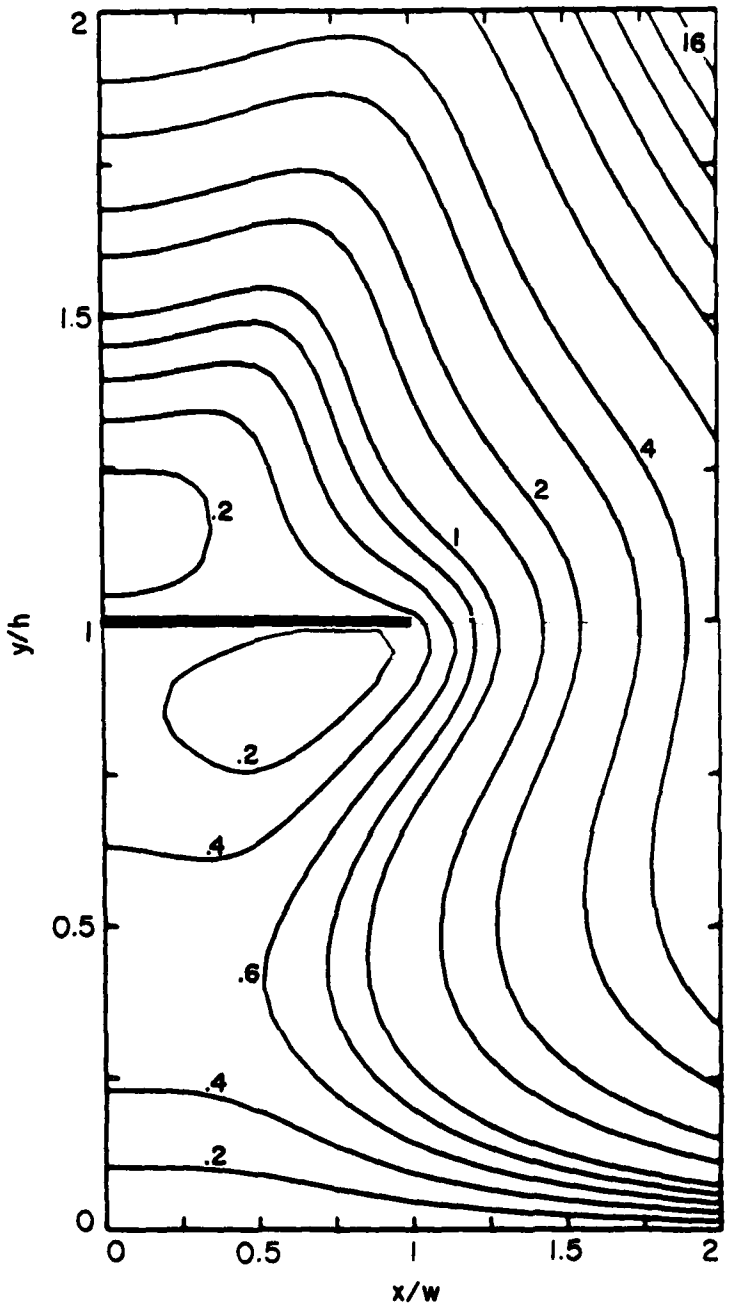

Figure 15c. Constant Value Contours for Normalized Field Component $|E_z/w|$ of the $TM_{1,2}$ Mode when $h/w = 2$. The Fields are Normalized so that $|p^2/\zeta|\sqrt{|E_x|^2 + |E_y|^2} = 1$ at $x = y = 0$.

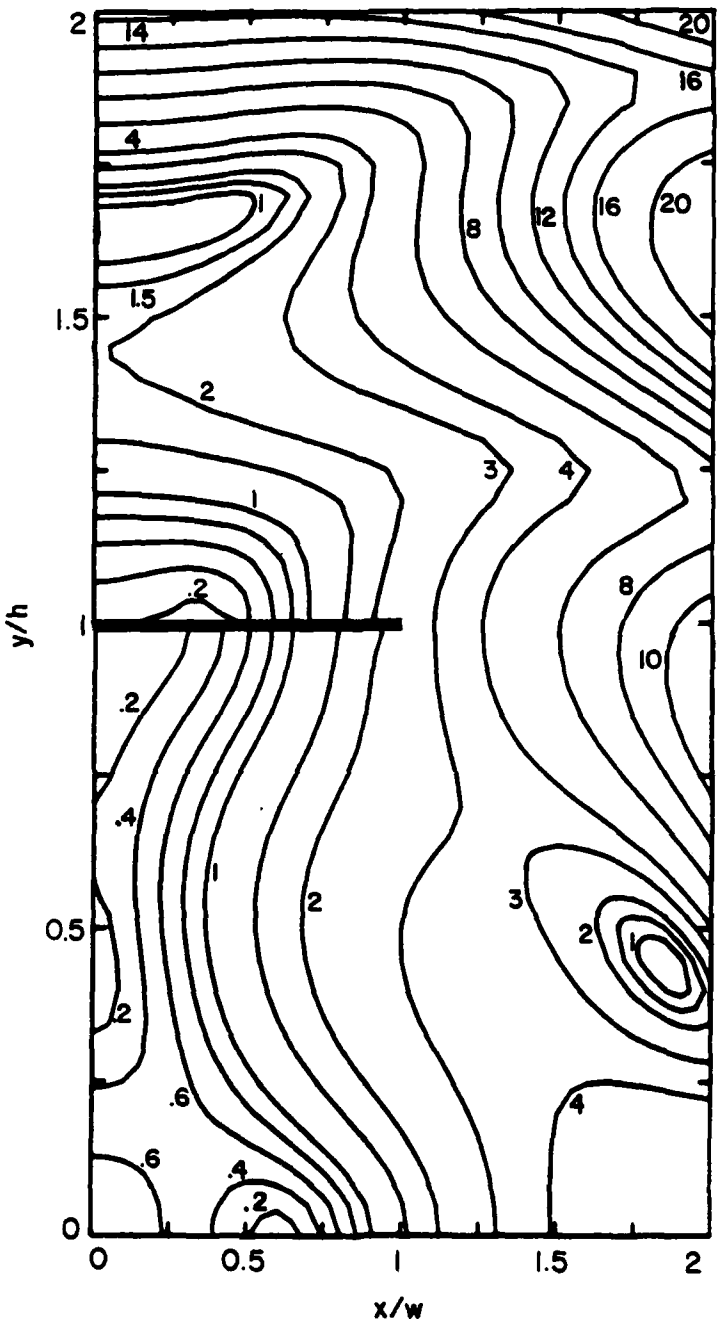

Figure 15d. Constant Value Contours for Normalized Field Component $\sqrt{(\mathrm{Re}(p^2E_x/\zeta))^2 + (\mathrm{Re}(p^2E_y/\zeta))^2} = \sqrt{(\mathrm{Re}(p^2H_y/s\varepsilon_o))^2 + (\mathrm{Re}(p^2H_x/s\varepsilon_o))^2}$ of the $TM_{1,2}$ Mode when $h/w = 2$. The Fields are Normalized so that $|p^2/\zeta|\sqrt{|E_x|^2 + |E_y|^2} = 1$ at $x = y = 0$.

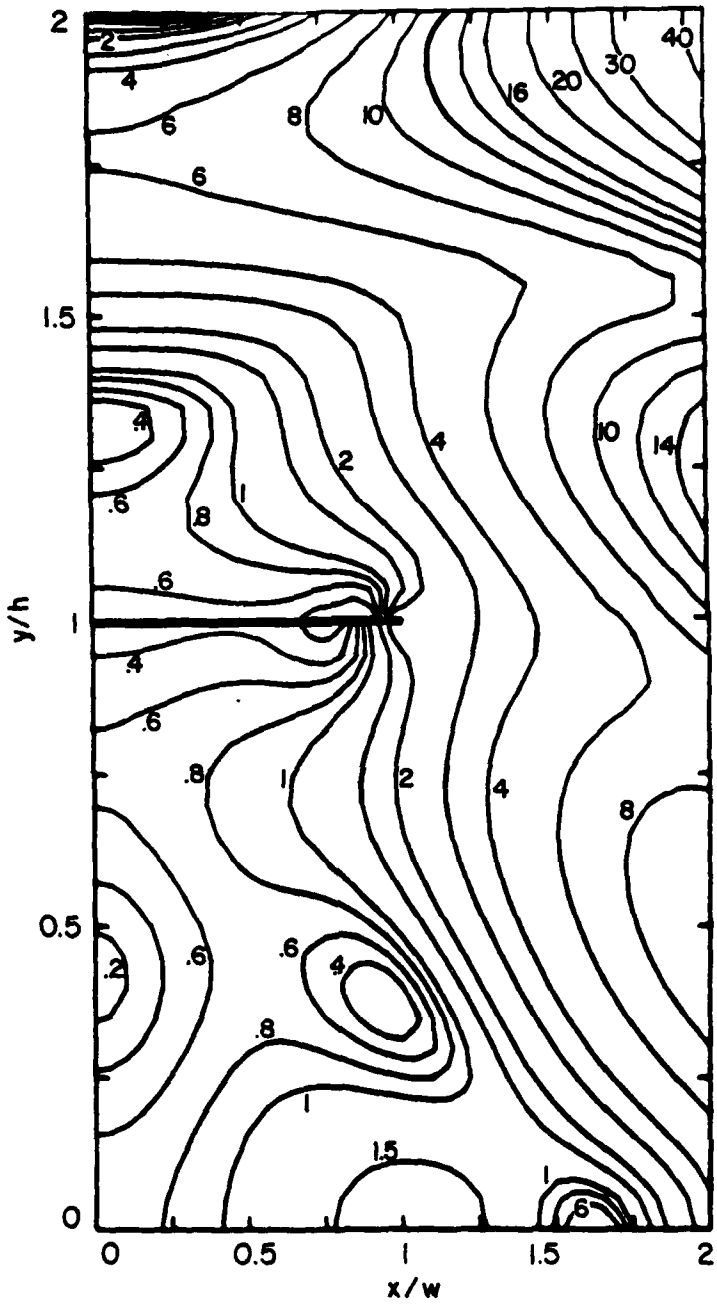

Figure 15e. Constant Value Contours for Normalized Field Component $\sqrt{(\mathrm{Im}(p^2E_x/\zeta))^2 + (\mathrm{Im}(p^2E_y/\zeta))^2} = \sqrt{(\mathrm{Im}(p^2H_y/s\varepsilon_o))^2 + (\mathrm{Im}(p^2H_x/s\varepsilon_o))^2}$ of the $TM_{1,2}$ Mode when $h/w = 2$. The Fields are Normalized so that $|p^2/\zeta|\sqrt{|E_x|^2 + |E_y|^2} = 1$ at $x = y = 0$.

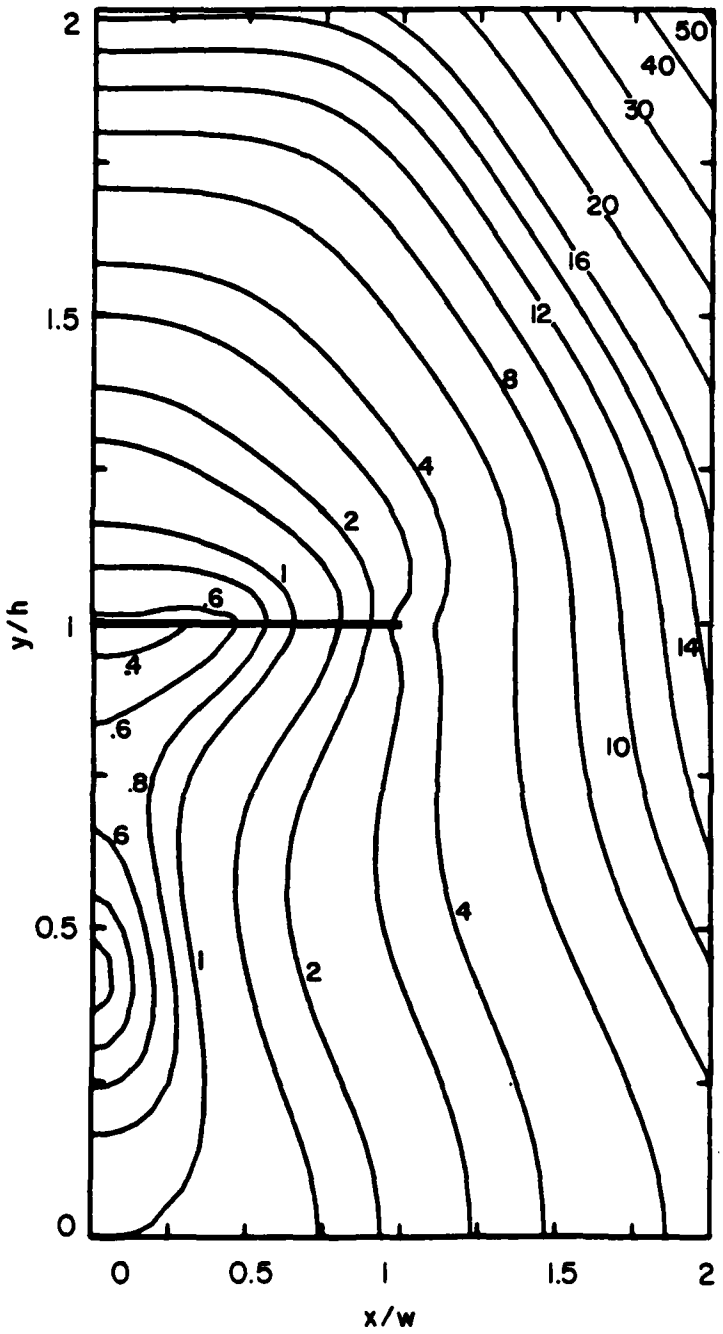

Figure 15f. Constant Value Contours for Normalized Field Component $|p^2/\zeta|\sqrt{|E_x|^2 + |E_y|^2} = |p^2(s\varepsilon_o)^{-1}|\sqrt{|H_x|^2 + |H_y|^2}$ of the $TM_{1,2}$ Mode when h/w = 2. The Fields are Normalized so that $|p^2/\zeta|\sqrt{|E_x|^2 + |E_y|^2} = 1$ at $x = y = 0$.

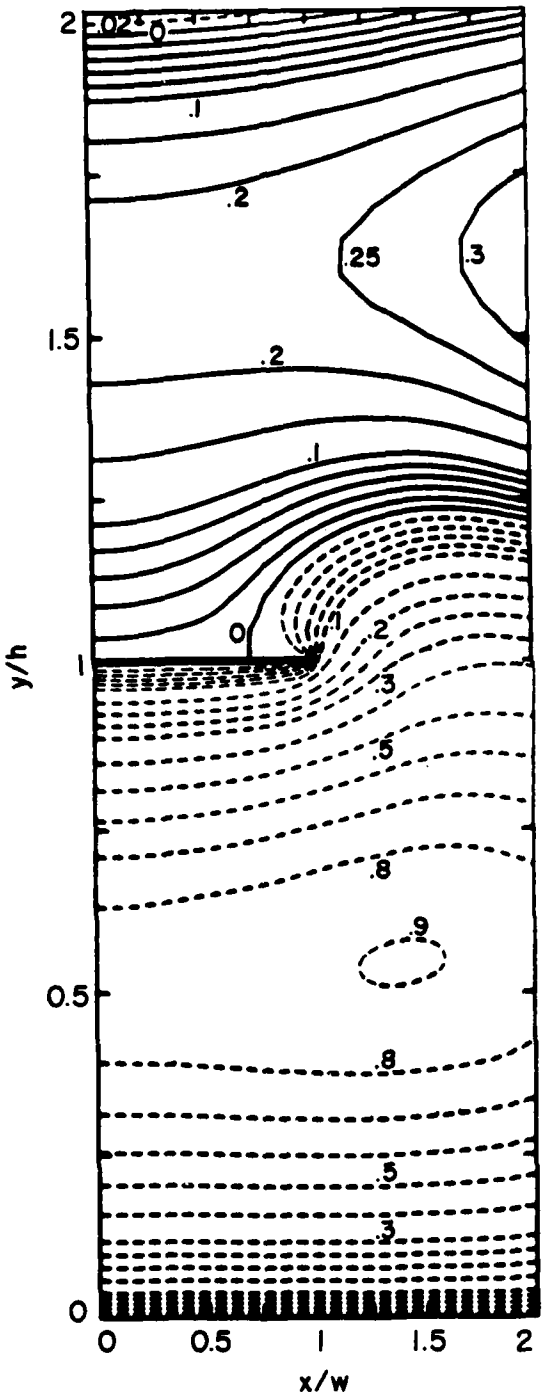

Figure 16a. Constant Value Contours for Normalized Field Component $Re(E_z/w)$ of the $TM_{0,1}$ Mode when $h/w = 3$. The Fields are Normalized so that $|p^2/\zeta|\sqrt{|E_x|^2 + |E_y|^2} = 1$ at $x = y = 0$. Broken Lines are for Negative Values.

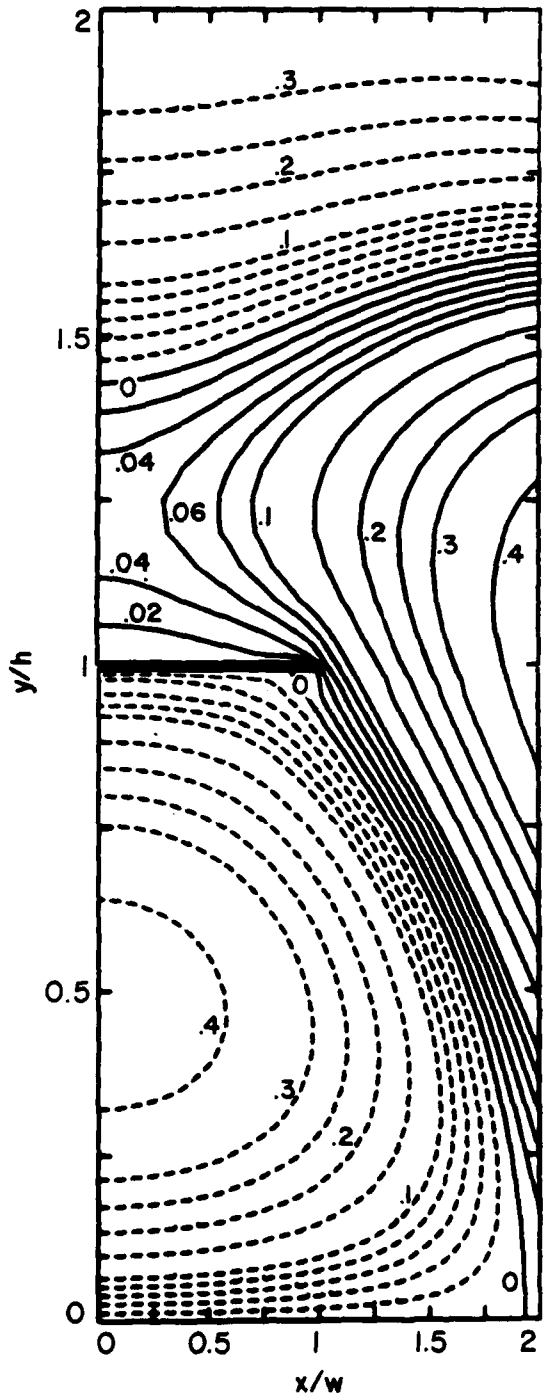

Figure 16b. Constant Value Contours for Normalized Field Component $\mathrm{Im}(E_z/w)$ of the $TM_{0,1_2}$ Mode when $h/w = 3$. The Fields are Normalized so that $|p^2/\zeta|\sqrt{|E_x|^2 + |E_y|^2} = 1$ at $x = y = 0$. Broken Lines are for Negative Values.

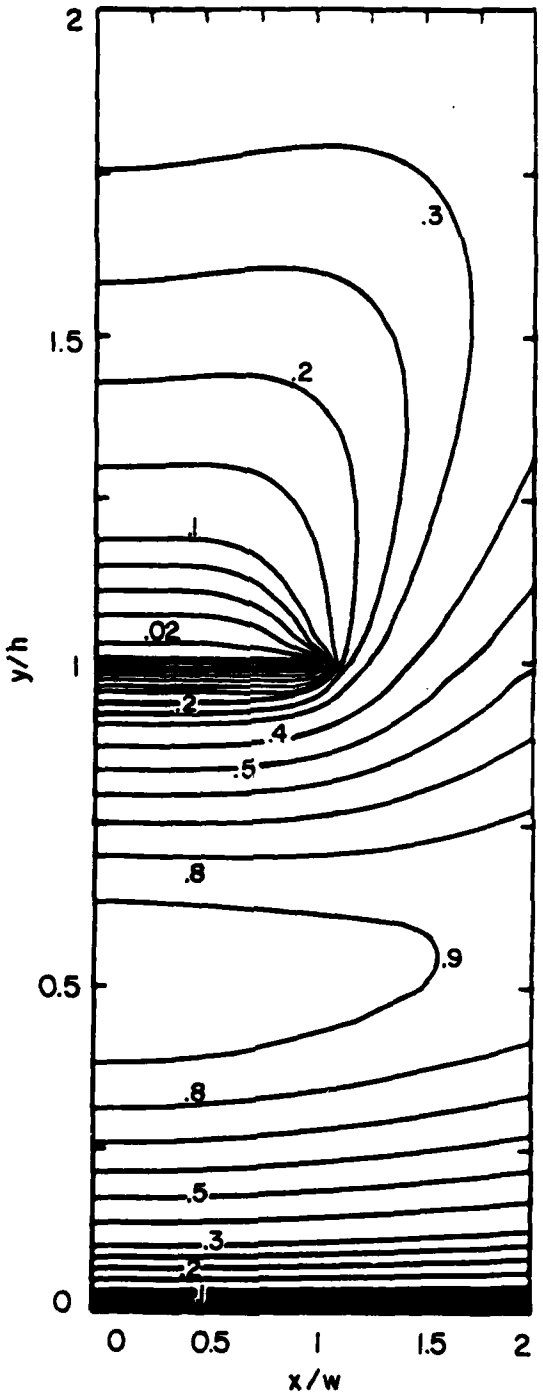

Figure 16c. Constant Value Contours for Normalized Field Component $|E_z/w|$ of the $TM_{0,1}$ Mode when $h/w = 3$. The Fields are Normalized so that $|p^2/\zeta|\sqrt{|E_x|^2 + |E_y|^2} = 1$ at $x = y = 0$.

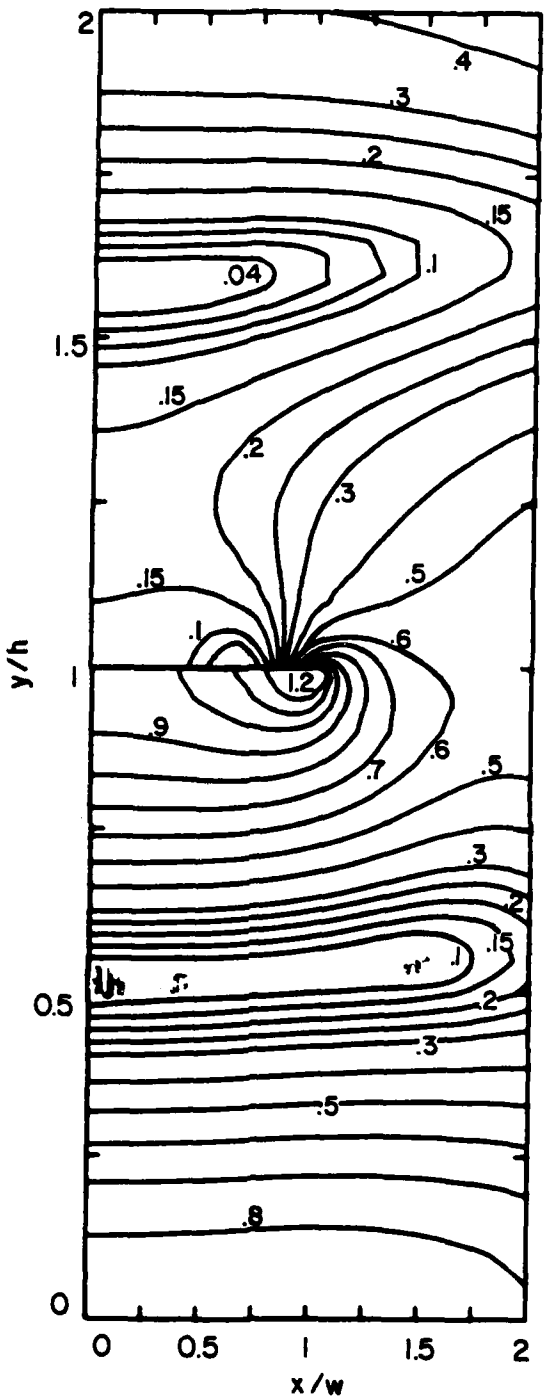

Figure 16d. Constant Value Contours for Normalized Field Component $\sqrt{(\mathrm{Re}(p^2E_x/\zeta))^2 + (\mathrm{Re}(p^2E_y/\zeta))^2} = \sqrt{(\mathrm{Re}(p^2H_y/s\varepsilon_o))^2 + (\mathrm{Re}(p^2H_x/s\varepsilon_o))^2}$ of the $TM_{0,1}$ Mode when $h/w = 3$. The Fields are Normalized so that $|p^2/\zeta|\sqrt{|E_x|^2 + |E_y|^2} = 1$ at $x = y = 0$.

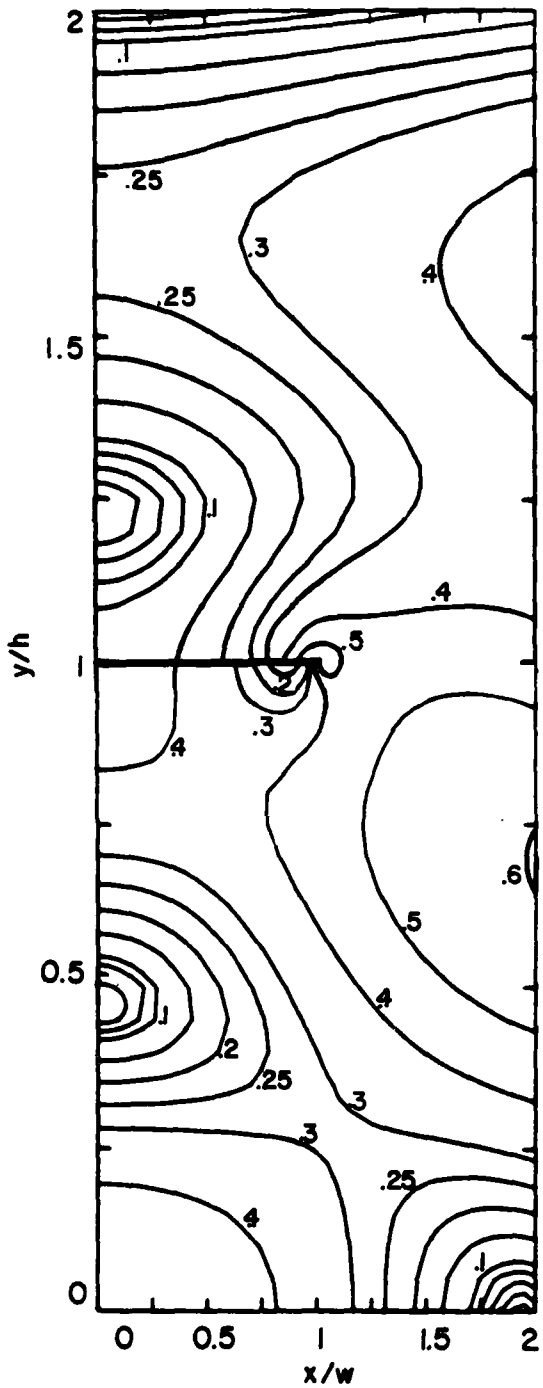

Figure 16e. Constant Value Contours for Normalized Field Component $\sqrt{(\mathrm{Im}(p^2E_x/\zeta))^2 + (\mathrm{Im}(p^2E_y/\zeta))^2} = \sqrt{(\mathrm{Im}(p^2H_y/s\varepsilon_o))^2 + (\mathrm{Im}(p^2H_x/s\varepsilon_o))^2}$ of the $TM_{0,1}$ Mode when $h/w = 3$. The Fields are Normalized so that $|p^2/\zeta|\sqrt{|E_x|^2 + |E_y|^2} = 1$ at $x = y = 0$.

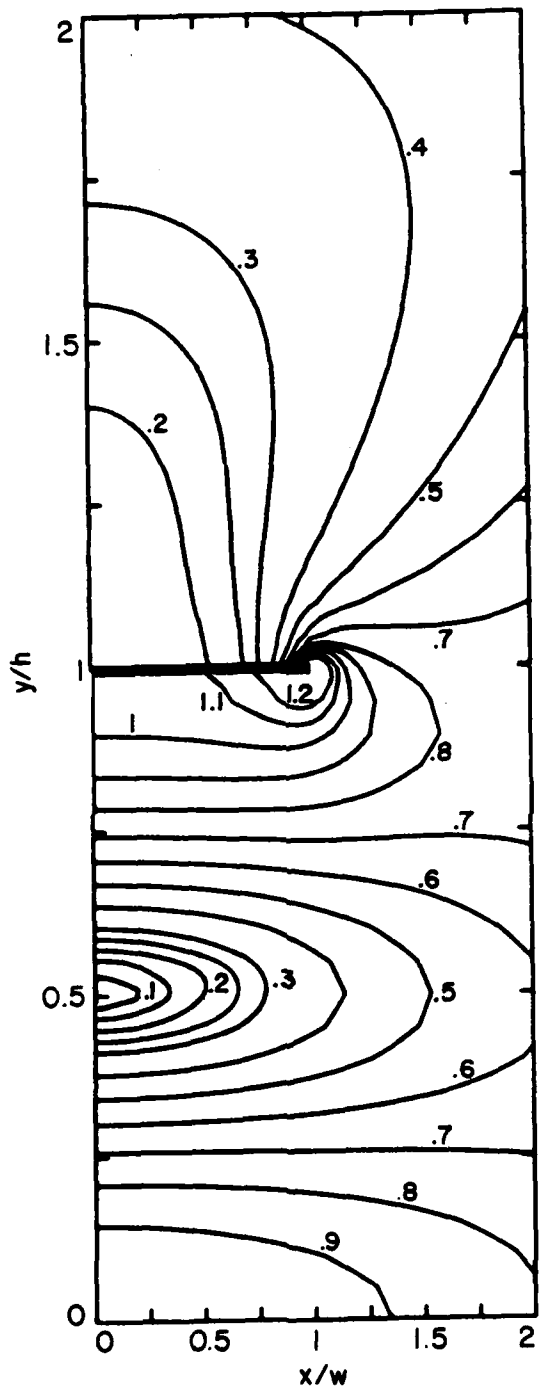

Figure 16f. Constant Value Contours for Normalized Field Component $|p^2/\zeta|\sqrt{|E_x|^2+|E_y|^2} = |p^2(s\varepsilon_o)^{-1}|\sqrt{|H_x|^2+|H_y|^2}$ of the $TM_{0,1}$ Mode when h/w = 3. The Fields are Normalized so that $|p^2/\zeta|\sqrt{|E_x|^2+|E_y|^2} = 1$ at $x = y = 0$.

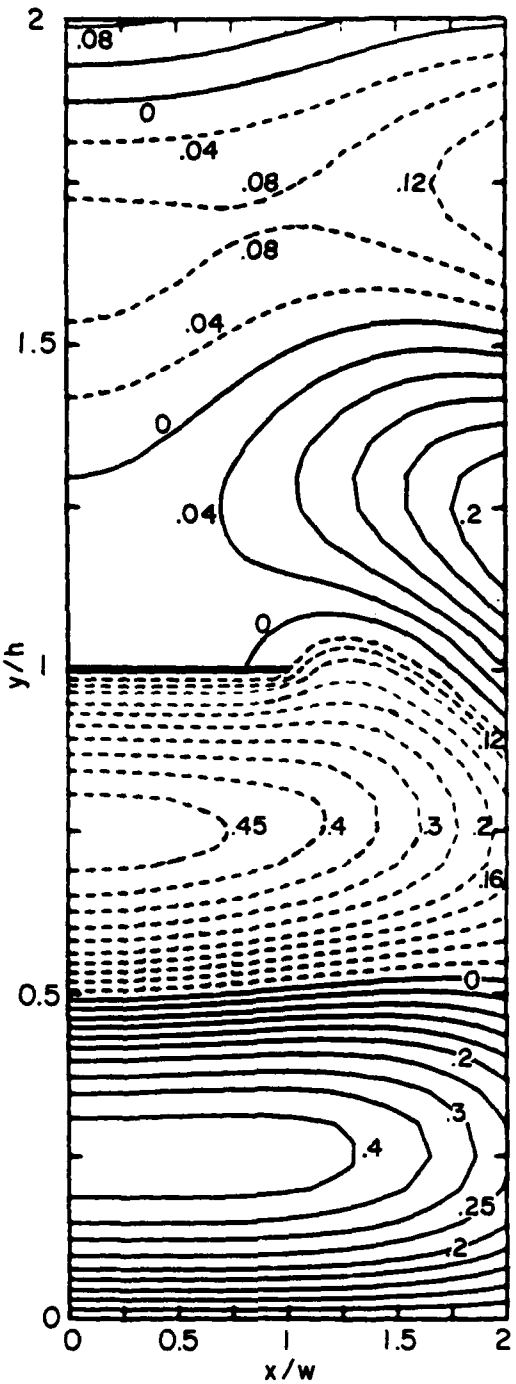

Figure 17a. Constant Value Contours for Normalized Field Component $Re(E_z/w)$ of the $TM_{0,2}$ Mode when $h/w = 3$. The Fields are Normalized so that $|p^2/\zeta|\sqrt{|E_x|^2 + |E_y|^2} = 1$ at $x = y = 0$. Broken Lines are for Negative Values.

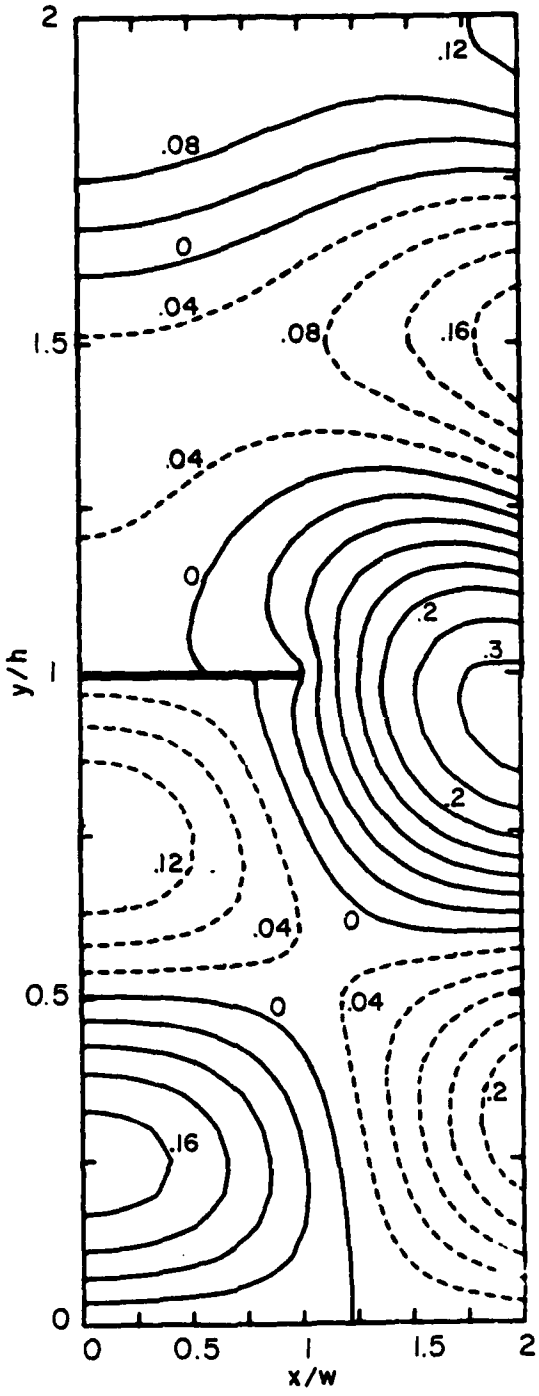

Figure 17b. Constant Value Contours for Normalized Field Component $\mathrm{Im}(E_z/w)$ of the $TM_{0,2_2}$ Mode when $h/w = 3$. The Fields are Normalized so that $|p^2/\zeta|\sqrt{|E_x|^2 + |E_y|^2} = 1$ at $x = y = 0$. Broken Lines are for Negative Values.

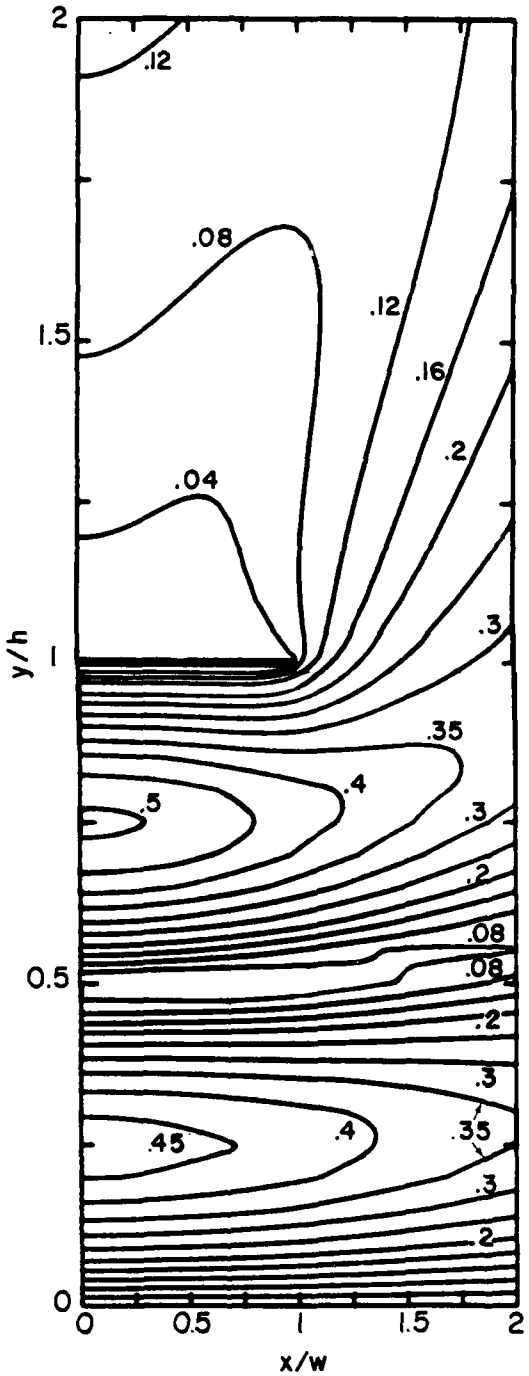

Figure 17c. Constant Value Contours for Normalized Field Component $|E_z/w|$ of the $TM_{0,2}$ Mode when $h/w = 3$. The Fields are Normalized so that $|p^2/\zeta|\sqrt{|E_x| + |E_y|^2} = 1$ at $x = y = 0$.

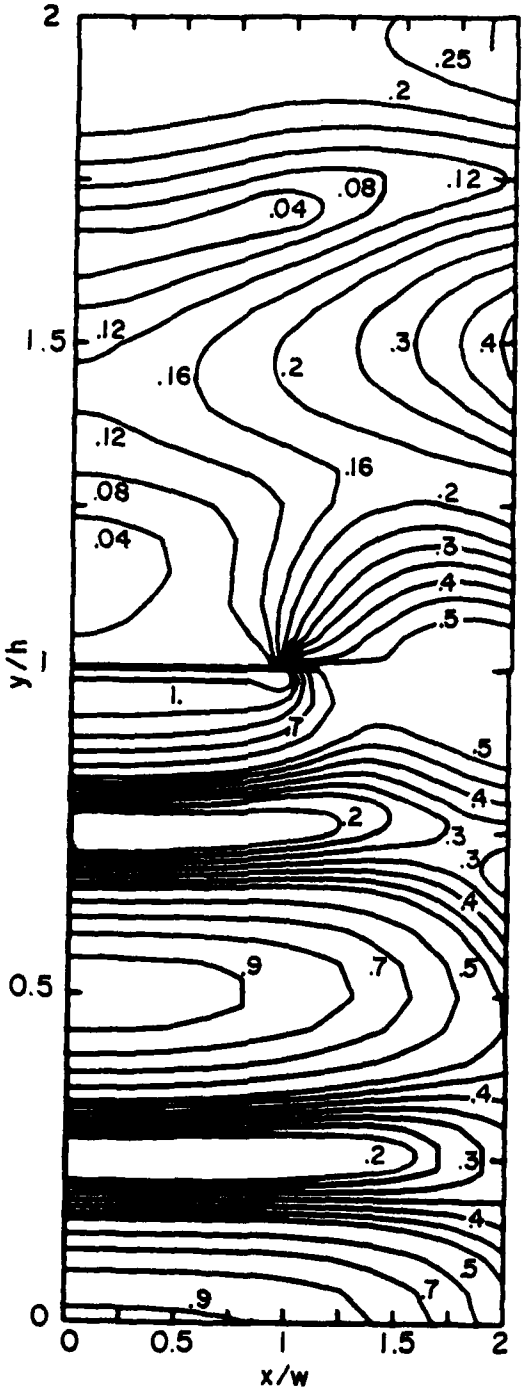

Figure 17d. Constant Value Contours for Normalized Field Component $\sqrt{(\mathrm{Re}(p^2E_x/\zeta))^2 + (\mathrm{Re}(p^2E_y/\zeta))^2} = \sqrt{(\mathrm{Re}(p^2H_y/s\varepsilon_o))^2 + (\mathrm{Re}(p^2H_x/s\varepsilon_o))^2}$ of the $TM_{0,2}$ Mode when $h/w = 3$. The Fields are Normalized so that $|p^2/\zeta|\sqrt{|E_x|^2 + |E_y|^2} = 1$ at $x = y = 0$.

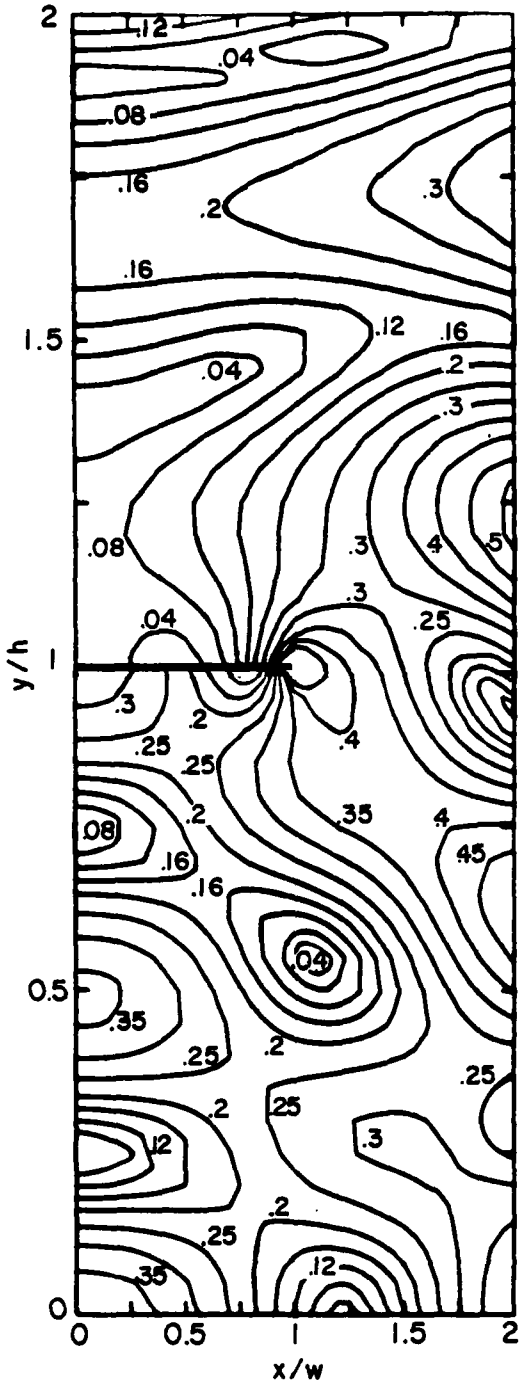

Figure 17e. Constant Value Contours for Normalized Field Component $\sqrt{(\mathrm{Im}(p^2E_x/\zeta))^2 + (\mathrm{Im}(p^2E_y/\zeta))^2} = \sqrt{(\mathrm{Im}(p^2H_y/s\varepsilon_o))^2 + (\mathrm{Im}(p^2H_x/s\varepsilon_o))^2}$ of the $TM_{0,2}$ Mode when $h/w = 3$. The Fields are Normalized so that $|p^2/\zeta|\sqrt{|E_x|^2 + |E_y|^2} = 1$ at $x = y = 0$.

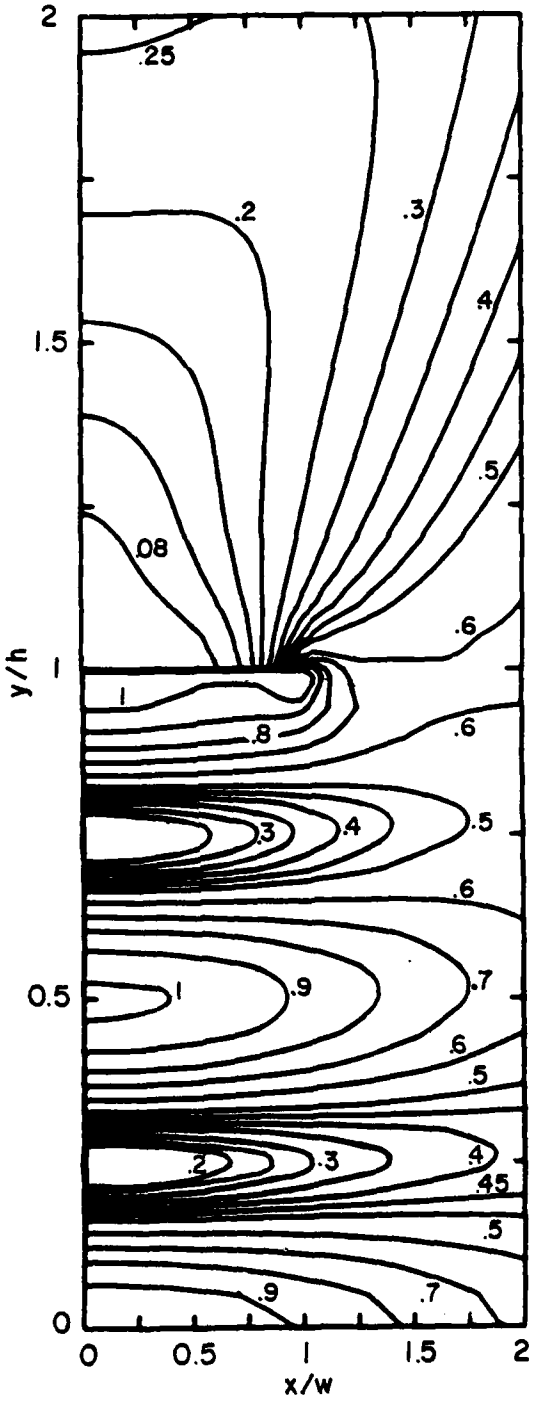

Figure 17f. Constant Value Contours for Normalized Field Component $|p^2/\zeta|\sqrt{|E_x|^2+|E_y|^2} = |p^2(s\varepsilon_o)^{-1}|\sqrt{|H_x|^2+|H_y|^2}$ of the $TM_{0,2}$ Mode when h/w = 3. The Fields are Normalized so that $|p^2/\zeta|\sqrt{|E_x|^2+|E_y|^2} = 1$ at $x = y = 0$.

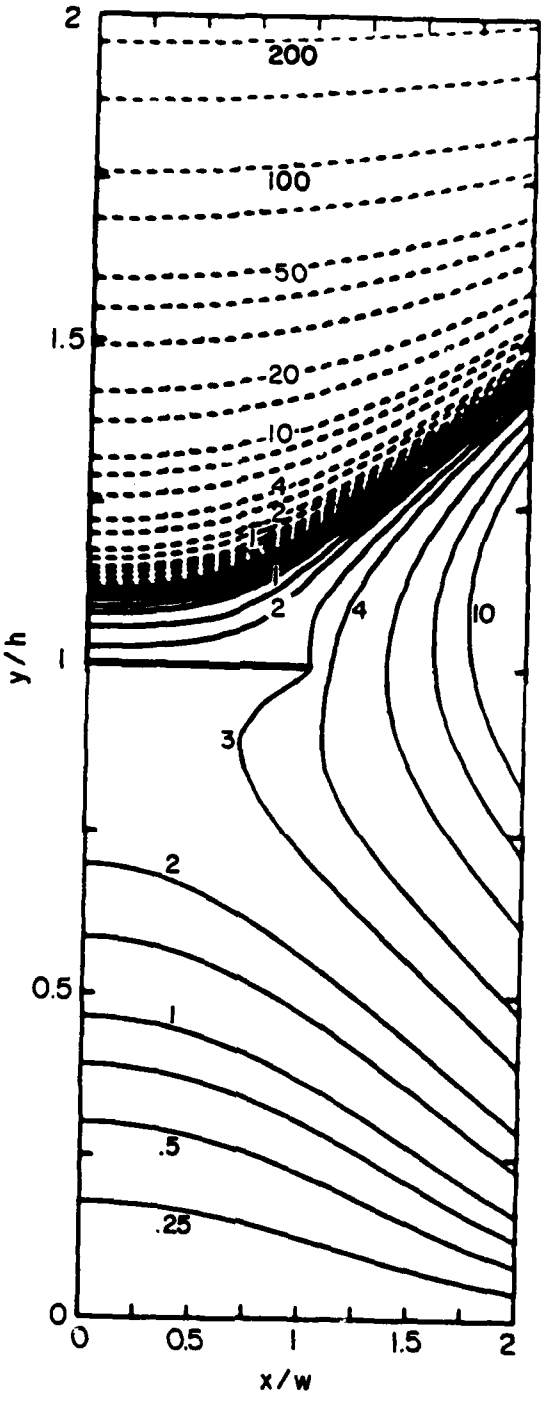

Figure 18a. Constant Value Contours for Normalized Field Component $Re(E_z/w)$ of the $TM_{1,1}$ Mode when $h/w = 3$. The Fields are Normalized so that $|p^2/\zeta|\sqrt{|E_x|^2 + |E_y|^2} = 1$ at $x = y = 0$. Broken Lines are for Negative Values.

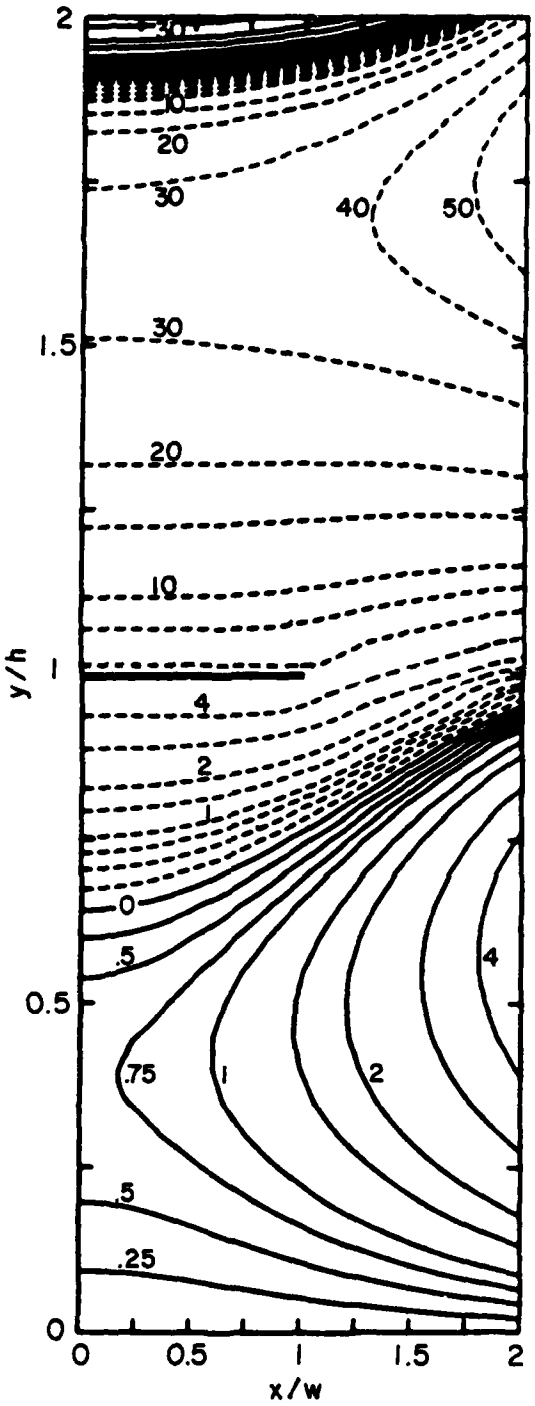

Figure 18b. Constant Value Contours for Normalized Field Component $\mathrm{Im}(E_z/w)$ of the $TM_{1,1}$ Mode when $h/w = 3$. The Fields are Normalized so that $|p^2/\zeta|\sqrt{|E_x|^2 + |E_y|^2} = 1$ at $x = y = 0$. Broken Lines are for Negative Values.

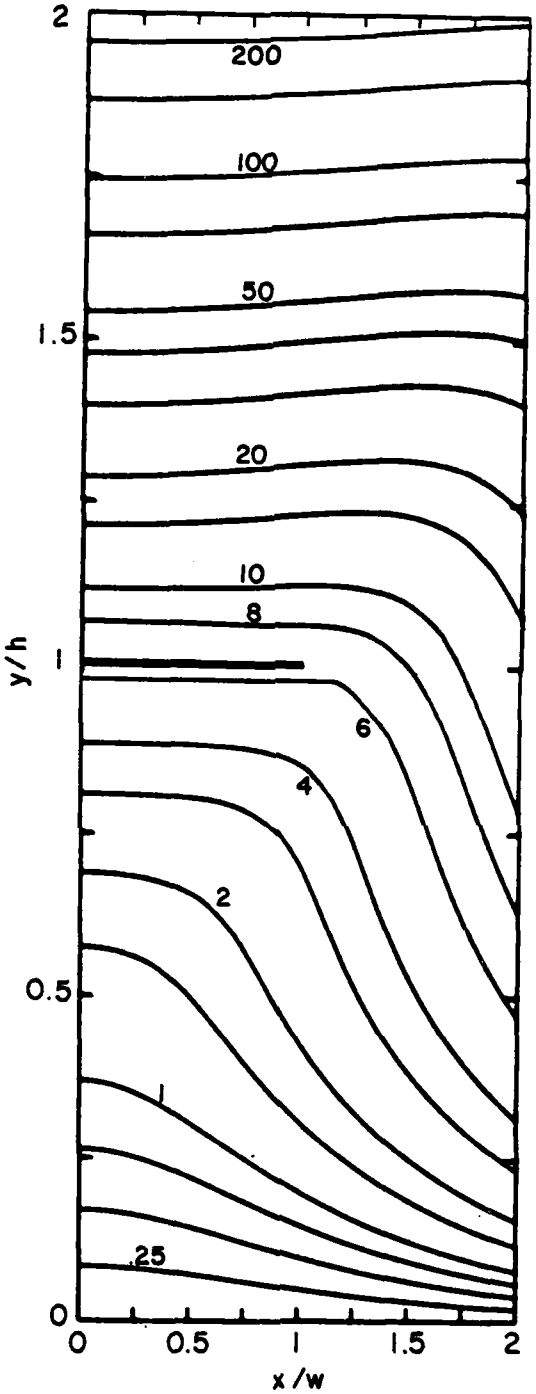

Figure 18c. Constant Value Contours for Normalized Field Component $|E_z/w|$ of the $TM_{1,1}$ Mode when h/w = 3. The Fields are Normalized so that $|p^2/\zeta|\sqrt{|E_x|^2 + |E_y|^2} = 1$ at $x = y = 0$.

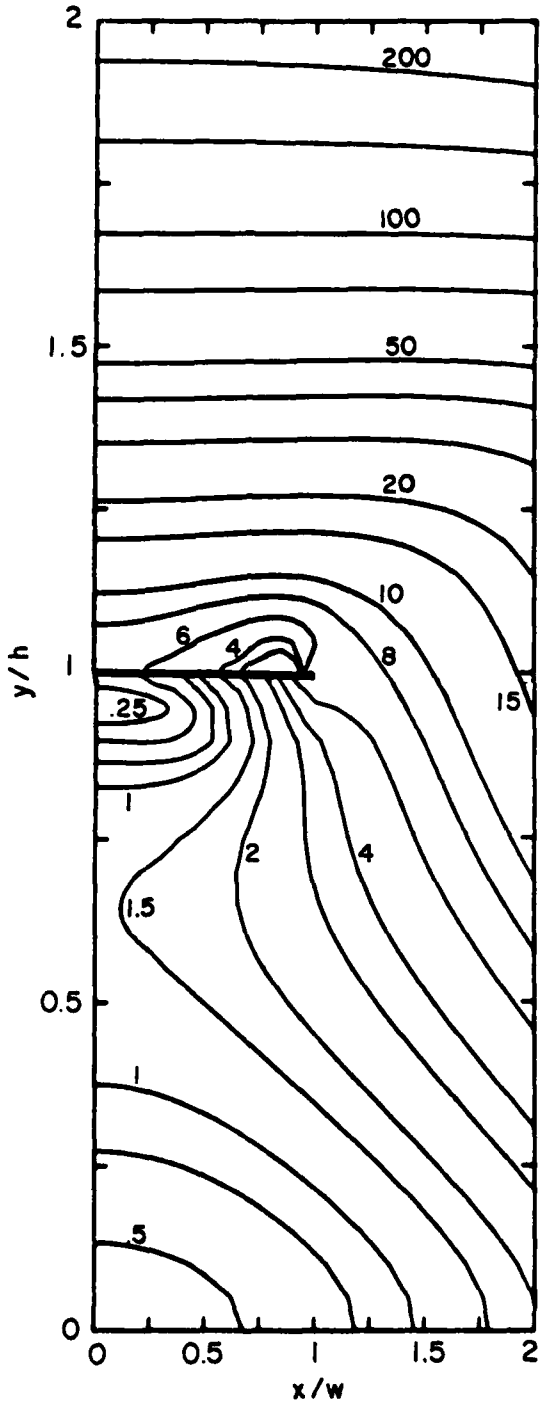

Figure 18d. Constant Value Contours for Normalized Field Component $\sqrt{(\mathrm{Re}(p^2E_x/\zeta))^2 + (\mathrm{Re}(p^2E_y/\zeta))^2} = \sqrt{(\mathrm{Re}(p^2H_x/s\varepsilon_o))^2 + (\mathrm{Re}(p^2H_y/s\varepsilon_o))^2}$ of the $TM_{1,1}$ Mode when $h/w = 3$. The Fields are Normalized so that $|p^2/\zeta|\sqrt{|E_x|^2 + |E_y|^2} = 1$ at $x = y = 0$.

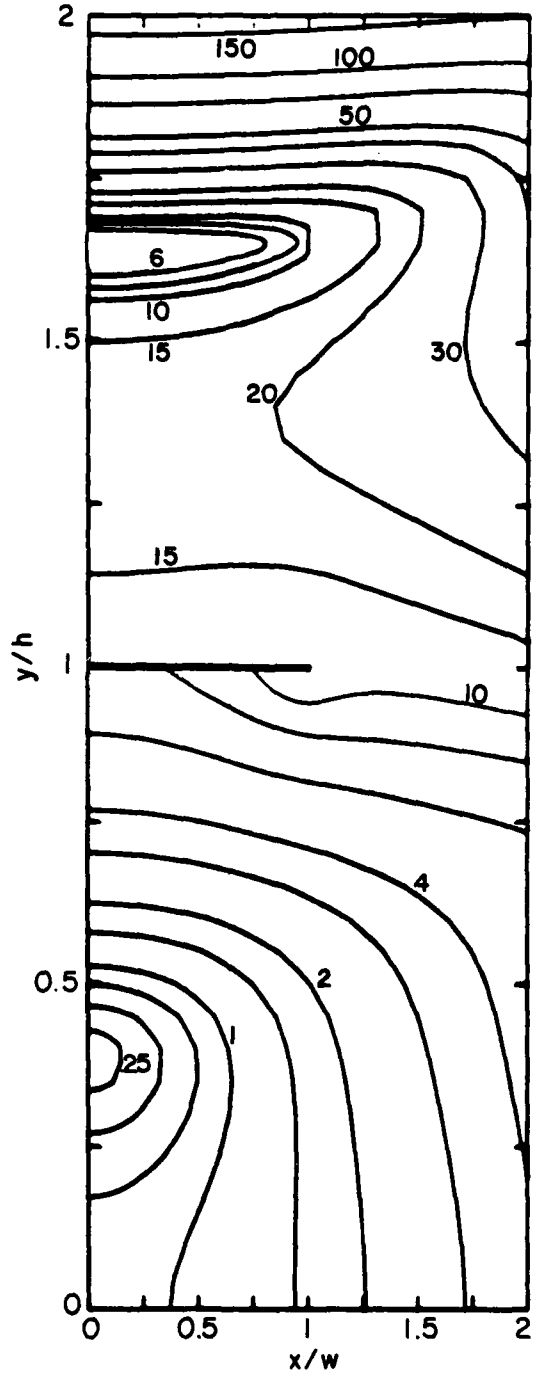

Figure 18e. Constant Value Contours for Normalized Field Component $\sqrt{(\mathrm{Im}(p^2E_x/\zeta))^2 + (\mathrm{Im}(p^2E_y/\zeta))^2} = \sqrt{(\mathrm{Im}(p^2H_x/s\varepsilon_o))^2 + (\mathrm{Im}(p^2H_y/s\varepsilon_o))^2}$ of the $TM_{1,1}$ Mode when $h/w = 3$. The Fields are Normalized so that $|p^2/\zeta|\sqrt{|E_x|^2 + |E_y|^2} = 1$ at $x = y = 0$.

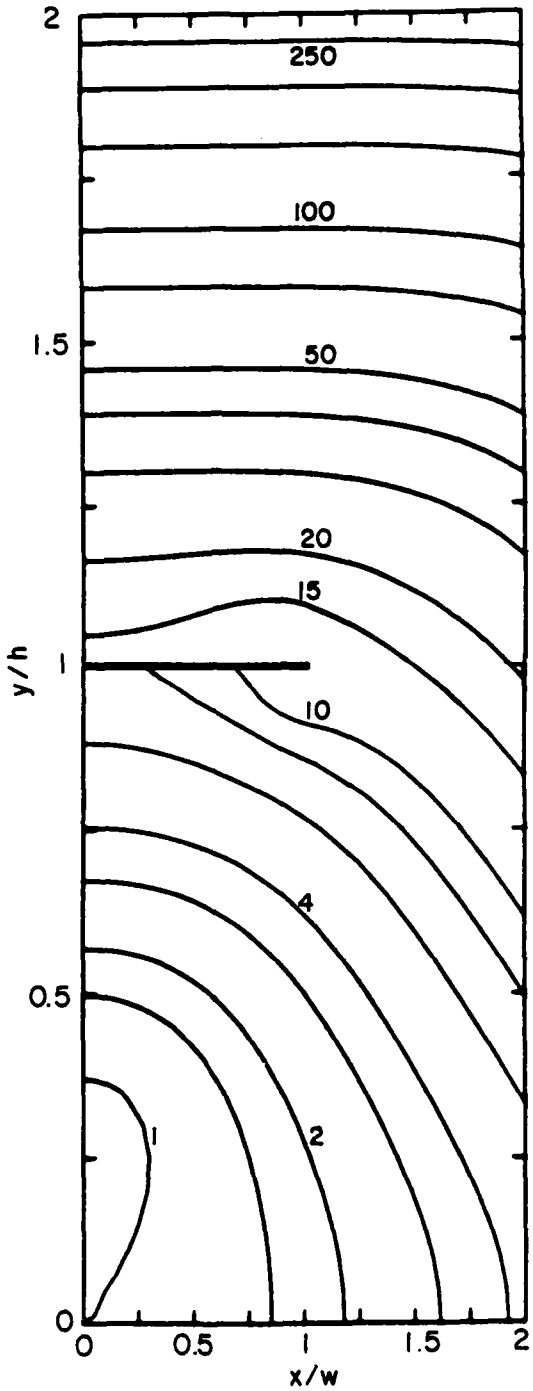

Figure 18f. Constant Value Contours for Normalized Field Component $|p^2/\zeta|\sqrt{|E_x|^2+|E_y|^2} = |p^2(s\varepsilon_o)^{-1}|\sqrt{|H_x|^2+|H_y|^2}$ of the $TM_{1,1}$ Mode when $h/w = 3$. The Fields are Normalized so that $|p^2/\zeta|\sqrt{|E_x|^2+|E_y|^2} = 1$ at $x = y = 0$.

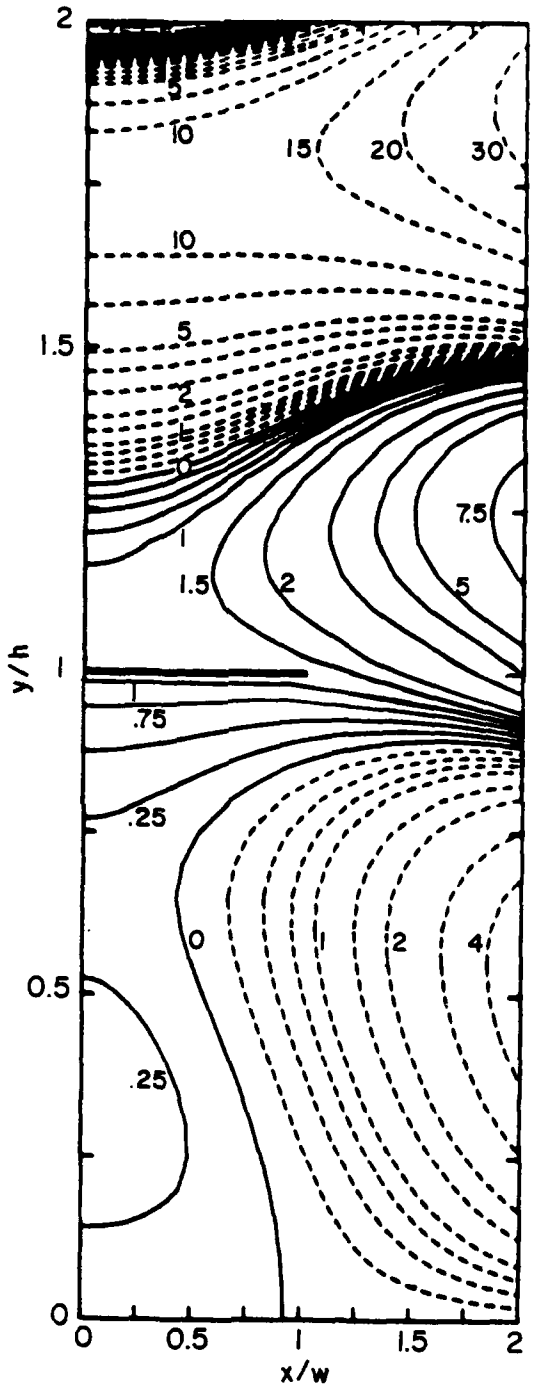

Figure 19a. Constant Value Contours for Normalized Field Component $Re(E_z/w)$ of the $TM_{1,2}$ Mode when $h/w = 3$. The Fields are Normalized so that $|p^2/\zeta|\sqrt{|E_x|^2 + |E_y|^2} = 1$ at $x = y = 0$. Broken Lines are for Negative Values.

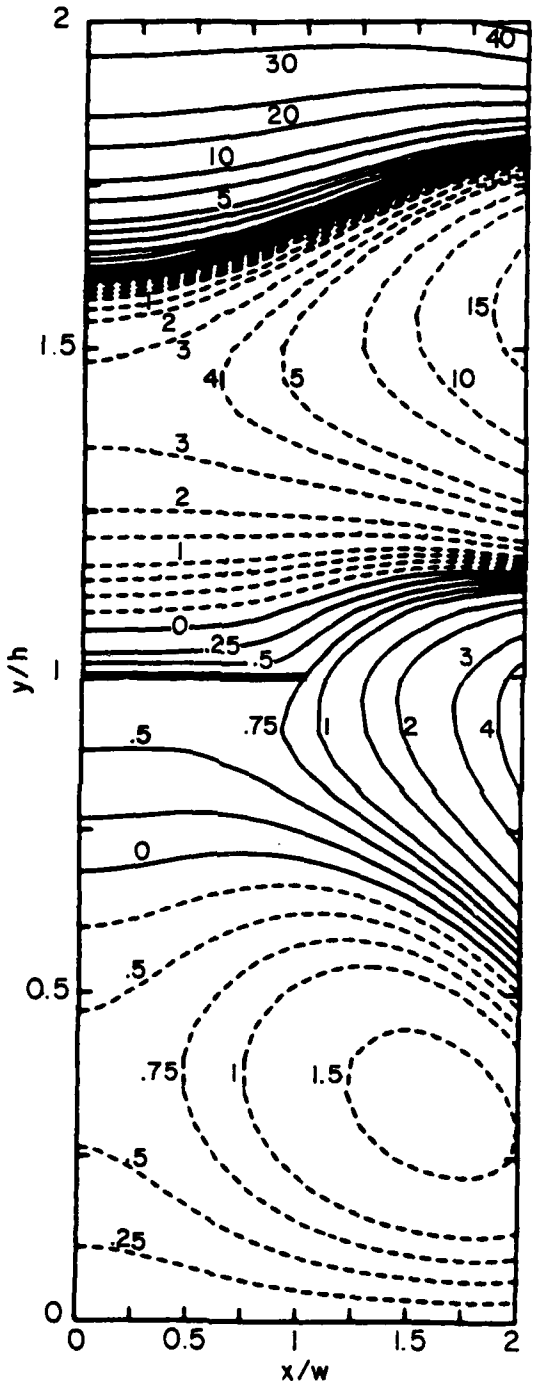

Figure 19b. Constant Value Contours for Normalized Field Component $\mathrm{Im}(E_z/w)$ of the $TM_{1,2}$ Mode when $h/w = 3$. The Fields are Normalized so that $|p^2/\zeta|\sqrt{|E_x|^2 + |E_y|^2} = 1$ at $x = y = 0$. Broken Lines are for Negative Values.

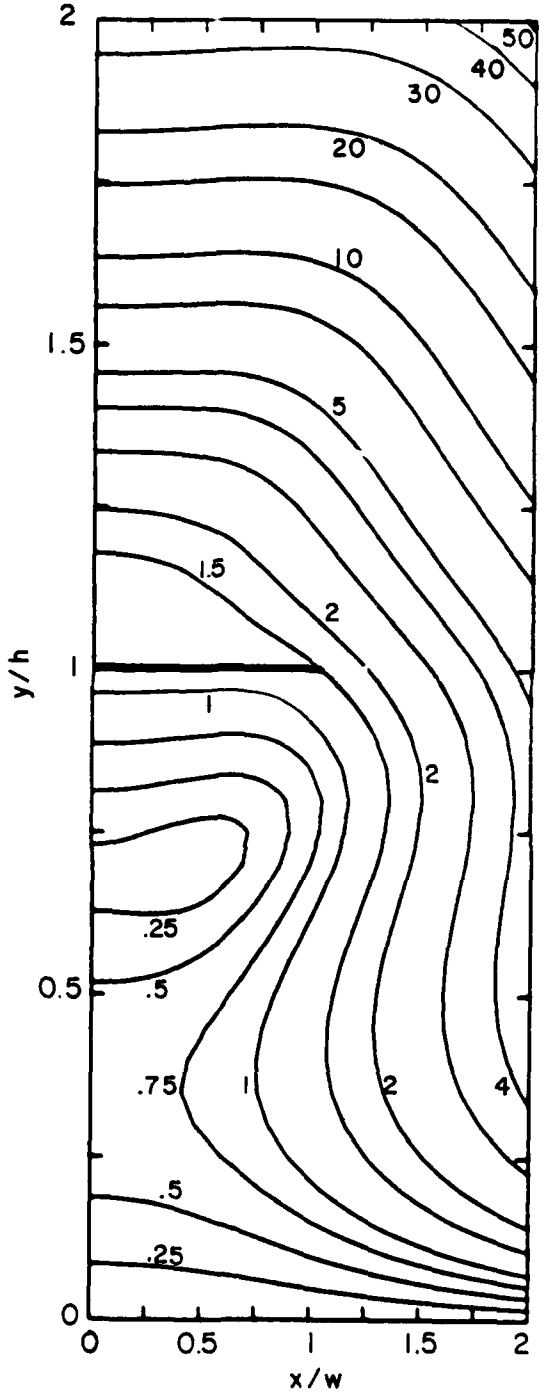

Figure 19c. Constant Value Contours for Normalized Field Component $|E_z/w|$ of the $TM_{1,2}$ Mode when $h/w = 3$. The Fields are Normalized so that $|p^2/\zeta|\sqrt{|E_x|^2 + |E_y|^2} = 1$ at $x = y = 0$.

AD-A086 813 DIKEWOOD INDUSTRIES INC ALBUQUERQUE NM F/G 20/14
DISCRETE AND CONTINUOUS SPECTRA OF FINITE-WIDTH, PARALLEL-PLATE--ETC(U)
MAY 80 F C YANG F29601-78-C-0045
UNCLASSIFIED DC-FR-1299-2 AFWL-TR-79-137 NL

2 OF 2
AD
A086813

END
DATE
FILMED
8-80
DTIC

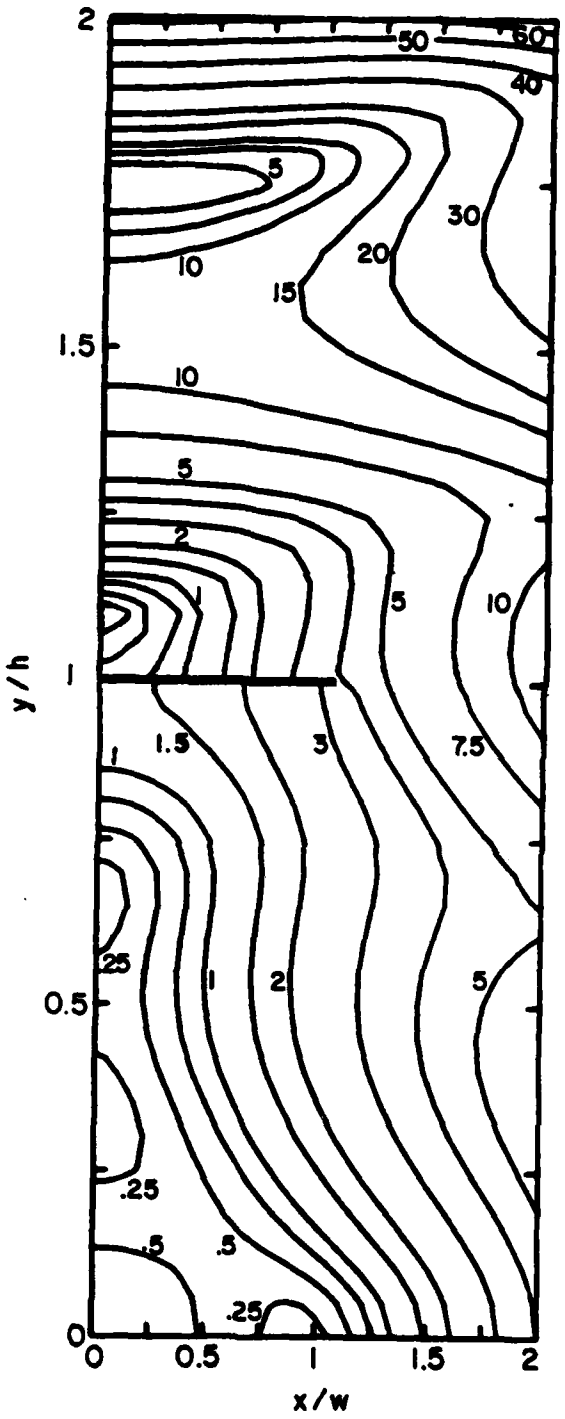

Figure 19d. Constant Value Contours for Normalized Field Component $\sqrt{(\mathrm{Re}(p^2E_x/\zeta))^2 + (\mathrm{Re}(p^2E_y/\zeta))^2} = \sqrt{(\mathrm{Re}(p^2H_y/s\varepsilon_o))^2 + (\mathrm{Re}(p^2H_x/s\varepsilon_o))^2}$ of the $TM_{1,2}$ Mode when $h/w = 3$. The Fields are Normalized so that $|p^2/\zeta|\sqrt{|E_x|^2 + |E_y|^2} = 1$ at $x = y = 0$.

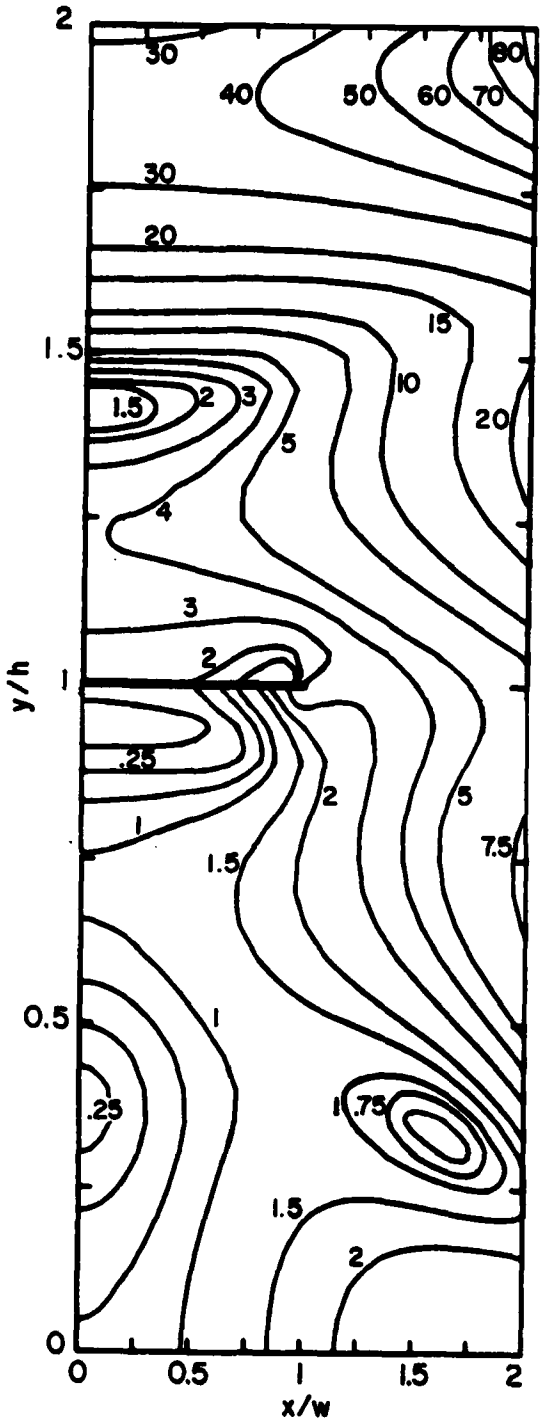

Figure 19e. Constant Value Contours for Normalized Field Component $\sqrt{(\mathrm{Im}(p^2E_x/\zeta))^2 + (\mathrm{Im}(p^2E_y/\zeta))^2} = \sqrt{(\mathrm{Im}(p^2H_y/s\varepsilon_o))^2 + (\mathrm{Im}(p^2H_x/s\varepsilon_o))^2}$ of the $TM_{1,2}$ Mode when $h/w = 3$. The Fields are Normalized so that $|p^2/\zeta|\sqrt{|E_x|^2 + |E_y|^2} = 1$ at $x = y = 0$.

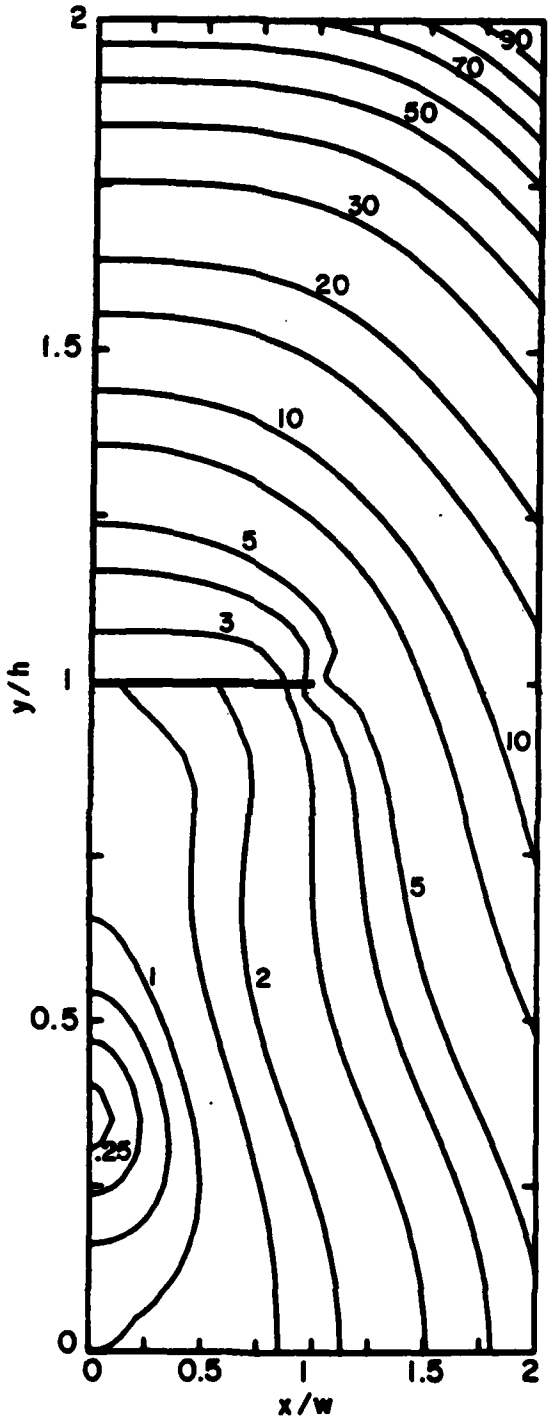

Figure 19f. Constant Value Contours for Normalized Field Component $|p^2/\zeta|\sqrt{|E_x|^2+|E_y|^2} = |p^2(s\varepsilon_o)^{-1}|\sqrt{|H_x|^2+|H_y|^2}$ of the $TM_{1,2}$ Mode when h/w = 3. The Fields are Normalized so that $|p^2/\zeta|\sqrt{|E_x|^2+|E_y|^2} = 1$ at $x=y=0$.

SECTION V

CONTINUOUS SPECTRUM CONTRIBUTION

In this section, an asymptotic estimation of the continuous spectrum contribution to the TM fields at a given ω will be presented.

From equations 2 and 19, the continuous spectrum contribution to E_z for a fixed ω is given by

$$E_z^c(x,y,z,j\omega) = \frac{1}{2\pi j}\int_{B_-}\int_{-w}^{w}\frac{1}{2\pi}\left\{K_o\left(p\sqrt{(x-x')^2+(y-h)^2}\right)-K_o\left(p\sqrt{(x-x')^2+(y+h)^2}\right)\right\}$$

$$\times\, f^{-e}(x'/w)e^{\zeta z}dx'd\zeta \tag{22}$$

where $p = -j\sqrt{\zeta^2+\omega^2/c^2}$, B_- is the contour shown in figure 3, and $f^{-e}(\xi)$ is calculated from equations 11 and 18. Along B_-, it can be shown that the p-values above and below the branch cut are related by p(above) = $e^{j\pi}$p(below). Thus, with the variable change from ζ to $-j\omega/c-\kappa$, equation 22 becomes

$$E_z^c(x,y,z,j\omega) = \frac{1}{4\pi}e^{-j\omega z/c}\int_{-w}^{w}dx'\int_0^{\infty}d\kappa\; e^{-\kappa z}f^{-e}(x'/w)$$

$$\times\left\{I_o\left(p\sqrt{(x-x')^2+(y-h)^2}\right)-I_o\left(p\sqrt{(x-x')^2+(y+h)^2}\right)\right\} \tag{23}$$

where I_o is the modified Bessel function of the first kind and the parameter p is given by $p = -j\sqrt{\kappa^2+2j\kappa\omega/c}$.

The asymptotic behavior for large z of the continuous spectrum contribution $E_z^c(x,y,z,j\omega)$ can now be estimated. Due to the exponential term $\exp(-\kappa z)$, it is clear that the κ-integral in equation 23 comes mainly from the region where $1 \geq \kappa z \geq 0$. For field points in the working volume of the simulator, the arguments of the Bessel functions are small for $1 \geq \kappa z \geq 0$, provided that $z \gg \omega(h^2+\omega^2)/c$ and $z^2 \gg (h^2+\omega^2)$. The small-argument expansion can be applied to the Bessel functions to get (ref. 9)

$$I_o\left(p\sqrt{(x-x')^2 + (y-h)^2}\right) - I_o\left(p\sqrt{(x-x')^2 + (y+h)^2}\right)$$

$$\simeq \left(\kappa^2 + 2j\kappa\omega/c\right)yh \tag{24}$$

For the term $f^{-e}(\xi)$, one obtains, under the same conditions, from equations 11 and 18

$$f^{-e}(\xi) = \frac{1}{\sqrt{1-\xi^2}}\left[T_{2n}(\xi)\right]^T\left[\delta_{nm} + K^e_{nm} - L^e_{nm}\right]^{-1}\left[S^{-e}_m\right]$$

$$\simeq \frac{1}{\sqrt{1-\xi^2}}\left[T_{2n}(\xi)\right]^T\left[\delta_{nm} + \delta_{om}\delta_{on}\frac{1}{\ln 2}\left(\ln\frac{2}{\Gamma pw} - K_o(2ph)\right)\right]^{-1}\left[S^{-e}_m\right]$$

$$\simeq \frac{1}{\sqrt{1-\xi^2}}\sum_{n=0}^{\infty}\left(1 + \delta_{on}\frac{1}{\ln 2}\ln\frac{4h}{\Gamma w}\right)^{-1} S^{-e}_n T_{2n}(\xi) \tag{25}$$

where $[T_{2n}(\xi)]^T$ is the transpose of the column vector $[T_{2n}(\xi)]$ (i.e., a row vector with $T_{2n}(\xi)$ as the elements).

Combining equations 23, 24 and 25, one has

$$E^c_z(x,y,z,j\omega) \simeq \frac{wyh}{4\pi}e^{-j\omega z/c}\sum_{n=0}^{\infty}\left\{\left(1 + \delta_{no}\frac{1}{\ln 2}\ln\frac{4h}{\Gamma w}\right)^{-1}\right.$$

$$\left.\times\int_{-1}^{1}d\xi'\,\frac{T_{2n}(\xi')}{\sqrt{1-\xi'^2}}\int_0^{\infty}d\kappa\, S^{-e}_n e^{-\kappa z}(\kappa^2 + 2j\kappa\omega/c)\right\} \tag{26}$$

$$\text{for } z \gg \omega(h^2+w^2)/c \quad \text{and} \quad z^2 \gg h^2 + w^2$$

Now, if one assumes that S^{-e}_n has no singularities close to the branch cut, which is generally true, equation 26 immediately becomes

$$E^c_z(x,y,z,j\omega) \simeq \frac{1}{2}\left(1 + \frac{1}{\ln 2}\ln\frac{4h}{\Gamma w}\right)^{-1} S^{-e}_o e^{-j\omega z/c}\,\frac{1}{z^3}\left(1 + j\,\frac{\omega}{c}\,z\right) \tag{27}$$

From equation 27, it is seen that the continuous spectrum contribution to $E_z(x,y,z,j\omega)$ decays as z^{-2} when the wave propagates along the +z direction. The above asymptotic estimation can also be applied to other field components to obtain similar results. Hence, within the region where $z^2 >> yhw\omega/c$, (h^2+w^2), $\omega^2(h^2+w^2)^2/c^2$, the continuous spectrum contribution is negligible compared to the TEM mode contribution.

REFERENCES

[1] Marin, L., "Transient Electromagnetic Properties of Two Parallel Wires," Sensor and Simulation Notes, Note 173, Air Force Weapons Laboratory, Kirtland Air Force Base, New Mexico, March 1973.

[2] Marin, L., "Modes on a Finite-Width, Parallel-Plate Simulator, I. Narrow Plates," Sensor and Simulation Notes, Note 201, Air Force Weapons Laboratory, Kirtland Air Force Base, New Mexico, September 1974.

[3] Marin, L., "Modes on a Finite-Width, Parallel-Plate Simulator, II. Wide Plates," Sensor and Simulation Notes, Note 223, Air Force Weapons Laboratory, Kirtland Air Force Base, New Mexico, March 1977.

[4] Marin, L. and Lewis, G.C. Jr., "Modes on a Finite-Width, Parallel-Plate Simulator, III. Numerical Results for Modes on Wide Plates," Sensor and Simulation Notes, Note 227, Air Force Weapons Laboratory, Kirtland Air Force Base, New Mexico, September 1977.

[5] Baum, C.E., "Impedances and Field Distributions for Parallel Plate Transmission Line Simulators," Sensor and Simulation Notes, Note 21, Air Force Weapons Laboratory, Kirtland Air Force Base, New Mexico, June 1966.

[6] Brown, T.L. and Granzow, K.D., "A Parameter Study of Two-Parallel-Plate Transmission Line Simulators of EMP Sensor and Simulation Note 21," Sensor and Simulation Notes, Note 58, Air Force Weapons Laboratory, Kirtland Air Force Base, New Mexico, April 1968.

[7] Baum, C.E., Giri, D.V., and Gonzales, R.D., "Electromagnetic Field Distribution of the TEM Mode on a Symmetrical Two-Parallel-Plate Transmission Line," Sensor and Simulation Notes, Note 219, Air Force Weapons Laboratory, Kirtland Air Force Base, New Mexico, April 1976.

[8] Carrier, G.F., Krook, M., and Pearson, C.E., Functions of a Complex Variable: Theory and Technique, McGraw-Hill, pp.428 - 429, 1966.

[9] Abramowitz, M. and Stegun, I.A., Handbook of Mathematical Functions, Dover Publications, Inc., New York, November 1970.

APPENDIX

MATRIX-EQUATION FORMULATION FOR THE TE FIELDS

In this appendix, the matrix equation for the TE fields of the two parallel-plates will be formulated. The procedure will be the same as that used for the TM fields given in section III.

Under the source condition 6, the coupled differential-integral equations 5 are simplified to the single equation

$$\left(\frac{d^2}{dx^2} - p^2\right)\left(\int_{-w}^{w} \left\{G(x,h,x',h;p) - G(x,h,x',-h;p)\right\} g^{-o}(x')dx'\right)$$
$$= \beta^{-o}(x) \qquad \text{for} \quad |x| \leq w \tag{A1}$$

To solve equation A1, one first integrates the equation to yield the following integral equation

$$\int_{-w}^{w} \left\{G(x,h,x',h;p) - G(x,h,x',-h;p)\right\} g^{-o}(x')dx'$$
$$= B^{-o}\sinh(px) + \int_{-w}^{w} (2p)^{-1}\sinh\left(p|x-x'|\right)\beta^{-o}(x')dx' \qquad \text{for } |x| \leq w \tag{A2}$$

where the integration constant B^{-o} will be determined from the edge conditions.

Equation A2 has the same form as equation 7. Hence, by following the same procedure used to solve equation 7, one can transform equation A2 into a Fredholm integral equation of the second kind given by

$$g^{-o}(\xi) + \int_{-1}^{1} \left(K(\xi,\xi';\gamma) - L(\xi,\xi';\gamma)\right) g^{-o}(\xi')d\xi'$$
$$= \frac{2\gamma B^{-o}}{\pi\sqrt{1-\xi^2}} \fint_{-1}^{1} \frac{\cosh(\gamma\xi')\sqrt{1-\xi'^2}}{\xi-\xi'} d\xi' + \frac{2}{\pi\sqrt{1-\xi^2}} \fint_{-1}^{1} \frac{v^{-o'}(\xi')\sqrt{1-\xi'^2}}{\xi-\xi'} d\xi'$$
$$\text{for } |\xi| \leq 1 \tag{A3}$$

where the variables are normalized according to equation 8, $K(\xi,\xi';\gamma)$ and $L(\xi,\xi';\gamma)$ are defined in equation 10, and

$$v^{-o}(\xi) = w^2 \int_{-1}^{1} (2\gamma)^{-1} \sinh\left(\gamma|\xi - \xi'|\right) \beta^{-o}(\xi')d\xi'$$

The unknown quantities in equation A3 are $g^{-o}(\xi)$ and B^{-o}. By applying the edge conditions, one can derive a relationship between them. The edge and symmetry conditions for $g^{-o}(\xi)$ suggest the following expansion

$$g^{-o}(\xi) = \sqrt{1-\xi^2} \sum_{m=o}^{\infty} g_m^{-o} U_{2m+1}(\xi) \tag{A4}$$

After using the expansion A4 in equation A3 it is observed that both left-hand and right-hand sides of equation A3 contain the term $\xi/\sqrt{1-\xi^2}$ which is the dominant term when $\xi \to \pm 1$. By letting $\xi \to \pm 1$, one can equate the left-hand and right-hand coefficients of the term $\xi/\sqrt{1-\xi^2}$ and thus obtain

$$\int_{-1}^{1} \int_{-1}^{1} \left(M'(\xi''-\xi';\gamma) - N'(\xi''-\xi';\gamma)\right)\sqrt{1-\xi'^2}\sqrt{\frac{1+\xi''}{1-\xi''}} \sum_{m=0}^{\infty} g_m^{-o} U_{2m+1}(\xi')d\xi''d\xi'$$

$$= \gamma B^{-o} \int_{-1}^{1} \cosh(\gamma\xi')\sqrt{\frac{1+\xi'}{1-\xi'}}\, d\xi' + \int_{-1}^{1} v^{-o'}(\xi')\sqrt{\frac{1+\xi'}{1-\xi'}}\, d\xi'$$

Or, after simplification

$$B^{-o} = \sum_{m=0}^{\infty} a_m^o g_m^{-o} - v_{edge}^{-o} \tag{A5}$$

where

$$a_m^o = 2\left(\pi\gamma I_o(\gamma)\right)^{-1} \int_{-1}^{1} \left(M'(2\eta;\gamma) - N'(2\eta;\gamma)\right) R_m^o(\eta)d\eta$$

$$R_m^o(\eta) = \int_{-1+|\eta|}^{1-|\eta|} \frac{\left(1-(\eta'-\eta)^2\right)U_{2m+1}(\eta'-\eta)}{\sqrt{\left(1-(\eta'+\eta)^2\right)\left(1-(\eta'-\eta)^2\right)}}\, d\eta'$$

$$v_{edge}^{-o} = \left(\pi\gamma I_o(\gamma)\right)^{-1} \int_{-1}^{1} v^{-o'}(\xi')(1-\xi'^2)^{-\frac{1}{2}}\, d\xi'$$

Having determined B^{-o} in terms of g_m^{-o}, the matrix equation for g_m^{-o} can then be derived. By removing the term $\xi/\sqrt{1-\xi^2}$ from both sides of equation A3, it is easy to see that the equation can be cast into the following form

$$g^{-o}(\xi) + \sqrt{1-\xi^2}\int_{-1}^{1} \{P(\xi,\xi';\gamma) - Q(\xi,\xi';\gamma)\} g^{-o}(\xi')d\xi'$$
$$= \sqrt{1-\xi^2}\left(B^{-o}H^o(\xi) + V^{-o}(\xi)\right) \tag{A6}$$

where

$$H^o(\xi) = \frac{2\gamma}{\pi}\fint_{-1}^{1} \frac{\cosh(\gamma\xi')\sqrt{1-\xi'^2}}{1-\xi^2}\left(\frac{1}{\xi-\xi'} - \frac{\xi}{1-\xi'}\right)d\xi'$$

$$= \frac{2\gamma}{\pi}\fint_{-1}^{1} \frac{\cosh(\gamma\xi')}{(\xi-\xi')\sqrt{1-\xi'^2}}\, d\xi'$$

$$\{P(\xi,\xi';\gamma) - Q(\xi,\xi';\gamma)\}$$

$$= \frac{2}{\pi}\fint_{-1}^{1} \frac{M'(\xi''-\xi';\gamma) - N(\xi''-\xi';\gamma)}{(\xi-\xi'')\sqrt{1-\xi''^2}}\, d\xi''$$

$$V^{-o}(\xi) = \frac{2}{\pi}\fint_{-1}^{1} \frac{v^{-o'}(\xi')}{(\xi-\xi')\sqrt{1-\xi'^2}}\, d\xi'$$

By inserting the expansion A4 into equation A6 and using the orthogonality of the Chebyshev polynomials, one finally obtains the desired algebraic equations for g_m^{-o} given by

$$g_n^{-o} + \sum_{m=o}^{\infty}\left(P_{nm}^o - Q_{nm}^o - H_n^o a_m^o\right)g_m^{-o} = -v_{edge}^{-o}H_n^o + V_n^{-o} \tag{A7}$$

Or, in matrix form,

$$\left[\delta_{nm} + P^{o}_{nm} - Q^{o}_{nm} - H^{o}_{n} a^{o}_{m}\right]\left[g^{-o}_{m}\right] = \left[- v^{-o}_{edge} H^{o}_{n} + V^{-o}_{n}\right] \tag{A8}$$

where

$$P^{o}_{nm} - Q^{o}_{nm} = \frac{2}{\pi}\int_{-1}^{1}\int_{-1}^{1}\sqrt{1-\xi^2}\,U_{2n+1}(\xi)\sqrt{1-\xi'^2}\;U_{2m+1}(\xi') \times$$

$$\left\{P(\xi,\xi';\gamma) - Q(\xi,\xi';\gamma)\right\}d\xi' d\xi$$

$$= -\frac{16}{\pi}\int_{0}^{1}\left(M'(2\eta;\gamma) - N'(2\eta;\gamma)\right)F^{o}_{nm}(\eta)d\eta$$

$$H^{o}_{n} = \frac{2}{\pi}\int_{-1}^{1}\sqrt{1-\xi^2}\;U_{2n+1}(\xi)H^{o}(\xi)d\xi$$

$$= -\frac{8\gamma}{\pi}\int_{0}^{\pi/2}\cosh(\gamma\cos\phi)\cos\left(2(n+1)\phi\right)d\phi$$

$$V^{-o}_{n} = \frac{2}{\pi}\int_{-1}^{1}\sqrt{1-\xi^2}\;U_{2n+1}(\xi)V^{-o}(\xi)d\xi$$

$$= -\frac{8}{\pi}\int_{0}^{1} v^{-o'}(\xi')T_{2n+2}(\xi')(1-\xi'^2)^{-\frac{1}{2}}\,d\xi'$$

$$F^{o}_{nm}(\eta) = \int_{-1+|\eta|}^{1-|\eta|}\frac{\left(1-(\eta'-\eta)^2\right)U_{2m+1}(\eta'-\eta)T_{2n+2}(\eta'+\eta)}{\sqrt{\left(1-(\eta'-\eta)^2\right)\left(1-(\eta'+\eta)^2\right)}}\,d\eta'$$

$$= \sum_{k=0}^{n+1}\sum_{\ell=0}^{m} u^{o}_{m\ell}t^{o}_{nk}\left\{\sum_{j=0}^{\ell+k}\left(b_j(2k,\,2\ell+1) - \eta^2 b_j(2k,\,2\ell+3)\right)\times\right.$$

$$\left.\times\,\eta^{2\ell+2k-2j+1}D_j(\eta) - b_{\ell+k+1}(2k,\,2\ell+3)\eta D_{\ell+k+1}(\eta)\right\}$$

$$u^{o}_{m\ell} = (-1)^{m-\ell} \frac{(m+\ell+1)!}{(m-\ell)!(2\ell+1)!} 2^{2\ell+1}$$

$$t^{o}_{nk} = (-1)^{n-k+1} \frac{(n+k)!(n+1)}{(n-k+1)!(2k)!}$$

and $b_j(k,\ell)$, $D_j(\eta)$ are given in equations 16 and 17; $\bar{v}^{o}_{edge}$ and a^{o}_{m} are given in equation A5 with

$$R^{o}_{m}(\eta) = \sum_{\ell=o}^{m} u^{o}_{m\ell} \left\{ \sum_{j=0}^{\ell} \left(b_j(0,\ 2\ell+1) - \eta^2 b_j(0,\ 2\ell+3) \right) \eta^{2\ell-2j+1} D_j(\eta) \right.$$
$$\left. -\eta\ b_{\ell+1}(0,\ 2\ell+3) D_{\ell+1}(\eta) \right\}$$

The solution of equation A8 is simply given by

$$\left[\bar{g}^{o}_{m} \right] = \left[\delta_{nm} + P^{o}_{nm} - Q^{o}_{nm} - H^{o}_{n} a^{o}_{m} \right]^{-1} \left[\bar{V}^{o}_{n} - \bar{v}^{o}_{edge} H^{o}_{n} \right] \qquad \text{(A9)}$$

This solution can be used in equations A4, 4 and 2 to calculate the TE fields of the two-parallel-plate simulator.